Synchronization and interdependence between the cycles of Colombia's hydroclimatology and El Niño-Southern Oscillation

Hernán Darío Salas Parra

Universidad Nacional de Colombia
Facultad de Minas, Departamento de Geociencias y Medio Ambiente
Medellín, Colombia
2020

Synchronization and interdependence between the cycles of Colombia's hydroclimatology and El Niño-Southern Oscillation

Hernán Darío Salas Parra

Thesis submitted as partial requirement for the degree of:
Doctor en Ingeniería - Recursos Hidráulicos

Advisors:
Germán Poveda, Ph.D. and Oscar J. Mesa, Ph.D.

Research area:
Hydroclimatology
Universidad Nacional de Colombia
Facultad de Minas, Departamento de Geociencias y Medio Ambiente
Medellín, Colombia
2020

I dedicate this work to my family: My wife Marcela, my daughter Julieta, and my son Juan Miguel. Their love and patience did this possible.

Also, I dedicate this to Susann Reininger, whom my family and I deeply miss.

Aknowledgments

I express my deep gratitude to Professors Germán Poveda and Óscar J. Mesa for their patience, advice, motivation, and friendship. Without their deep questions and suggestions, this work would not have been possible.

Thanks to Professor Jürgen Kurths at Potsdam Institute for Climate Impact Research (PIK) in Germany for his kind hospitality and support during my stay there.

Thanks to Susann and Klaus Reininger, who did wonderful our stay in Caputh - Schwielowsee (Potsdam, Germany). My family and I have deep gratitude and appreciation.

Thanks to Niklas Boers and Norbert Marwan at PIK for their contribution to this research. I learned a lot in my talks with them.

Thanks to Professors: Francina Dominguez, Jorge M. Ramírez and Andrés Ochoa Jaramillo. For their participation in the qualification exam and Ph.D proposal.

Thanks to the Ph.D committee: Isabel Hoyos, Marcelo Barreiro, and A. Ochoa for constructive comments on this work.

Thanks to my friends in Emergente S.A.S - Energía Sostenible : Óscar A. Rueda, Joany Sánchez, Óscar Álvarez-Villa.

This thesis was developed with the financial support of the program *Becas para Doctorados Nacionales - Convocatoria 617–2* by COLCIENCIAS.

Synchronization and interdependence between the cycles of Colombia's hydroclimatology and El Niño-Southern Oscillation

Abstract

Hydroclimatology of Colombia is highly influenced by El Niño - Southern Oscillation (ENSO), which conditions the hydrological response over Colombia, increasing (decreasing) rainfall and streamflows during La Niña (El Niño) depending on the location in the country. This dissertation presents an approach based on synchronization techniques to study the interdependence between ENSO and hydrological variables in Colombia. To that end, we use synchronization techniques such as: Phase synchronization (PS) that is based on the physical properties of weakly coupled periodic oscillators, and Generalized Synchronization (GS) that is based on properties of recurrence of non-linear dynamical systems. Furthermore, we quantify interannual hydroclimatic anomalies (HyAns) using diverse methods to evaluate the sensitivity of linear and non-linear interdependence quantifiers. Our main findings reveal that: (1) we need of quantifying the uncertainty of HyAns in terms of magnitude, sign, timing, and phase of ENSO, because HyAns methods induce an important error source and bias on the interdependence analysis and modeling of climate time series; (2) We find that the positive (negative) HyAns experienced in the Pacific, the Caribbean and the Andean regions of Colombia, during La Niña (El Niño), are phase-locked with the ENSO. Moreover, we provide evidence that the ENSO signal is phase-locked with the annual cycle of rainfall in some regions of Colombia. Furthermore, other macro-climatic processes also show significant PS such as the Pacific Decadal Oscillation (PDO) and the North Atlantic Oscillation (NAO); (3) The Caribbean, the CHOCO and the Orinoco Low-Level Jets (LLJs), and the Cross-Equatorial Flow (CEF) constitute an interdependence mechanism and contribute to explain hydrological anomalies in Colombia during the phases of ENSO. During La Niña (El Niño), GS is strong (weak) for the Caribbean and the CHOCO LLJs whereas GS is moderate (strong) for the Orinoco LLJ. Moreover, moisture advection by the Caribbean and CHOCO LLJs exhibit synchrony with HyAns at 0 to 2 (2 to 4) month-lags over north-western Colombia and the Orinoco LLJ moisture advection synchonizes with HyAns at similar month-lags over the Amazon region of Colombia. This work provides new evidence on the non-linear interactions between hydro-climatic processes in Colombia and ENSO, and constitute an unexplored approach to the understanding of climatic anomalies in tropical South America.

Keywords: Hydrology, Climatology, El Niño - Southern Oscillation (ENSO), Rainfall, Streamflows, Anomalies, Phase Synchronization, Generalized Synchronization.

Sincronización e interdependencia entre los ciclos de la hidroclimatología de Colombia y El Niño-Oscilación del Sur

Resumen

La hidroclimatología de Colombia está fuertemente influenciada por El Niño - Oscilación del Sur (ENSO), el cuál condiciona la respuesta hidrológica en Colombia, incrementando (disminuyendo) la lluvia y los caudales durante La Niña (El Niño) según la región de Colombia. Esta disertación presenta un enfoque basado en técnicas de sincronización para estudiar la interdependencia entre ENSO y las variables hidrológicas en Colombia. Para tal fin, usamos técnicas de sincronización tales como: Sincronización de Fases (PS) que está basada en propiedades físicas de osciladores periodicos debilmente acoplados, y Sincronización Generalizada (GS) que está basada en propiedades de recurrencia de sistemas dinámicos no-lineales. Además, cuantificamos las anomalies hidroclimáticas a escala interanual (HyAns) usando diversos métodos para evaluar la sensibilidad de los cuantificadores de interdependencia lineales y no-lineales. Nuestros principales hallazgos revelan que: (1) Es necesario cuantificar la incertidumbre de las HyAns en términos de la magnitud, signo, momento de ocurrencia y fase de ENSO porque los métodos HyAns inducen una importante fuente de error y sesgo para el análisis de interdependencia y modelación de series climáticas; (2) Encontramos que las anomalías positivas (negativas) en las regiones Pacífico, Caribe, y Andes de Colombia, durante La Niña (El Niño), están enfasadas con el ENSO. Además, presentamos evidencia que la señal de ENSO está enfasada con el ciclo anual de la lluvia en algunas regiones de Colombia. Adicionalmente, otros procesos macroclimáticos también exhiben sincronización de fase significativa tales como la Oscilación Decadal de Pacífico (PDO) y la Oscilación del Atlántico Norte (NAO); (3) La advección de humedad por las corrientes de Chorro de bajo nivel del Caribe, CHOCO y Orinoco, así como el Flujo Cruzado Ecuatorial (CEF) constituyen mecanismos de interdependencia y contribuyen a explicar las anomalías hidrológicas en Colombia durante las fases de ENSO. Durante La Niña (El Niño), GS es fuerte (débil) para las corrientes del Caribe y CHOCO mientras GS is moderada (fuerte) para la corriente del Orinoco. Además, la advección de humedad por las corrientes del Caribe y CHOCO exhiben sincronización con las anomalías con 0 a 2 (2 a 4) meses de rezago sobre el noroccidente Colombiano y la advección de humedad por la corriente del Orinoco se sincroniza con las anomalias de lluvia con tiempos de rezago similares sobre la región amazónica de Colombia. Este trabajo proporciona nueva evidencia sobre las interaciones no-lineales entre los procesos hidroclimáticos en Colombia y ENSO, y además constituye un enfoque inexplorado para el entendimiento de las anomalias climáticas en el norte de Sur America

Palabras Clave: Hidrología, Climatología, El Niño - Oscilación del Sur, Lluvia, Caudales, Anomalías, Sincronización de Fases, Sincronización Generalizada.

Table of contents

. Aknowledgments vii

. Abstract ix

. Resumen x

1. Introduction 1

1.1. Some hydroclimatic features of the region of study . . . 3

2. On the definition of hydro-climatic anomalies 6

2.1. Abstract . . . 6

2.2. Introduction . . . 7

2.3. Region of study . . . 9

2.3.1. Data . . . 9

2.4. Methods . . . 11

2.4.1. Hydro-climatic anomalies using TAC (HyAns–TAC) . . . 12

2.4.2. Hydro-climatic anomalies using Fourier transform (HyAns–Fourier) . 13

2.4.3. Hydro-climatic anomalies using F-Filtering (HyAns–FAC) . . . 14

2.4.4. Hydro-climatic anomalies using Singular Spectrum Analysis (HyAns-SSAC) . . . 15

2.4.5. Hydro-climatic anomalies using MAC (HyAns–MAC) . . . 16

2.4.6. Pearson Correlations and Composite Analysis . . . 17

2.4.7. k-sample tests based on likelihood ratio . . . 18

2.5. Results and Discussion . . . 18

2.5.1. Spatial patterns of rainfall anomalies during ENSO at the national scale 19

2.5.2. Temporal patterns of rainfall anomalies during ENSO . . . 20

2.5.3. Repercussions of HyAns methods on Pearson correlation analysis between rainfall anomalies and the ENSO signal . . . 22

2.5.4. Implications of HyAns methods on Composite Analysis considering the phases of ENSO . . . 26

2.5.5. The role of *the scale factor* and *the reference climatology* on traditional HyAns . . . 26

2.6. Concluding Remarks . . . 27

2.7. Acknowledgments . . . 29

3. Regional rainfall anomalies in Colombia and their association with ENSO: A phase synchronization approach 30
3.1. Abstract . . . 30
3.2. Introduction . . . 31
3.3. Region of study . . . 33
3.3.1. Natural regions of Colombia . . . 33
3.4. Data sets . . . 34
3.4.1. SSTs in the tropical Pacific Ocean and the ENSO signal . . . 34
3.4.2. Colombian Precipitation datasets . . . 34
3.4.3. Other Macro-climatic Indices . . . 35
3.4.4. Reanalysis . . . 35
3.5. Methods . . . 36
3.5.1. Generalized Phase Difference (GPD) . . . 36
3.5.2. Synchronization metrics . . . 37
3.5.3. Phase-Lag estimator . . . 37
3.5.4. Decomposition method . . . 38
3.5.5. Significance Tests . . . 38
3.5.6. On the sensitivity of PS metrics in relation to diverse HyAns methods 39
3.5.7. PS between other Macro-climatic Indices and hydro-climatic anomalies in Colombia . . . 40
3.6. Results and Discussion . . . 40
3.6.1. PS between SST3.4 and rainfall in Colombia using raw data . . . 40
3.6.2. PS between SST3.4 and HyAns in Colombia at inter-annual timescales 43
3.6.3. Composites of hydro-climatic variables from ERA5 during ENSO . . 47
3.6.4. PS analysis between ENSO and the AC of rainfall in Colombia 54
3.6.5. PS between other macro-climatic indices and HyAns in Colombia . . 58
3.7. Conclusions and future work . . . 62
3.8. Acknowledgments . . . 64
3.9. Appendix A:Phase Synchronization:Theoretical basis . . . 64
3.10. Appendix B: Decomposition methods based on EMD . . . 65
3.10.1. Empirical Mode Decomposition (EMD) . . . 65
3.10.2. Ensemble EMD (EEMD) . . . 66

4. Generalized Synchronization between ENSO and hydrological variables in Colombia: A recurrence quantification approach 67
4.1. Abstract . . . 67
4.2. Introduction . . . 68
4.2.1. ENSO effects on hydro-climatology of Colombia . . . 69
4.2.2. Objectives . . . 70

4.3. Data and region of study . . . 71
4.3.1. The ENSO signal . . . 71
4.3.2. Colombian hydrology . . . 73
4.3.3. Moisture Advection through Low-Level Jets . . . 75
4.3.4. The Amazonian Cross-Equatorial Flow . . . 76
4.4. Methods . . . 76
4.4.1. Generalized synchronization using the Recurrence Quantification Analysis . . . 76
4.4.2. Significance tests . . . 78
4.4.3. Joint Probability of Recurrences during ENSO . . . 78
4.4.4. Sensitivity of the GS metrics to diverse HyAns methods . . . 79
4.5. Results and discussion . . . 80
4.5.1. Rainfall anomalies in Colombia and their association with ENSO by means of Pearson correlations . . . 80
4.5.2. Moisture Advection Anomalies by LLJs during ENSO . . . 80
4.5.3. Time Delay and Embedding Dimension . . . 82
4.5.4. Sensitivity of the GS-metrics regarding diverse HyAns methods . . . 84
4.5.5. GS between SST3.4 anomalies and hydrological anomalies in Colombia 85
4.5.6. GS between the moisture advection by Low-Level Jets and rainfall in Colombia . . . 87
4.5.7. GS between the Cross-Equatorial Flow and rainfall in Colombia . . . 91
4.5.8. GS between indices for different types of ENSO and hydrologic anomalies in Colombia . . . 92
4.6. Final remarks and future work . . . 94
4.7. Acknowledgments . . . 96

5. General conclusions and Future work 98
5.1. General conclusions . . . 98
5.2. Future work . . . 99

A. Supplementary Material – Chapter 2 120

B. Supplementary Material – Chapter 3 126
B.1. Pre-processing data: Filtering and Definition of HyAns . . . 126

C. Supplementary Material – Chapter 4 146

Abbreviations

Abbreviations

Abbreviation	Definition
ENSO	El Niño - Southern Oscillation
HyAns	Hydroclimatic anomalies
TAC	Traditional Annual Cycle
FAC	F-Filtering of the Annual Cycle
MAC	Modulated Annual Cycle
SSA	Singular Spectrum Analysis
SSAC	Annual Cycle defined using SSA
PCA	Principal Component Analysis
EMD	Empirical Mode Decomposition
EEMD	Emsemble Empirical Mode Decomposition
PS	Phase Synchronization
SPS	Strength of Phase Synchronization
NAO	North Atlantic Oscillation
PDO	Pacific Decadal Oscillation
NTA	North Tropical Atlantic
NASH	North Atlantic Subtropical High
LLJ	Low Level Jet
STS	Synthetic Time Series
LN	La Niña; Cold state of ENSO
EN	El Niño; Warm state of ENSO
GS	Generalized Synchronization
AC	Annual Cycle
CDF	Cumulative Distribution Function
SIR	Solar Incoming Radiation
GPD	Generalized Phase Difference

1. Introduction

Northern South America is a highly relevant region to study hydro-climatic processes, their interrelations and their socio-economical, environmental and ecological impacts [*Poveda and Mesa*(1997), *Coelho et. al.*(2002), *Grimm et al.(2009)*, *Poveda et al.*(2011), Andreoli et al.(2017), *Bedoya-Soto et. al.*(2018)]. In particular, the continental territory of Colombia is located in the northwestern corner of South America and it is influenced by a suite of hydro-climatic processes from diurnal to inter-annual timescales [*Poveda et al.*(2004)]. The hydro-climatic variability of Colombia is influenced by climatic processes occurring in the tropical Pacific Ocean, the Atlantic Ocean and land-atmosphere-ocean feedbacks in conjunction with the orographic influence of the Andean mountains [*Poveda and Mesa*(1997), *Poveda et al.*(2005), *Bedoya-Soto and Poveda*(2017)]. The occurrence of both phases of ENSO at interannual timescales are associated with anomalies of diverse hydro-climatic variables and processes, depending on the location in the country [*Poveda and Mesa*(1997), *Poveda et al.*(2001), *Poveda et al.*(2011), *Bedoya-Soto et. al.*(2018)]. In general, according to the literature, negative anomalies in rainfall, river flows, soil moisture and vegetation activity are witnessed during the warm phase (El Niño), and the opposite during La Niña in most of the country [*Poveda and Mesa*(1997), *Poveda et al.*(2001), *Poveda et al.*(2011), *Bedoya-Soto et. al.*(2018)].

This dissertation is a novel approach in order to reveal new insights regarding the impacts of ENSO on northern South America. To that end, we use a set of non-linear methods because the complex dynamics of the relation between ENSO and Colombian rainfall makes hard the whole picture and also because traditional approaches are based on linear methods (composites and linear correlations). In this sense, previous works that have investigated the influence of ENSO on Colombian hydro-climatology can be classified in two large groups: (1) the physical mechanisms that explain the impact of Pacific Oceanic-Atmospheric dynamics over Colombia ([*Poveda and Mesa*(1997), *Poveda and Mesa*(1999), *Poveda et al.*(2001), *Poveda et al.*(2011), *Poveda et al.*(2014), *Muñoz et al.*(2017), *Jaramillo et al.*(2017), *Hoyos et al.*(2017)]; among others) and, (2) the statistical characterization and modeling of hydro-climatic variables, under ENSO influence, using linear and non-linear techniques ([*Carvajal et al.*(1998), *Poveda et al.*(2003), *Hurtado and Poveda*(2009), *Carmona and Poveda*(2014)], among others). It is remarkable emphasize that although not only ENSO has influence over hydro-climatic variables of Colombia, it is a key component to understand the Colombian water cycle dynamics. Then, although there is evidence of the interdependence between hydro-climatic variables of Colombia and the Pacific ocean-atmospheric dynamics at ENSO

timescales [*Poveda et al.*(2001), *Poveda et al.*(2011), *Bedoya-Soto and Poveda*(2017), *Bedoya-Soto et. al.*(2018)], such interdependence has not been studied using an approach based on *the interaction between the oscillations* under the assumption that physical phenomena are generated by multiple oscillatory interacting systems or *synchronization* in the sense of [*Pikovsky et al.*(2001)]. There are different methods to investigate synchronization, based on recurrences [*Marwan et al.*(2007), *Donner et al.*(2010), *Arnhold et al.*(1999), *Le Van Quyen et al.*(1999), *Shiff et al.*(1996)], phase differences [*Rosenblum et al.*(1997), *Pikovsky et al.*(2001)], or the quasi-simultaneous appearance of events [*Stolbova et al.*(2014), *Malik et al.*(2012), *Rheinwalt et al.*(2016), *Agarwal et al.*(2017)]. In particular, the phase differences method has physical basis deduced from weakly coupled oscillators whereas the method based on recurrences is deduced on properties of the non-linear dynamical systems.

In Chapter 2, we study the definition of the so-called hydro-climatic anomalies (HyAns) because extracting the annual cycle of hydro-climatic data is a widely used procedure in Geosciences such as Meteorology, Hydrology, and Climatology, among others and, although diverse methodologies are used to filter out the seasonal cycle, little effort has been made to assess the uncertainties implied in the estimation of HyAns. To advance in dealing with this issue, it is necessary to compare diverse methods to estimate HyAns, which are based on diverse reference 'climatologies' in order to investigate the differences and biases among different HyAns methods (in terms of their sign, timing, and magnitude) as well as their repercussions for linear and non-linear analysis and modeling of climate time series.

In Chapter 3, we investigate Phase Synchronization (PS) between the El Niño - Southern Oscillation (ENSO) signal and the (inter-annual and annual) cycles of rainfall in Colombia. To that end, we carry out a detailed data analysis in order to define the annual cycle (AC), eliminating the seasonal residual frequencies in hydro-climatic anomalies (HyAns), assessing the statistical significance of PS metrics, and checking the sensitivity of the PS metrics in relation to diverse HyAns estimation methods. In this chapter, we characterize the seasonal regional patterns of rainfall anomalies in relation to the ENSO's states. We look for PS between HyAns in the five natural regions of Colombia and the ENSO signal as well as the PS between the AC of rainfall and the ENSO signal. Furthermore, we explore possible PS between HyAns and other macro-climatic processes such as the Pacific Decadal Oscillation (PDO) and the North Atlantic Oscillation (NAO), among others.

In Chapter 4, we use Recurrence Quantification Analysis (RQA) to study features of Generalized Synchronization (GS) between El Niño-Southern Oscillation (ENSO) and monthly HyAns (rainfall and streamflows) in Colombia. To that end, we check the sensitivity of the RQA concerning diverse HyAns estimation methods. In general, the GS and its sensitivity to HyAns methods are quantified by means of time-lagged joint recurrence analysis. Then, we link the GS results with the dynamics of some important physical mechanisms that modulate Colombia's hydroclimatology, including the Caribbean, the CHOCO and the Orinoco Low-Level Jets (LLJs), and the Cross-Equatorial Flow (CEF) over northwestern Amazonia (southern Colombia). In this chapter, we characterize the zones of Colombian territory un-

der the influence of mentioned moisture advection sources during the phases of ENSO and possible physical basis behind the synchronization patterns.
Finally, Chapter 5 contains general conclusions and future work.

1.1. Some hydroclimatic features of the region of study

The continental territory of Colombia can be divided into five major natural regions (see Fig 2-1) with different hydro-climatological, geomorphological and bio-ecological characteristics due to the influence of diverse geographical features and processes at different spatial and temporal scales.
Some remarkable aspects of annual and inter-annual rainfall and streamflow variability in those regions are influenced by ENSO as follows:
The **Pacific** region comprises 7% of the total Colombian territory. The Atrato and San Juan rivers drain most of the region to the Caribbean Sea and the Pacific Ocean. The region witness one of the `the rainiest regions on Earth`, which has been explained in terms of land-ocean-atmosphere interactions enhanced by the Choco low-level jet (Choco Jet) [*Poveda and Mesa*(2000), *Mapes et al.*(2003a), *Mapes et al.*(2003b), *Warner et al.*(2003), *Bedoya-Soto et. al.*(2018)]. [*Poveda and Mesa*(2000)] found that zonal wind at 925 hPa penetrates into western Colombia as a low-level westerly jet, located at 5^oN. Those winds are almost absent during February–March, attain its maximum core wind velocities during October–November (6-8 m/s) and decrease onwards, which explain combined with the activity of Mesoscale Convective Complexes the high annual precipitation in this region. The annual cycle of rainfall is bimodal with the rainiest periods in March–April–May (MAM) and September–October–November (SON) and, the minima rainy periods in December–January–February (DJF) and June–July–August (JJA). This characterization was based on IDEAM and TRMM datasets [*Hoyos et al.*(2017)]. However, the recent work by urrea shows that rainfall seasonality in the Pacific region depends also on the location in the region. The central Pacific region exhibits a non-seasonal annual cycle while, that in northern Pacific is unimodal, and in southern Pacific is bimodal. In particular, during El Niño, the strength of CHOCO jet winds diminish as a result of reduction of the temperature gradient between surface air temperatures over the Pacific coast off Colombia and the Niño 1+2 zone. Such weakening of CHOCO jet winds causes a reduction of moisture advection from Pacific to Colombia and contribute to explain negative anomalies in rainfall during El Niño [*Poveda and Mesa*(1997), *Poveda and Mesa*(2000), *Rueda and Poveda*(2006), *Bedoya-Soto et. al.*(2018)].
The **Caribbean** region constitutes 12% of the total Colombian territory. The western Caribbean region exhibits a bimodal annual cycle with the rainiest periods in MAM and SON, and the driest ones in JJA and DJF, whereas the eastern Caribbean region exhibits a mixed seasonality [*Urrea et al.*(2018)]. This region is strongly influenced by the Caribbean Low Level jet (CLLJ), whose easterly zonal wind at 925 hPa has a bimodal annual cycle, with maxima in July and February, in response to the sea level pressure changes in the

North Atlantic Subtropical High (NASH) [*Wang*(2007), *Poveda et al.*(2014)]. According to [*Hoyos et al.*(2017)], the main influence of the CLLJ in the region occurs at the end of the SON season, when the blocking effect of the CHOCO jet over the Tropical Pacific is weakened and the southward component of low-level transport is intensified when the ITCZ is in its southernmost position. Then, as a result, the low level transport that crosses Central America deflects towards western Colombia, enhancing the convergence moisture in this area in DJF [*Hoyos et al.*(2017)]. Notwithstanding, during La Niña, the easterly CLLJ winds are weak (strong) in JJA (DJF), whereas during El Niño, the easterly CLLJ winds are strong (weak) in JJA (DJF) [*Wang*(2007)]. Hence, the CLLJ influence over northern South America contributes to explain rainfall anomalies during ENSO over the Caribbean basin and the nearest continental areas [*Wang*(2007), *Muños et al.*(2008), *Arias et al.*(2015)].

The **Andean** region is delimited by the three branches of the Andes mountains, its area constitutes 19% of the total Colombian territory. The Magdalena and Cauca constitute the most important river basins draining river flows into the Caribbean Sea. Precipitation in this region exhibits bimodal annual cycles with the rainiest periods in March–April–May (MAM) and September–October–November (SON). In this region, the latitudinal migration of the ITCZ and its interactions with topography play an important role in the annual distribution of hydro-climatic variables, whose ACs spatially vary in agreement with the migration of the ITCZ and other physical mechanisms [*Poveda and Mesa*(1997), *Hoyos et al.*(2017), *Urrea et al.*(2018)]. At interannual time scales, precipitation and streamflows in this region exhibit strong correlations with ENSO, overall with severe droughts during El Niño and severe floods during La Niña [*Poveda and Mesa*(1997), *Poveda et al.*(2001), *Poveda et al.*(2011), *Poveda et al.*(2015), *Córdoba-Machado et al.*(2015), *Córdoba-Machado et al.*(2014), *Bedoya-Soto et. al.*(2018)]. The work by poveda11 on the relationship between the hydro-climatic anomalies over the Andes of Colombia and their relation to ENSO, concludes that the ENSO's effects are phase-locked to the seasonal cycle, being stronger during December–January–February (DJF) but weaker during March–April–May (MAM). Furthermore, such relation between ENSO and the seasonal cycle is evidenced in rainfall, river discharges, soil moisture and, the vegetation index (NDVI) as a surrogate of evapotranspiration [*Poveda et al.*(2011)].

The **Orinoco** region is a vast plain whose area constitutes 22% of the total Colombian territory. The main rivers of its fluvial system are the Orinoco, Guaviare and Meta and its hydro-climatology is strongly influenced by the Orinoco LLJ (also known as Corriente de los Andes Orientales (CAO) or Low Level Jet in the Eastern Plains) [*Montoya*(2001), *Torrealba and Amador*(2010), *Jiménez-Sánchez*(2019)], whose strong northeasterly flux crosses through the Orinoco and Amazon river basins. Such flux causes a localized weak moisture convergence over this area, which conjointly with the slower latitudinal migration of the ITCZ explains the unimodal annual cycle of precipitation with the rainiest and driest months in June and January, respectively [*Hoyos et al.*(2017)]. The most important sources of moisture of this region are the Atlantic Ocean, local recycling and terrestrial recycling from the Amazon and Orinoco Basins [*Poveda et al.*(2014), *Arias et al.*(2015)]. In this region, hydro-climatic

variability can be influenced by the Cross-Equatorial winds, which have an annual cycle with negative values (northern winds) between October and March with peak in December and positive values (southern winds) between April and September, with peak in June. The V-index for the Cross-Equatorial winds explains a high percentage of the seasonal variance of precipitation (37%) in northern South America [*Wang and Fu*(2002)].

The **Amazon** region is located north of the Amazon Basin and south of the Colombian territory. Its area constitutes 40% of the total Colombian territory. The main rivers of its fluvial system are Amazonas, Caquetá, Putumayo, Guaviare, Apaporis and Vaupes and, the moisture transport from the Amazon basin to Colombia induces temporal and spatial water cycle variability [*Poveda and Mesa*(1997)]. The AC of precipitation is unimodal with maxima in May [*Hoyos et al.*(2017)], and its main sources of moisture, as in the case of Orinoco, are the Atlantic Ocean, local recycling and terrestrial recycling from the Amazon and Orinoco Basins [*Hoyos et al.*(2017), *Arias et al.*(2015)]. In this region as well as in the Orinoco region, the annual and inter-annual cycles of hydro-climatic variables are significantly influenced by the Cross-Equatorial winds [*Wang and Fu*(2002)]. Notwithstanding, the literature does not provide information regarding the response of the Cross-Equatorial winds during different ENSO phases.

2. On the definition of hydro-climatic anomalies

Hernán D. Salas, Germán Poveda, Óscar J. Mesa, Niklas Boers, and Jürgen Kurths

2.1. Abstract

The implications of the estimation of inter-annual hydro-climatic anomalies (HyAns) need careful consideration, but the importance of the process does not correspond with the usual practice. For instance, common estimation techniques do not consider error sources or induced biases in subsequent interdependency analysis with other time series or climatic indices. Consequently, there is room for ambiguity in the physical interpretation of results. To advance in dealing with this issue, we quantify rainfall anomalies over Colombia (in terms of their sign, timing, and magnitude) and their interdependence with the El Niño - Southern Oscillation (ENSO) as a paradigmatic case to illustrate the problems, to compare different methods to define HyAns, and to infer recommendations. In general, we compare five HyAns estimation methods that consider both constant and variable definitions of the annual cycle. Next, we use the Pearson correlation analysis as well as the composite analysis to investigate the influence of those HyAns methods on the analysis of time series. Our results reveal significant differences among the HyAns methods regarding the influence of ENSO on monthly precipitation in Colombia in terms of magnitude, timing, spatial patterns, spectral properties, correlations, and probability distribution functions. This assessment study allows us to conclude that the method to estimate inter-annual HyAns based on moving averages is most adequate because of its *(i)* clear theoretical foundation, *(ii)* non-constant annual cycle, and *(iii)* adequate filtering of high-frequencies, among other criteria. Our identification of the differences between the diverse HyAns methods reveals biases and error sources toward the analysis and modeling of climate time series, which generate ambiguities for the physical interpretation of results. Our study presents methods that can be used anywhere in the world and evidences the need to tackle this fundamental but often overlooked problem. In particular, we stress its importance in assessing ENSO's effects on hydro-climatic processes.

2.2. Introduction

The seasonal component is the strongest signal in the temporal dynamics of hydro-climatic data. In order to investigate other signals and processes at different timescales, it is customary to remove the seasonality to obtain the so-called hydro-climatic anomalies (HyAns). This de-seasonalization is a widely used procedure in Geosciences and especially Meteorology, Hydrology, and Climatology, among others [*Fraedrich and Müller (1992)*, *Chandler (1992)*, *Mason et al. (2001)*, *Brohan et al.(2006)*, *Hegerl et al.(2018)*] and, although there are diverse methodologies to filter out the seasonal cycle, comparably less effort has been made to assess the uncertainties implied in the estimation of HyAns. In this sense, recent studies have shown that the analysis of hydro-climatic time series requires careful pre-processing steps to filter out the seasonal cycle in order to look for robust results and interpretations, because minor differences in data pre-processing can produce contradictory or even spurious results [*Lange et al.(2018)*, *Salas et al.(2020)*].

To advance in dealing with this issue, we compare five widely used methods to estimate HyAns, which are based on diverse reference 'climatologies': *(i)* the Traditional Annual Cycle (TAC) or constant climatology, which use long-term monthly averages as the annual cycle, which in turn assumes a constant response of the climate system to the periodic forcing of the annual solar incident radiation (SIR), and does not consider the non-linear and non-stationary responses of the climate system to the external forcing of SIR [*Salas et al.(1980)*], (ii) Fourier filtering of the annual cycle (hereafter Fourier), *(iii)* filtering of the annual cycle by Moving Averages (hereafter FAC), whose mathematical properties allow to filter out the seasonal frequencies and their harmonics from the original climatic time series [Douglass (2011), Douglass (2015)], *(iv)* Singular-Spectrum Analysis to extract the annual cycle (hereafter SSAC), which enables us to decompose a time series into its elementary patterns using a Principal Component Analysis (PCA) in the vector space of delay coordinates. After this decomposition, the elementary temporal patterns are distinguished into noise, semi-annual, annual and inter-annual components [*Vautard et al.(1992)*, *Ghil (2002)*], *(iv)* Subtraction of the Modulated Annual Cycle (MAC), which is based on the Ensemble Empirical Mode Decomposition (EEMD) technique. This method decomposes the signal into seasonal frequencies and other oscillation modes [*Huang et al.*(1998), *Wu and Huang*(2009)]. Hence, HyAns defined using the TAC and Fourier methods imply a constant climatology, whereas to define HyAns using FAC, SSAC, and MAC a non-constant annual cycle is implied.

To carry out our comparative analysis among HyAns methods, we study interannual rainfall anomalies during two extreme phases of ENSO (El Niño and La Niña) over South America because, despite the progress in understanding climate interactions in this region, uncertainty remains regarding the robustness of the impacts [*Cai et al.(2020)*]. In particular, we focus our research on the continental territory of Colombia, located in the northwestern corner of South America (see Fig. **2-1**). A suite of hydro-climatic processes from diurnal to inter-annual timescales influence Colombia's climate [*Poveda et al.*(2004)]. Besides, it is a highly

relevant region where the hydro-climatic anomalies associated with ENSO produce strong socio-economical, environmental and ecological impacts [*Poveda and Mesa*(1997), *Coelho et al.(2002)*, *Grimm et al.(2009)*, *Poveda et al.*(2011), Andreoli et al.(2017), *Bedoya-Soto et. al.*(2018), *Poveda et al.(2020)*]. The main controls of the hydro-climatic variability of Colombia are processes occurring in the tropical Pacific Ocean, the Atlantic Ocean, and land-atmosphere-ocean feedback in conjunction with the orographic influence of the Andean mountains [*Poveda and Mesa*(1997), *Poveda et al.*(2005), *Bedoya-Soto and Poveda*(2017)]. During both phases of ENSO, there are characteristic hydroclimatic anomalies, depending on location in the country [*Poveda and Mesa*(1997), *Poveda et al.*(2001), *Poveda et al.*(2011), *Bedoya-Soto et. al.*(2018)]. In general, negative anomalies in rainfall (decrease in rainfall), river flows, soil moisture, and vegetation activity occur during the warm phase (El Niño) and the opposite during La Niña. Hence, Colombia is an adequate and interesting region to study how to characterize HyAns and investigate the differences and biases among different methods to quantify HyAns and their implications for analysis and modeling of climate time series.

Depending on the estimation method, temporal and spatial properties of HyAns could considerably differ, leading to significantly different physical interpretations about the interannual variability. Furthermore, some HyAns methods are widely accepted in climate sciences research [*Salas et al.(1980)*, *Vautard et al.(1992)*], although they lack physical justification, especially given the non-linear character of the climate processes [*Wu et al.*(2008), *Fedorov et al.(2000)*, *Thoning and Tans (1989)*]. Hence, in order to quantify the differences between HyAns methods, we compare the probability distributions of the HyAns estimations using the k-sample tests, a powerful method based on likelihood ratio that improves the conventional Kolmogorov-Smirnov, Cramér-von Mises and Anderson-Darling tests [*Zhang and Wu (2007)*].

Moreover, we explore the influence of the studied HyAns methods through Pearson's correlations, a well-known and straightforward measure of linear association [*Pearson (1895)*]. Then, we quantify Pearson correlations between an index of ENSO in the tropical Pacific Ocean, the Multivariate ENSO Index (MEI) [*Wolter and Timlin (2011)*], and rainfall anomalies in Colombia using the five different HyAns methods. Furthermore, we investigate whether the HyAns methods can induce significant differences in the composite analysis, a frequently used tool to infer the relationships among different climate phenomena [*Terray et al.(2003)*, *Boschat et al.(2016)*, *Xie et al.(2017)*] and we validate our results using parametric and non-parametric tests [*Nicholls (2001)*, *Terray et al.(2003)*]. As a complement, we discuss the role of *the scale factor* and *the reference climatology* in the formal definition of climate anomalies.

The purpose of this work is threefold: *(i)* to quantify and compare rainfall anomalies throughout Colombia estimated by the five different HyAns methods, namely HyAns–TAC, HyAns–Fourier, HyAns–FAC, HyAns–SSAC, and HyAns–MAC. *(ii)* To investigate the influence of HyAns methods on the analysis of the mutual dependence between macro-climatic phenom-

ena and hydrological time series. (iii) To recommend a HyAns method for practical purposes based on essential criteria, such as firm theoretical foundation, variable climatology, and adequate filtering of inter-annual frequencies.
This work is structured as follows: Section 2.3 describes the region of study and the precipitation data sets. Section 4.4 presents definitions of hydro-climatic anomalies using the five methods described above, as well as comparison methods such as Pearson correlation, composite analysis, and k-sample tests. Results are discussed in Section 4.5 and the conclusions are drawn in Section 4.6.

2.3. Region of study

There are five regions in the continental territory of Colombia: Andes, Orinoco, Pacific, Amazon, and the Caribbean. Each exhibits different hydro-climatological, geomorphological, and bio-ecological characteristics due to the influence of diverse geographical characteristics and climate processes [$IGAC(2002)$]. Figure **2-1** shows the continental location of Colombia as well as the five different regions.

2.3.1. Data

Colombian precipitation

- **Dataset No. 1**: We use data from a precipitation reanalysis performed by Hurtado-Montoya and Mesa [*Hurtado and Mesa*(2014)], which produced monthly precipitation fields for Colombia, spanning the period from 1975 to 2006, at a spatial resolution of 5 minutes of arc, in the region 5^oS–15^oN and 80^oW–65^oW. Those authors used a set of 2270 rain gauges from diverse institutions including Instituto de Hidrología, Meteorología y Estudios Ambientales de Colombia (IDEAM), Empresas Públicas de Medellín (EPM), Centro Nacional de Investigaciones del Café (CENICAFE) and The Global Historical Climatology Network (GHCN). Besides, they also used satellite images from the Global Precipitation Climatology Project (GPCP)-V2, National Centers for Environmental Prediction (NCEP)/National Center for Atmospheric Research (NCAR), Tropical Rainfall Measuring Mission (TRMM), and the Geostationary Satellite System (GOES). Finally, the monthly precipitation fields resulted from an optimal combination of the available data and the implementation of the PRISM model [*Daly et al.(2002)*] for space interpolation, taking into account the topography of the Colombian territory. This dataset is freely available through personal communication with the authors [*Hurtado and Mesa*(2014)].

- **Dataset No. 2**: Climate Hazards Group InfraRed Precipitation with Station data (CHIRPS) is a high resolution (0.05^o), daily, pentad, and monthly quasi-global rainfall

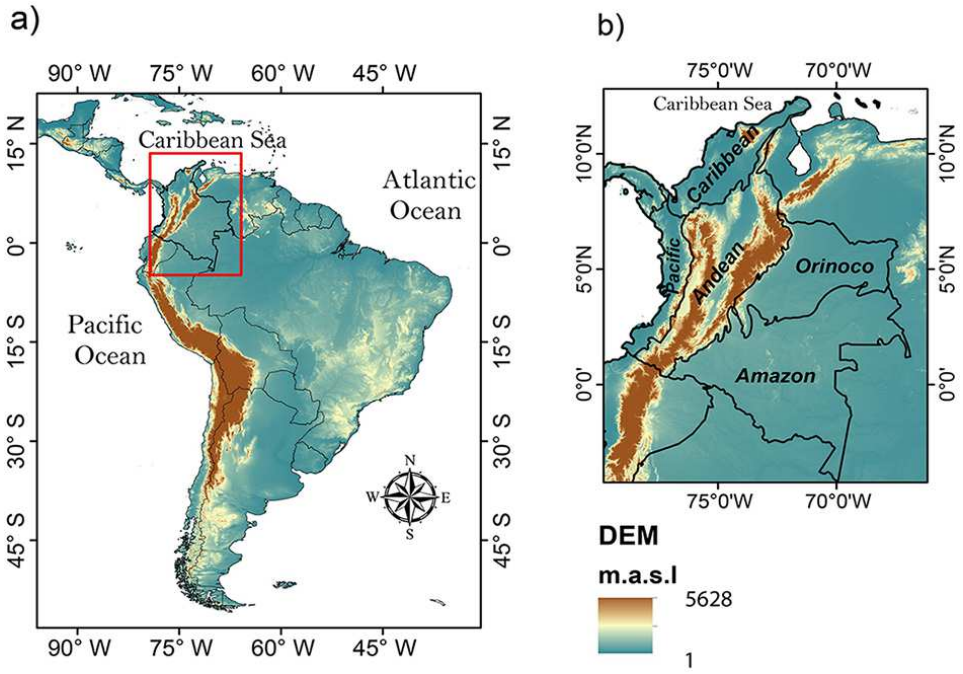

Figures 2-1.: Region of study. a) Continental context. b) National context including the five major natural regions [*IGAC*(2002)] (Andes, Orinoco, Pacific, Amazon and Caribbean). Figure was created using the void-filled elevation (30 sec DEM) raster obtained from the World Wildlife Fund HydroSHEDS project [*Lehner et al.(2008)*], and used under the following license. This product incorporates data from the HydroSHEDS database which is ©World Wildlife Fund, Inc. (2006-2013) and has been used herein under license. WWF has not evaluated the data as altered and incorporated within, and therefore gives no warranty regarding its accuracy, completeness, currency or suitability for any particular purpose. Portions of the HydroSHEDS database incorporate data which are the intellectual property rights of ©USGS (2006-2008), NASA (2000-2005), ESRI (1992-1998), CIAT (2004-2006), UNEP-WCMC (1993), WWF (2004), Commonwealth of Australia (2007), and Her Royal Majesty and the British Crown and are used under license. The HydroSHEDS database and more information are available at http://www.hydrosheds.org.

data set [*Funk et al.(2015)*]. It covers the 50^{o}S–50^{o}N latitudinal band (and all longitudes), ranging from 1981 to near-present. The purpose of CHIRPS was to support the United States Agency for International Development Famine Early Warning Systems Network (FEWS NET) [*Funk et al.(2015)*]. In this work, we use 0.05^o spatial resolution and the monthly time resolution from 1 January 1981 to 31 December 2018 over Colombia (5^{o}S–15^{o}N and 80^{o}W–65^{o}W).

ENSO signal

To characterize the ENSO signal, we use the monthly Multivariate ENSO Index (MEI) version 2.0 (MEI.v2) [*Wolter and Timlin (1998)*, *Wolter and Timlin (2011)*]. Five variables enter into the definition of the index: sea level pressure, sea surface temperature, surface zonal winds, surface meridional winds, and Outgoing Longwave Radiation (OLR). The MEI.v2 uses observations of OLR from NOAA Climate Data Record, whereas the original MEI used observations based on the International Comprehensive Ocean-Atmosphere Data Set (ICOADS) cloud cover fraction data. MEI is a more reliable estimator of the ENSO state compared to other indices such as Nino3.4 (based only on sea surface temperatures) or SOI (based on sea-level pressures) [Rasmusson and Carpener (1982), Trenberth and Stepaniak (2001)]. Values of the MEI index greater (lesser) than +0.5 (-0.5) define the occurrence of El Niño (La Niña) events, whereas the remaining periods are neutral. We classified the information of precipitation according to El Niño and La Niña events. See details on the classification of events per year at the webpage https://www.esrl.noaa.gov/psd/enso/mei.

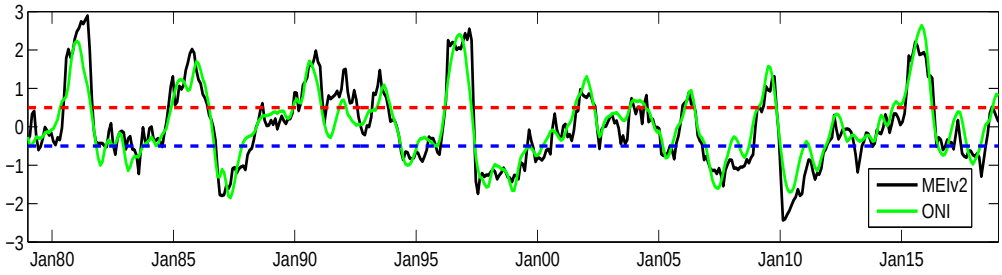

Figures 2-2.: Multivariate ENSO Index (MEI) version 2.0 (MEIv2) and the Oceanic Niño Index (ONI). (dashed red line) values above the 0.5 for warm (El Niño) events. (dashed blue line) values below the -0.5 for cold (La Niña) events.

Besides, we also use the Oceanic Niño Index (ONI), above the +0.5^{o}C threshold for warm (El Niño) events and at or below the -0.5^{o}C anomaly for cold (La Niña) events, in order to verify the consistency of our results https://psl.noaa.gov/data/correlation/oni.data. Figure **2-2** shows the MEIv2 and ONI indices while Table **2-1** shows El Niño and La Niña events according to the mentioned criteria.

2.4. Methods

We use five methods to estimate hydro-climatic anomalies (HyAns), which depend on the way the annual cycle is defined. In those methods, the main idea is to subtract the seasonal components from data to filter out the effect of the external solar forcing, common to all hydro-climatic time series, and define the intra-annual and inter-annual variability of the processes [*Wu and Huang*(2009)]. In this work, we calculate HyAns as,

Tables 2-1.: El Niño and La Niña events according to the classification mentioned in Section 2.3.1.

El Niño	**La Niña**
1976-77	1975-76
1977-78	1983-84
1979-80	1984-85
1982-83	1988-89
1986-87	1995-96
1987-88	1998-99
1991-92	1999-00
1994-95	2000-01
1997-98	2005-06
2002-03	2007-08
2004-05	2008-09
2006-07	2010-11
2009-10	2011-12
2014-15	2016-17
2015-16	2017-18

$$Y_{v,\tau}^{(j)} = \frac{X_{v,\tau} - AC_{v,\tau}^{(j)}}{\sigma_T}, \tag{2-1}$$

where $X_{v,\tau}$ denotes the original data for year v at the time interval τ (in our case τ=1 month). $AC_{v,\tau}^{(j)}$ indicates the annual cycle (or seasonal component) estimated by the method j. In this study, σ_T, the standard deviation of the original time series, is the scale factor. Thus, in Eq. (2-1), the HyAns, $Y_{v,\tau}$, are defined using the same scale factor and varying the technique to estimate the seasonal component. After that, we classify HyAns according to the extreme phases of ENSO (La Niña and El Niño), as mentioned in section 2.3.1.

2.4.1. Hydro-climatic anomalies using TAC (HyAns–TAC)

The most popular technique to extract the annual (and semi-annual) components from hydro-climatic data is by monthly standardization. It is defined as,

$$Y_{v,\tau} = \frac{X_{v,\tau} - \hat{\mu}_\tau}{\hat{\sigma}_\tau}, \;\; \tau = 1, 2, ..., 12 \;\text{ months}, \;\; v = 1, 2, ..., n \;\text{ years}. \tag{2-2}$$

Here, $\hat{\mu}_\tau$ and $\hat{\sigma}_\tau$ denote the estimates of the monthly mean (or Traditional Annual Cycle - TAC) and the monthly standard deviation, respectively [*Salas et al.(1980)*]. Eq.2-2 assumes

cycle-stationary and constant climatology [*Wu et al.*(2008)]. Besides, it leaves aside the non-linear character of the climate system, and therefore the response to a periodic incoming solar radiation could not be perfectly periodic [*Wu et al.*(2008)]. Finally, it does not remove all of the seasonal frequencies [Douglass (2015)].
This approach attempts to separate the forced and the free responses of the climate system. Then, the TAC method looks for removing the part of the time series that is forced by cyclo-stationary astronomical driving. Given that such forcing is cyclo-stationary, one assumes that its variability is entirely predictable. Therefore, although this attempt is valuable in predicting the unforced component, the assumption of a linear response might bias the analysis, measures, and skills of prediction of models.

2.4.2. Hydro-climatic anomalies using Fourier transform (HyAns–Fourier)

This well-known method for analysis of time series considers that a time series is the superposition of oscillations of different frequencies. In this sense, a time series $X_{v,\tau}$ is given by

$$X_{v,\tau} = \alpha_o + \sum_{k=1}^{N/2} \alpha_k cos(2\pi f_k t) + \beta_k sin(2\pi f_k t) + \xi_t; \qquad t = 1, 2, 3, ..., N, \tag{2-3}$$

where t denotes the time, $f_k = \frac{k}{N}$ denotes the frequency, k is the harmonic of the fundamental frequency, and N is the number of observations [*Hashyap and Ramachandra (1976)*]. The parameter $\alpha_o = \bar{X}_{v,\tau}$ is the mean of the time series, and α_k and β_k are

$$\alpha_k = \frac{2}{N} \sum_{t=1}^{N} X_{v,\tau} cos(2\pi f_k t) \qquad k = 1, 2, ..., N/2, \tag{2-4}$$

$$\beta_k = \frac{2}{N} \sum_{t=1}^{N} X_{v,\tau} sin(2\pi f_k t) \qquad k = 1, 2, ..., N/2. \tag{2-5}$$

For $k > N/2$, one considers a variance spectrum by decomposing the variance of the process into a number of frequency bands. The spectral density I_k is the amount of variance per frequency band f_k defined as,

$$I_k = \frac{N}{2} \left[\alpha_k^2 + \beta_k^2\right], \tag{2-6}$$

and the angular frequency is,

$$\omega_k = \frac{2\pi k}{N} \qquad k = 1, 2, ..., M. \tag{2-7}$$

The plot of ω_k vs. I_k is the spectrum. Its smooth representation is called *Power Spectrum*, where prominent spikes indicate periodicity and important contribution to the variance of

the process at frequencies close to the peak. The total area under the spectrum is equal to the variance of the process.
Using the prominent spikes of the spectrum, one can detect the natural frequencies f_k of the series. Then one can test the significance of the periodicity following a procedure described by [*Hashyap and Ramachandra (1976)*]. In our case, we need to test the significance of periodicity at semiannual (6 months) and annual (12 months) timescales, separately. Hence, we built each new time series S_k with significant seasonal periodicity as

$$S_k = \mu + \alpha_k cos(\omega_k t) + \beta_k sin(\omega_k t), \tag{2-8}$$

where k is the harmonic of the fundamental frequency at which data exhibit significant periodicity (associated with frequencies of 6 and 12 months) and μ is the mean of time series. Finally, we define the HyAns as,

$$Y_{v,\tau} = \frac{X_{v,\tau} - S_k}{\sigma_T}, \tag{2-9}$$

where $Y_{v,\tau}$ are the anomalies calculated by subtracting the seasonal frequency bands from the original time series and σ_T denotes the scale factor.

2.4.3. Hydro-climatic anomalies using F-Filtering (HyAns–FAC)

A moving average is a method to filter out the seasonal component of hydro-climatic time series from the inter-annual components [Douglass (2011), Douglass (2015)]. As first step, we calculate $\hat{X}_{v,\tau} = X_{v,\tau} - \mu$, μ denoting the overall mean. After that, we apply a 12-month filter to $\hat{X}_{v,\tau}$, such that if we represent the time series by $\left\{\hat{X}_{v,\tau}\right\}_{\tau=0}^{m}$, $m = 11$ for monthly series, then a two-sided moving average of the time series is given by,

$$\mathbf{F}(\hat{X}_{v,\tau}) = \frac{1}{2k} \sum_{j=-k}^{k-1} \hat{X}_{v^*,(\tau+j)^*},\ \tau = k, k+1, \ldots, m-k. \tag{2-10}$$

where $\mathbf{F}(\hat{X}_{v,\tau})$ is a filtered time series based on averages of the original time series, $\hat{X}_{v,\tau}$, $m+1$ indicates the total number of months, and k is a positive integer. Note that the denominator, $2k$, in Eq. (2-10) denotes the size of the average window (in our case $k = 6$, for a 12-month average window). For the sub-indices, $(\tau + j)^* = (\tau + j) \mathrm{mod}(m)$, and $v^* = v - 1$ if $\tau + j \leq 0$, or $v^* = v + 1$ if $\tau + j > m$, or $v^* = v$ in the other cases. The result is intended to be a season-free signal and the anomalies for this method are

$$Y_{v,\tau} = \frac{\mathbf{F}(\hat{X}_{v,\tau})}{\sigma_T}, \tag{2-11}$$

where $\mathbf{F}(\hat{X}_{v,\tau})$ is a low frequency signal without seasonal components. A high frequency signal that contains the seasonal and intra-seasonal frequencies and its harmonics is $\hat{X}_{v,\tau} -$

$\mathbf{F}(\hat{X}_{v,\tau})$. In Eq. 2-11, σ_T is the standard deviation of $X_{v,\tau}$. According to Douglass [Douglass (2011), Douglass (2015)], this filter has two important mathematical properties: (1) it is similar to a low-pass filter that allows frequencies lower than 1.0 cycle/yr to pass and, (2) the Fourier transform of $\mathbf{F}(\hat{X}_{v,\tau})$ contains a factor $H12(f) = sin(12\pi f)/sin(\pi f)$, which has zeros at multiples of the frequency [*Smith (1997)*] $f = (1/12)$ month^{-1}. Thus, both the components of $\mathbf{F}(\hat{X}_{v,\tau})$ whose frequencies are exactly $f = (1/12)$ month^{-1} and all its harmonics are completely removed.
In this work, we use a 12-month filter that is also denoted as "6-1-5" where "1" is the reference [Douglass (2011)]. Hence, we lost six data points at the beginning of the time series and five at end of the time-series. That is, in Eq. (2-10), $k = 6$ and $\tau \geq 6$. It is necessary to point out that the filtered signal $\mathbf{F}(\hat{X}_{v,\tau})$ is a displaced signal in relation to $\hat{X}_{v,\tau}$ but this can be corrected using lagged-cross Pearson correlations between $\mathbf{F}(\hat{X}_{v,\tau})$ and $\hat{X}_{v,\tau}$.

2.4.4. Hydro-climatic anomalies using Singular Spectrum Analysis (HyAns-SSAC)

The basis of Singular-Spectrum Analysis (SSA) is the Principal Component Analysis (PCA) in the vector space of delay coordinates for a time series [*Vautard et al.(1992)*]. The classical PCA is used with multi-channel time series and gives the principal axes of a sequence of M-dimensional vectors x_i $(1 \leq i \leq N)$, by expanding it according to an orthonormal basis $(E^k, 1 \leq k \leq M)$.

$$X_{ij} = \sum_{k=1}^{M} a_i^k E_j^k, 1 \leq j \leq M, \tag{2-12}$$

where the coefficients a_i^k are the *principal components* and the vectors E^k are the *empirical orthogonal functions*. The vectors E^k are the eigenvectors of the cross-covariance matrix of the sequence (X_i). For a scalar time series denoted by x_i, $1 \leq i \leq M$, an equivalent expansion is

$$x_{i+j} = \sum_{k=1}^{M} a_i^k E_j^k, 1 \leq j \leq M. \tag{2-13}$$

The analogy is made by augmenting the single time series x_i into the multi-variate time series $X_i = (x_{i+1}, x_{i+2}, ..., x_{i+M})$. Therefore, there is no formal difference between Eqs. 2-12 and 2-13 [*Vautard et al.(1992)*, *Ghil (2002)*]. In the latter, M is the *window length*, chosen by the user, in contrast with the classical PCA, where M is the fixed dimension of data vectors. As we shall see, SSA allows extracting information embedded in the delay-coordinate phase space by decomposing the sequence of augmented vectors into simple patterns of behavior, which one can classify into trends, oscillatory patterns, and noise [*Ghil (2002)*]. A

possible interpretation of SSA is a data-adaptive filter that decomposes the time series into components that are statistically independent at zero lag, with no use of prescribed waves (sines, cosines, or wavelets) as classical spectral analysis [*Vautard et al.(1992)*, *Ghil (2002)*]. In our case, we define $\hat{X}_{v,\tau} = X_{v,\tau} - \mu$, μ denoting the overall mean after SSA decomposition. After SSA processing, we define the standardized anomalies as,

$$Y_{v,\tau} = \frac{\hat{X}'_{v,\tau}}{\sigma_T}, \tag{2-14}$$

where $\hat{X}'_{v,\tau}$ is the reconstructed signal after SSA decomposition, with predominant frequencies at inter-annual timescales. σ_T is the scale factor, the standard deviation of $X_{v,\tau}$.

2.4.5. Hydro-climatic anomalies using MAC (HyAns–MAC)

Wu et al. [*Wu et al.*(2008)] propose a method to quantify time series anomalies based on Ensemble Empirical Mode Decomposition (EEMD) and the so-called Modulated Annual Cycle (MAC) [*Wu and Huang*(2009)]. This method consists of decomposing a signal in a set of Intrinsic Mode Functions (IFM), associated with different frequency bands, and consequently, to diverse physical oscillation modes. The IMF's containing the seasonal frequencies (i.e., annual and semiannual) constitute the MAC, subtracted from the original time series to obtain the anomalies. The rationale of this method comes from properties of non-linear dynamical systems, for which the response of a non-linear dynamical system, under an external periodical forcing, might not be perfectly periodic [*Wu et al.*(2008)]. Then, when the (non-linear) Earth climate system is excited by the seasonal solar incident radiation (SIR), most likely, such non-linearities prevent the response (the hydro-climatic variables) from being perfectly periodic [*Wu et al.*(2008)].

The Empirical Mode Decomposition (EMD) is an adaptive time-frequency data analysis method that does not require a priori functional basis because its basis functions are derived adaptively from data. This property of EMD allows its application to non-linear and non-stationary data. However, the adaptive advantage of EMD has as the price the difficulty of laying a firm theoretical foundation [*Huang and Shen (2005)*]. A summary of EMD is [*Huang et al.*(1998)]: (1) The extreme maximum and minimum values are identified in $x(t)$, (2) the maximal values are connected using a cubic spline to find an upper envelope, $U_{max}(t)$. A similar procedure is carried out to the minimal values resulting a lower envelope, $L_{min}(t)$, (3) the average value between $U_{max}(t)$ and $L_{min}(t)$ is calculated [i.e. $\bar{U}(t) = \frac{U_{max}(t) - L_{min}(t)}{2}$], (4) the time series $\bar{U}$ is subtracted from $x(t)$ [i.e. $d(t) = x(t) - \bar{U}(t)$], (5) the time series $d(t)$ is considered as the new $x(t)$ and the steps 1-4 are repeated until finding a signal with zero mean that constitutes the first IMF, (6) the IMF is subtracted from the original time series $x(t)$ and the procedure is repeated to obtain the next IMF, and (7) stop the iterative process when $d(t)$ has only a maximum or a minimum value, so it is not longer possible to extract more functions using $d(t)$.

However, after decomposing a signal into a set of IMFs by EMD, each IMF contains information at several frequency bands, making its physical interpretation difficult. To solve that problem, [*Wu and Huang*(2009)] proposed the EEMD method. A summary is (1) add a white noise series to the original data $x(t)$, (2) apply the EMD method to $x(t)$ with added noise to find the IMFs, (3) repeat steps (1) and (2) several times and, (4) calculate the (ensemble) mean for each IMF, until finding stable values of the IMF at an error level ϵ.
According to Wu and Huang [*Wu and Huang*(2009)], EEMD uses statistical properties of noise and the EMD method serves as a dyadic filter for various types of noise [*Flandrin et al.(2005)*, *Wu and Huang (2004)*], to enable the EMD method as a dyadic filter bank for any data. Then, the EEMD method largely eliminates the mode mixing problem and preserves the physical uniqueness of decomposition. In brief, the EEMD method works because the added white noise populates the whole time-frequency space uniformly with the constituting components of different scales. Then, when one adds the signal to this uniformly distributed white back-ground, its components are projected onto the reference scales established by the white noise. Hence, each trial may produce very noisy results, each EMD decomposition of the noise-added signal yields to IMFs, which contain information of the signal and the added white noise. Notwithstanding, while the noise in each trial is different in separate trials, it cancels out in the ensemble mean of enough trials. Therefore, as more and more trials go into the ensemble, the only persistent part is the signal [*Wu and Huang*(2009)].
Finally, denoting $\hat{X}'_{v,\tau}$ the summation of IMFs with predominant frequencies at inter-annual timescales, identified using Fourier spectral analysis (in our experiment), the standardized anomalies are

$$Y_{v,\tau} = \frac{\hat{X}'_{v,\tau}}{\sigma_T}, \tag{2-15}$$

where the $Y_{v,\tau}$'s are the standardized anomalies and σ_T is the standard deviation of $X_{v,\tau}$.

2.4.6. Pearson Correlations and Composite Analysis

Pearson linear correlations [*Pearson (1895)*] and composite analysis [*Terray et al.(2003)*, *Boschat et al.(2016)*] are two well-know methods to infer association between climatic variables. On the one hand, the Pearson cross-correlation coefficient for a time-lag τ quantifies the linear association between two time-series. Let X_t^i and Y_t^j two time-series in the locations i and j, then the τ-lag correlation coefficient $r_{X,Y}$ can be estimated as [*Salas et al.(1980)*],

$$r_{X,Y}(\tau) = \frac{\sum_{t=1}^{n-\tau}(X_t^i - \mu_t^i)(Y_{t+\tau}^i - \mu_{t+\tau}^i)}{\left[\sum_{t=1}^{n-\tau}(X_t^i - \mu_t^i)^2 \sum_{t=1}^{n-\tau}(Y_{t+\tau}^i - \mu_{t+\tau}^i)^2\right]^{1/2}}, \tag{2-16}$$

where $\tau = 0, 1, 2, ..., n$. For $i = j$, eqn. (3-16) is the temporal autocorrelation function (ACF).
On the other hand, the composite analysis is a tool to infer the relationships between different climate phenomena [*Terray et al.(2003)*, *Boschat et al.(2016)*, *Xie et al.(2017)*]. In general,

following Xie et al. [*Xie et al.(2017)*] to investigate the association between an index I and a field variable F, at first, we try to define some events, usually defined in terms of the index I. If I satisfies some criteria, the timings of those events constitute the key times. After that, we isolate the signal in the variable F corresponding to I by calculating the average of F in all key times. Finally, through statistical tests, we check whether there is a significant connection between those two variables or not [*Terray et al.(2003)*, *Boschat et al.(2016)*, *Xie et al.(2017)*]. In our experiment, we compare the average anomalies computed using the five different HA methods listed above, for El Niño and La Niña, to those estimated for neutral epochs (according to the classification described in section 2.3.1). Also, we test the null hypothesis of difference on average anomalies using the commonly-applied (parametric) Student's t-test [*Nicholls (2001)*] and also using a non-parametric test proposed by Terray et al. [*Terray et al.(2003)*].

2.4.7. k-sample tests based on likelihood ratio

In the vast set of methods to quantify differences between data sets, we select a powerful goodness-of-fit k-sample test, based on the likelihood ratio, in order to determine significant differences among probability distributions of rainfall anomalies obtained from the different HyAns methods. Let us denote as $Y_{v,\tau}^{(i)}$ and $Y_{v,\tau}^{(k)}$ the estimated anomalies through methods i and k, respectively. Then, it is possible to test the null hypothesis that $Y_{v,\tau}^{(i)}$ and $Y_{v,\tau}^{(k)}$ belong to the same probability distribution function using a two-sample test.

According to Zhang [*Zhang and Wu (2007)*], the new k-sample tests have two main advantages to more traditional tests (Kolmogorov-Smirnov, Anderson-Darling and, Cramér-von Mises). The first is that traditional tests are derived based on the chi-squared statistic (χ^2), whereas the new k-sample tests use the likelihood-ratio statistic. The second is that traditional tests are sensitive to location differences among distributions and are comparably less strong in detecting variations in shape, whereas k-sample tests are sensitive to both location and shape [*Zhang (2002)*, *Zhang and Wu (2007)*]. Finally, k-sample tests allow us to compare the probability distribution functions from the complete data sets instead of using metrics based on a unique statistic attributes such as mean absolute error (MAE), mean square error (MSE), root mean square error (RMSE), Minkowski distances (L_λ), among others. In this work, Z_K, Z_A and, Z_C denote the new k-sample Kolmogorov-Smirnov, Anderson-Darling and, Cramér-von Mises tests, respectively.

2.5. Results and Discussion

The following is a discussion about the spatial and temporal analysis of differences among the five methods to estimate hydro-climatic anomalies.

2.5.1. Spatial patterns of rainfall anomalies during ENSO at the national scale

Overall, the Andes, Caribbean, and Pacific regions exhibit negative (positive) rainfall anomalies during El Niño (La Niña). In contrast, the Amazon and Orinoco regions experience positive (negative) rainfall anomalies during the warm (cold) phase of ENSO [*Poveda et al.*(2011), *Bedoya-Soto et. al.*(2018), *Cai et al.(2020)*, *Salas et al.(2020)*]. Figure **2-3** suggests that the studied HyAns methods yield consistent results classifying anomalies in terms of their sign during both phases of ENSO. However, Fig. **2-3** also evidences that the methods are not consistent in the magnitude of rainfall anomalies although for all five HyAns methods we used the same scale factor. A couple of examples regarding the differences among the HyAns methods are (1) during La Niña, the HyAns–TAC, HyAns–Fourier, and HyAns–MAC methods exhibit high-positive anomalies in the Pacific region, whereas HyAns–FAC and HyAns–SSA show lower-positive anomalies in the same region (Fig. **2-3**, top row); (2) during El Niño, the HyAns–TAC, HyAns–Fourier, and HyAns–MAC methods exhibit high negative rainfall anomalies over the Pacific and Andes regions, whereas the other methods show lower negative rainfall anomalies (Fig. **2-4**, bottom panels).

Furthermore, we compare the spatial patterns of rainfall anomalies over the continental territory of Colombia using the five HyAns methods. To that end, we compare the cumulative probability distribution functions (CDFs) of the anomaly fields using the k-sample tests based on the likelihood ratio, at the 5% significance level. Our results indicate that: (1) During El Niño (Fig. **2-5** a), 70% (30%) of the study region experiences negative (positive) rainfall anomalies. All HyAns methods coincide with this feature. Moreover, the k-sample tests indicate that CDFs of HyAns–TAC and HyAns–Fourier are statistically equal, whereas the comparison among the CDFs of HyAns–FAC, HyAns–SSA and HyAns–MAC indicates that those produce statistically different results; (2) During La Niña (Fig. **2-5** b), 70% (30%) of the study region experiences positive (negative) rainfall anomalies, and all HyAns methods show this characteristic. Also, the k-sample tests indicate that CDFs of HyAns–TAC and HyAns–Fourier are statistically equal, whereas the statistical comparison among HyAns–FAC, HyAns–SSA and HyAns–MAC indicates that their CDFs are dissimilar.

A similar analysis was done using Dataset No. 2 (CHIRPS), Fig. **2-4** shows a good consistency with the results from Dataset No.1 over the regions that exhibit negative (positive) rainfall anomalies during El Niño (La Niña). Figure **2-5** (c-d) shows the CDFs for the CHIRPS dataset. k-sample tests indicate that CDFs of HyAns methods based on a constant annual cycle are similar (HyAns–TAC and HyAns–Fourier). In contrast, CDF's of HyAns methods based on a non-constant annual cycle differ from each other.

It is necessary to point out that the magnitude of rainfall anomalies could change significantly depending on the dataset used and the phase of ENSO (e.g., see Figure **2-5**b and Figure **2-5**d). Furthermore, the classification of the ENSO events using the MEI and ONI indices provide similar results in terms of the composite rainfall anomaly fields, which suggest that

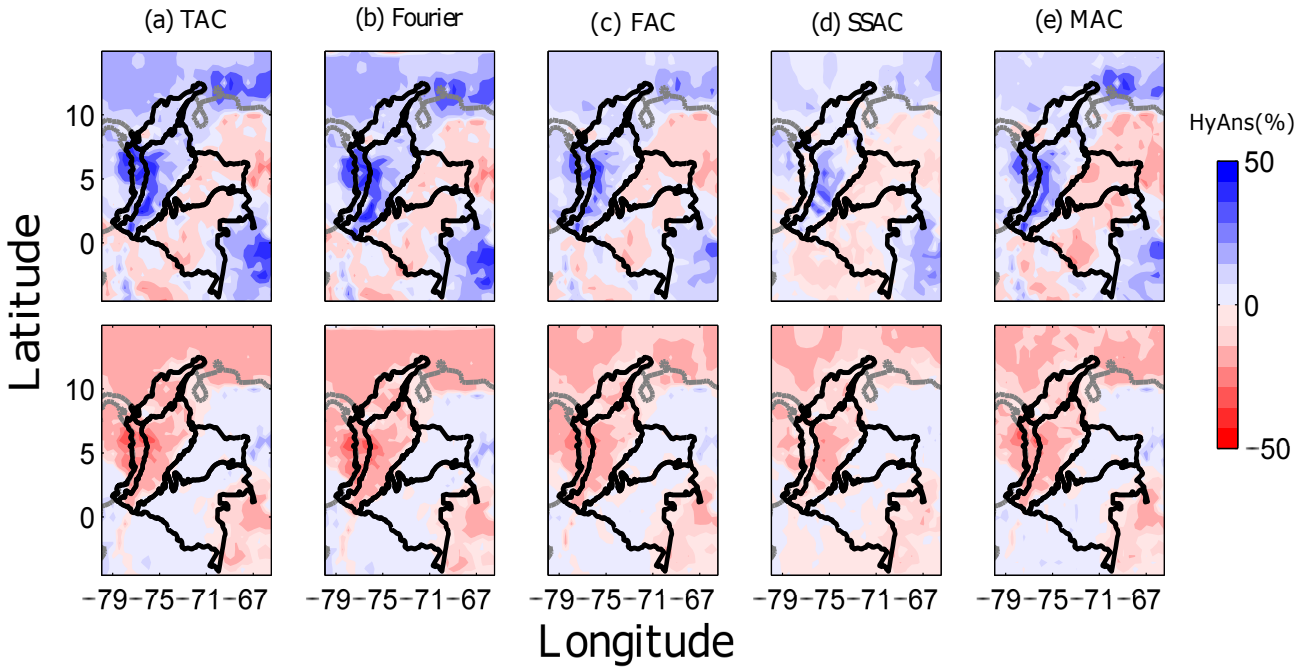

Figures 2-3.: Composite rainfall anomalies (HyAns) over Colombia (Dataset No. 1 – Hurtado-Montoya and Mesa (2014)), during ENSO, estimated by the five HyAns methods. (Top panels) HyAns during La Niña (LN). (Bottom panels) HyAns during El Niño (EN). (dark line) boundaries of the natural regions of Colombia. (gray line) northern South America boundaries of countries.

differences come from the HyAns methods of estimation (see Supplementary Information, Figures A-1 and A-2). It is remarkable that during El Niño (La Niña), k-sample tests over regions exhibiting only negative (positive) anomalies indicate that HyAns–FAC and HyAns–MAC have statistically similar CDFs. Our results reveal that composite HyAns fields calculated by different methods have significant statistical differences, although, at first glance, the differences seem to be minor.

2.5.2. Temporal patterns of rainfall anomalies during ENSO

First, we analyze the Cumulative Distribution Functions (CDFs) of monthly rainfall anomalies averaged across the five regions of Colombia. These analyses evidence that: (1) During La Niña (Fig. **2-6** top row), rainfall anomalies are 70% (30%) of the time positive (negative) in the Pacific, Andean and Caribbean regions whereas in the other regions are 70% (30%) of the time negative (positive); (2) During El Niño (Fig. **2-6** bottom row), rainfall anomalies are 70% (30%) of the time negative (positive) in the Pacific, Andean and Caribbean, whereas in the other regions are 70% (30%) of the time negative (positive). Moreover, for

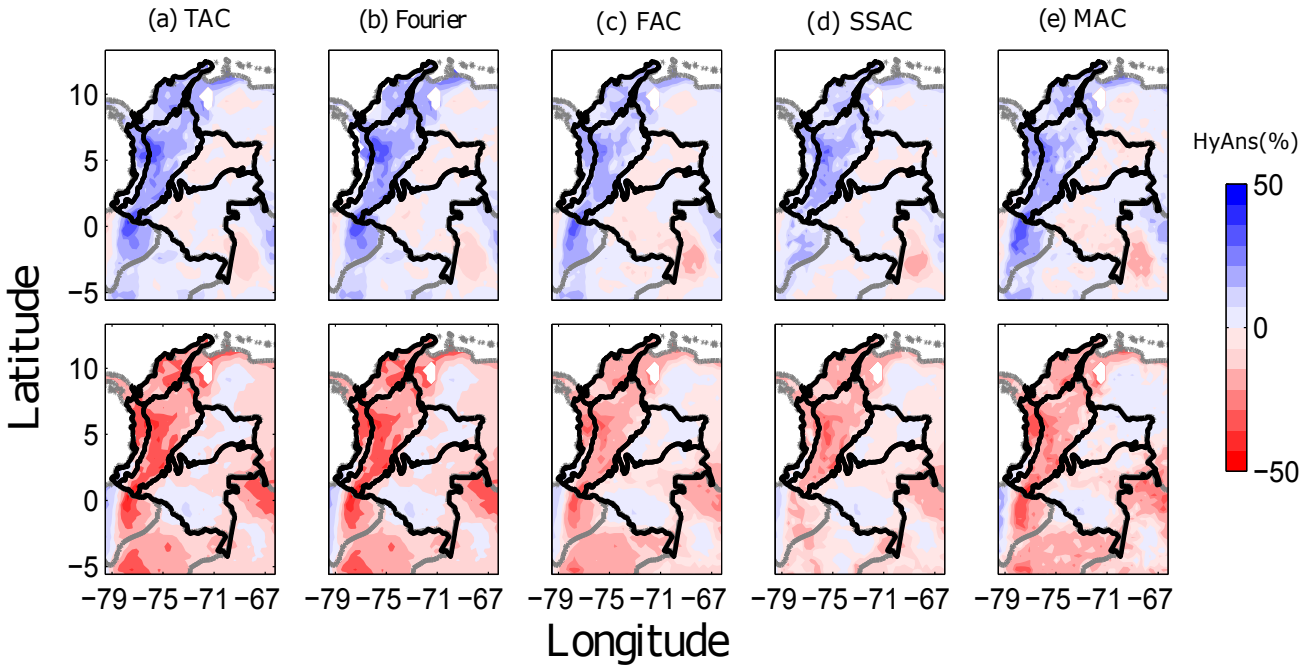

Figures 2-4.: Composite rainfall anomalies (HyAns) over Colombia (Dataset No. 2 – CHIRPS), during ENSO, estimated by the five HyAns methods. (Top panels) HyAns during La Niña (LN). (Bottom panels) HyAns during El Niño (EN). (dark line) boundaries of the natural regions of Colombia. (gray line) northern South America boundaries of countries.

both phases of ENSO, all k-sample tests at 0.05 significance level, suggest that CDFs of HyAns–TAC and HyAns–Fourier are similar. In contrast, the CDFs of the other HyAns methods are different to each other. Less rigorous k-sample tests, at the 0.10 significance level, indicate that HyAns–FAC and HyAns–MAC are similar in most cases. Those results show high sensibility in HyAns estimation depending on the method.

The autocorrelation functions (ACFs) in Fig **2-7** (top row) show that the HyAns–TAC and HyAns–Fourier rainfall anomalies exhibit a fast-decaying ACF. In contrast, the other HyAns methods show a slower decay. These mean that ACFs of HyAns methods based on a non-constant annual cycle (HyAns–FAC, HyAns–SSA and HyAns–MAC) are analogous. In contrast, the ACF of HyAns methods based on a constant climatology (HyAns–TAC and HyAns–Fourier) are different from those based on non-constant climatology. Regarding the power spectral density (PSD), Fig. **2-7** (bottom row) shows that HyAns–TAC and HyAns–Fourier are similar. Also, the PSDs exhibit significant differences among HyAns–FAC, HyAns–MAC and HyAns–SSA. Using the statistical test to detect significant periodic frequencies proposed by [*Ahdesmäki et al.(2005)*], one can demonstrate that HyAns–TAC and HyAns–Fourier leave significant residual frequencies at intra-annual and seasonal time

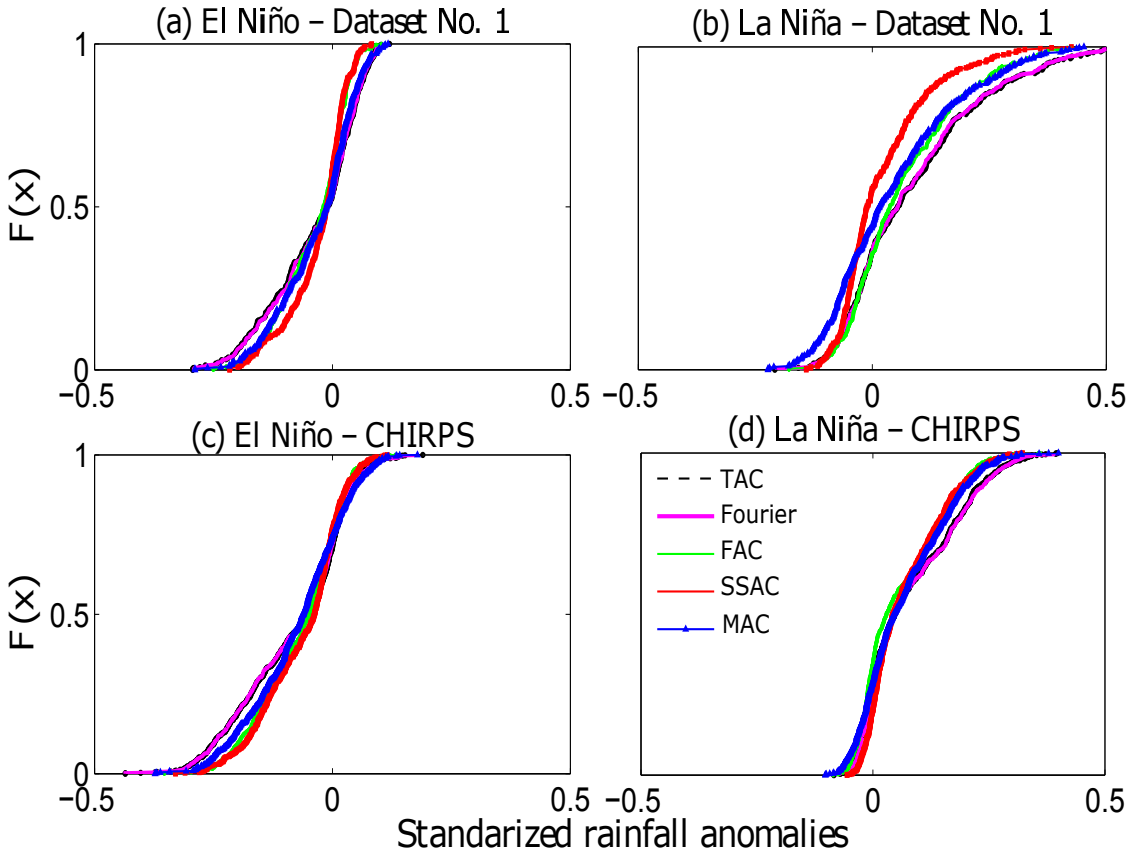

Figures 2-5.: Cumulative Distribution Functions (CDFs) of composite rainfall anomalies fields throughout the continental territory of Colombia, using diverse HyAns methods, during the extreme phases of ENSO (El Niño and La Niña). (a-b) CDFs using Data set No. 1. (c-d) CDFs using Data set No. 2 – CHIRPS.

scales, these residuals help explain the fast-decaying of ACF for these methods.
Moreover, the HyAns–SSA method mixes modes of variability with significant frequencies at intra-seasonal and seasonal time scales that are hard to link with physical processes (not shown). Meanwhile, the HyAns–FAC and HyAns–MAC methods allow removing the seasonal and intra-seasonal frequencies satisfactorily and contribute to attest to the reliability of the filtering to define inter-annual variability.

2.5.3. Repercussions of HyAns methods on Pearson correlation analysis between rainfall anomalies and the ENSO signal

The choice of the HyAns method has a substantial impact on the interdependence analysis and modeling of climate time series. In order to illustrate this we study the association between ENSO and rainfall anomalies over Colombia using a linear correlation analysis, which

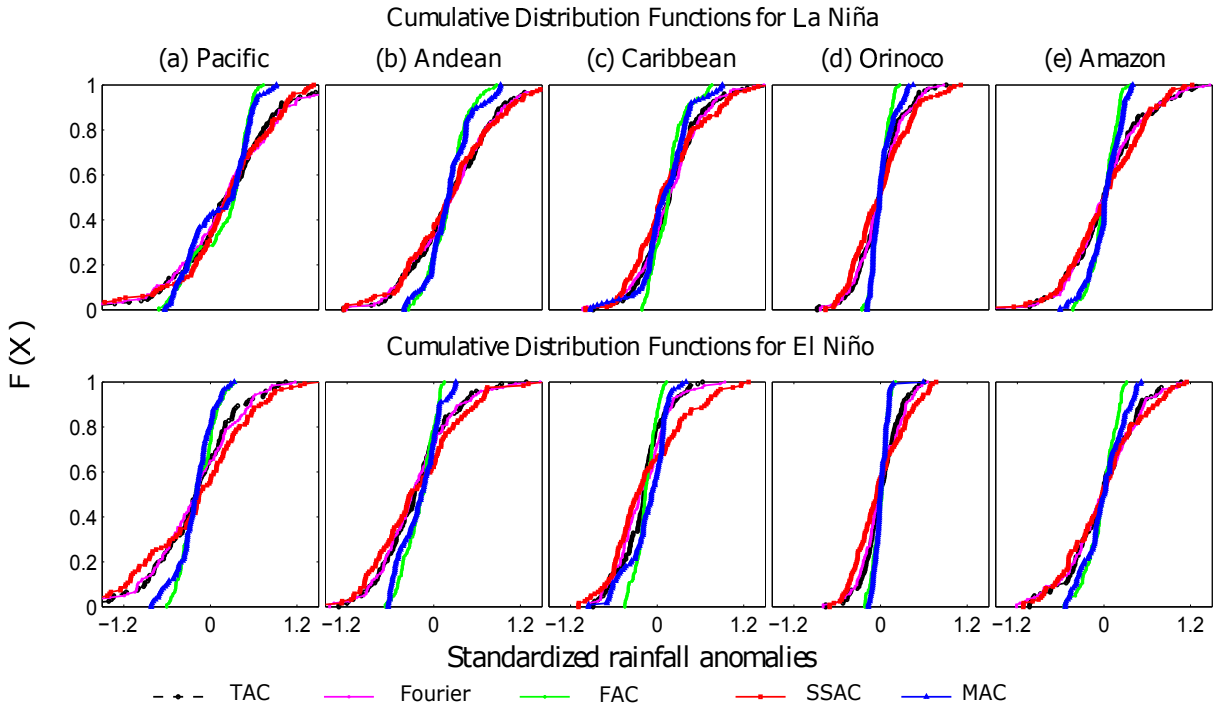

Figures 2-6.: Cumulative Distribution Functions (CDFs) of monthly rainfall anomalies (Dataset No. 2 –CHIRPS) averaged over the five regions of Colombia for La Niña (top row) and El Niño (bottom row). Each column denotes one of the Colombian regions.

is a well-known model to quantify the possible association between variables. Moreover, Pearson correlation has been used to investigate the relationship between ENSO indices and different hydro-climatic variables over Colombia (rainfall, streamflows, temperatures, vegetation indices, among others). Those investigations show significant linear correlations among the tropical Pacific Ocean dynamics and the land-atmosphere-ocean variability over northern South America [*Poveda and Mesa*(1997), *Poveda et al.*(2011), *Córdoba-Machado et al.*(2015), *Córdoba-Machado et al.*(2014), *Bedoya-Soto et. al.*(2018)].

In our experiment, we quantify the Pearson correlation coefficient r, between the MEI index and rainfall anomalies over Colombia and its statistical significance. To that end, we use 1200 monthly time series of rainfall, each one corresponding to a pixel of the rainfall fields for Colombia, spanning the period from 1975 to 2006 [*Hurtado and Mesa*(2014)]. For each time series, we estimate the anomalies using the HyAns methods based on constant and non-constant annual cycles. Then, we calculate r between the series of rainfall anomalies and the MEI index. Also, we test the null hypothesis of no relationship between the observed phenomena. If the p-value is smaller than the significance level (default is 0.05), the corresponding correlation is significant. In this sense, we find that significant r typically correspond to values higher than 0.50 or lower than -0.50.

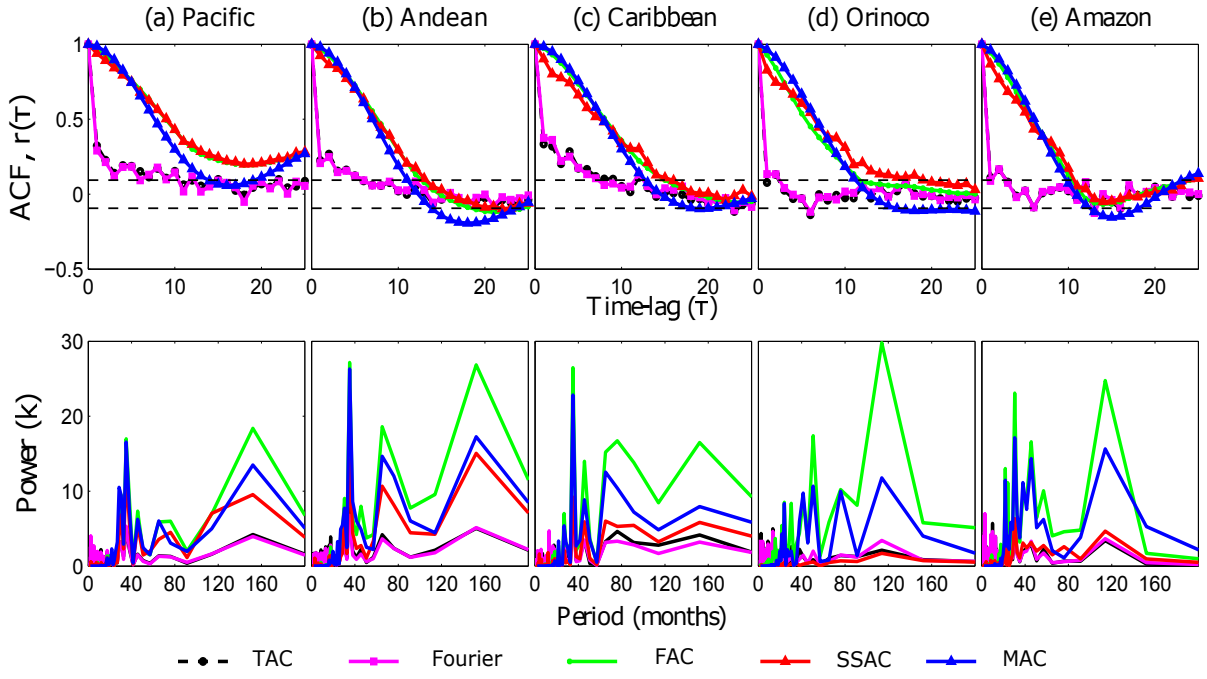

Figures 2-7.: Auto-correlation Functions, ACFs (top row) and Periodograms (bottom row) of monthly rainfall anomalies, spatially averaged over the five regions of Colombia using diverse HyAns methods.

In general, our results evidence that the Pearson correlation coefficients do not exhibit significant differences concerning the HyAns methods, when we use time series without classifying the data points according to the phases of ENSO. An explanation for those results is that 42% of the data points in the time series correspond to ENSO's neutral phase. In contrast, during the extreme phases of ENSO (El Niño and La Niña), maps of correlations exhibit significant differences with the HyAns methods (Fig.**2-8**). In such cases, Pearson correlations do not have a bias induced by neutral data points, where 41% (17%) of the data points correspond to El Niño (La Niña).

In particular, our findings allow us to conclude that: (1) the Andean, Pacific, and Caribbean regions of Colombia exhibit significant negative correlations, when we use the complete time series, for all HyAns methods as reported in several previous works [*Poveda and Mesa*(1997), *Poveda et al.*(2011)]. Furthermore, the Orinoco and Amazon regions show mainly non-significant correlations, although the HyAns–FAC and HyAns–MAC methods indicate some areas of positive significant r values (Fig.**2-8** top row). (2) During El Niño, the r-map using HyAns–TAC, HyAns–Fourier and HyAns–SSA suggest strong correlations across the Caribbean and western Colombia. In contrast, the r-map using HyAns–FAC and HyAns–MAC show a vast area of high significant r-values covering the continental territory

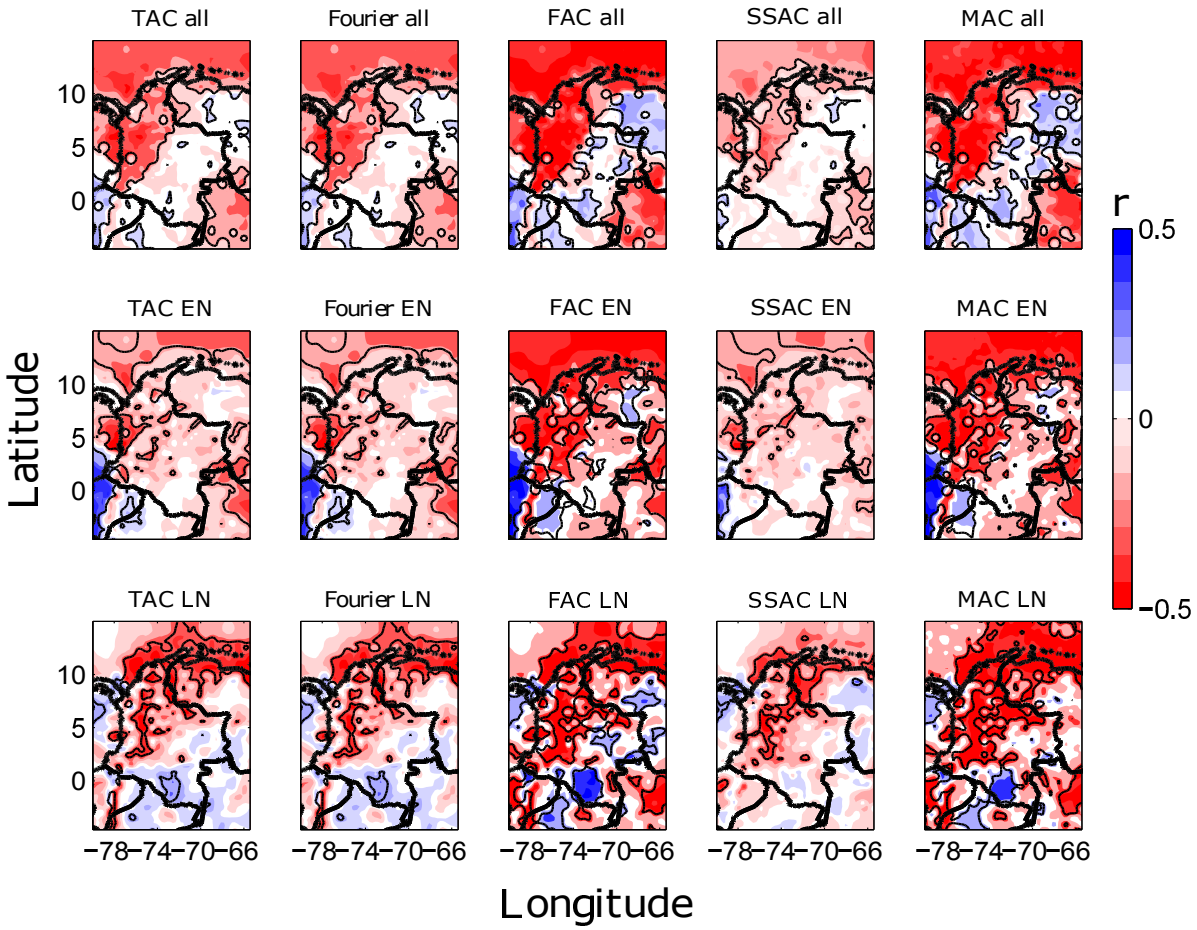

Figures 2-8.: Pearson Correlation, r, between the MEI index and rainfall anomalies over Colombia using diverse HyAns methods, each column denotes a HA method. (top row) r using complete time series without classification of data according to the ENSO phases. (middle row) r for the data points classified as El Niño (EN) following the MEI index. (bottom row) r for the data points classified as La Niña (LN) following the MEI index. (contour lines) Zones where the Pearson Correlation Coefficient, r, is significant at 5%.

of Colombia in the Pacific, Caribbean, and Andean regions, including the Caribbean sea zone in northern Colombia (Fig.**2-8** middle row). (3) During La Niña, the HyAns methods exhibit differences regarding the areas of r significance. r-maps using HyAns–TAC, HyAns–Fourier, and HyAns–SSA indicate smaller correlated areas over the country than r-maps using HyAns–FAC and HyAns–MAC. Besides, the r-map for most of the methods show high r-values covering the country to the north of 5^o N, whereas the r-map using HyAns–SSA suggests a weak connection towards the Caribbean Sea (Fig.**2-8** bottom row). (4) k-sample tests for datasets of significant r-values suggest equality of CDFs between methods based on

constant annual cycle as well as equality of CDFs among methods based on a non-constant annual cycle. Furthermore, there is a non-equality of CDFs in other cases (CDFs not shown here).

2.5.4. Implications of HyAns methods on Composite Analysis considering the phases of ENSO

We carry out a composite analysis to verify how HyAns methods affect the areas of the statistical significance of the composite fields. To this end, we compare the average anomalies for La Niña and El Niño phases in relation to the Neutral ones. We compare composite using the t-test (parametric) and the Terray's test (non-parametric). In general, our results reveal that the HyAns computed by the FAC and MAC methods include areas of statistical significance that the HyAns by TAC, Fourier, and SSA are not able to capture (see Figure **2-9**). Results are similar for both statistical tests and data sets (see Supplementary Information, Figures A-3 to A-6). Hence, these results show that the structure of composites can change significantly and requires a careful analysis of sensitivity regarding the estimation of anomalies. Boschat et al. [*Boschat et al.(2016)*] suggested that *"the message contained in the structure of composites may be quite misleading unless interpreted carefully, and that physical hypotheses framed from these need rigorous tests with appropriate tools"*. In this sense, our analysis allows us to conclude that the definition of anomalies plays a fundamental role in the adequate inference through composite analysis.

2.5.5. The role of the scale factor and the reference climatology on traditional HyAns

At this point, it is worth mentioning that the scale factor affects the interpretation of HyAns. For example, the American Meteorological Society (AMS) defines **climate anomaly** as "*the difference between the average climate over a period of several decades or more, and the climate during a particular month or season*" [*AMS(2015)*]. Such a definition implies that the scale factor is unity. At the same time, some well-known climate indexes are standardized (e.g., Southern Oscillation Index –SOI) and take as scale factor the standard deviation of each month [*NOAA(2018)*], which are the so-called standardized anomalies. Even though both cases consider constant climatology, the latter provides more information about the magnitude of the anomalies because they are in terms of the dispersion.

Both definitions above use the original time series, subtracting a base value from it. As we mentioned in 2.4.1, the monthly mean of data is the most used value. However, as discussed by Kawale et al. [*Kawale et al.(2011)*], the true theoretical mean is unknown, and most of the time, a short reference interval defines the reference climatology, typically, 30 years. Sometimes a shorter reference period can produce spurious results [*Kawale et al.(2011)*].

Then, the official definition of **climate anomaly** is different from the standardized climate

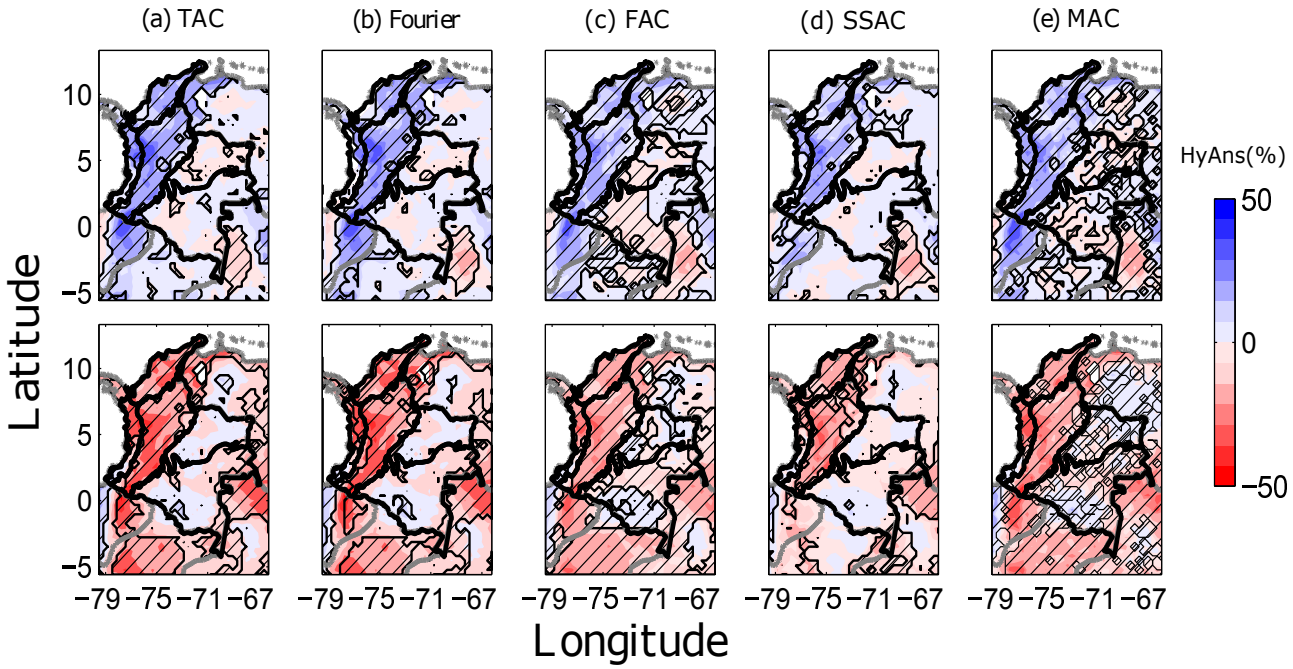

Figures 2-9.: Composite analysis for rainfall anomalies (Dataset No. 2; CHIRPS) showing the zones where mean anomalies for La Niña (top row) and El Niño (bottom row) are statistically different to the mean anomalies for the neutral phases of ENSO. (hatched lines) zones of statistically different mean values using the Terray's test [*Terray et al.(2003)*] at the 0.05 significance level.

anomaly that provides information on the magnitude of anomalies in terms of the dispersion of climate processes. Furthermore, the reference period is a subjective criterion that does not consider the non-stationarity and non-linear dynamics of Earth climate processes. Also, the most used definition of climate anomalies does not consider the behavior of hydro-climatic variables in response to climate change.

Our results evidence that HyAns methods based on constant and non-constant annual cycles can be strongly affected by the scale factor selected. In particular, the HyAns–Fourier method exhibits high anomaly values if the scale factor considers the seasonal dispersion of the climate time series.

2.6. Concluding Remarks

We study spatial and temporal patterns of hydro-climatic anomalies at interannual timescales throughout Colombia during ENSO's extreme phases. To that end, we use diverse HyAns methods that use constant and non-constant definitions of the seasonal variability or annual cycle: Traditional Annual Cycle (TAC), Fourier filtering of the annual cycle (Fourier),

filtering of the annual cycle by Moving Averages (FAC), annual cycle extracted by Singular Spectrum Analysis (SSA), and Modulated Annual Cycle (MAC). Our results unveil significant differences among time series of anomalies in terms of their: spatial patterns, magnitude, residual seasonal frequencies, the presence of noise, autocorrelations functions, spectral properties, and probability distribution functions.

Furthermore, we studied the influence of these HyAns methods to analyze interdependence among climate time series. We explored the relationship between ENSO and rainfall anomalies in Colombia using Pearson correlations. Our results evidence that the significant linear correlations might vary depending on the HyAns method and the phases of ENSO. For the composite analysis, our results allow us to conclude that the definition of anomalies plays a fundamental role in the proper inference of physical linkages through composites. Furthermore, the apparent minor differences in the HyAns estimation using diverse methods induce a significant error source and bias on the correlation analysis and modeling of climate time series. Moreover, these results evidence that data pre-processing for HyAns estimation requires verification of the adequate filtering of seasonal frequencies because some methods such as HyAns–TAC, HyAns–Fourier and HyAns–SSA do not remove satisfactorily such frequencies inducing differences in HyAns estimation and correlation metrics.

From these comparisons, for estimation of hydroclimatic anomalies at inter-annual timescale, we suggest using the filtering of the annual cycle using moving averages, here called HyAns–FAC because it (i) has a firm mathematical foundation, (ii) considers a varying climatology (annual cycle), (iii) adequately separates noise, intra-annual, seasonal and inter-annual components with (iv) not-significant residual seasonal frequencies in HyAns, (v) generates moderate extreme values of anomalies in comparison with the HyAns–SSA and HyAns–MAC methods, (vi) its autocorrelation function is comparable with HyAns–SSA and HyAns–MAC, and (vii) its computational cost is a one-tenth part of HyAns–SSA and hundreds of times less than HyAns–MAC.

Also, our results point out the need to quantify the uncertainty of HyAns in terms of magnitude, sign, timing, and phase of ENSO. It is also pertinent to revise the theoretical basis behind the diverse HyAns methods, not necessarily supported on physical grounds. Likewise, we discuss how the scale factor plays an essential role in the meaning of HyAns and how the period of the reference climatology affects HyAns estimations. e.g., climate reference varies depending on extreme phases of ENSO. On the other hand, HyAns can be affected by the datasets used, and hence we recommend to use different datasets in order to provide robustness to HyAns estimations.

Moreover, a large induced bias to correlation analysis of time series is a fundamental issue for future research, which needs consideration related to sophisticated non-linear methods reported in the literature. Likewise, it is essential to investigate the false "skill" in prediction models, whose input data contain a significant cyclo-stationary forced component. Our results evidence the need to tackle this fundamental overlooked problem regarding the effects of ENSO in hydroclimatic processes.

2.7. Acknowledgments

The work of H.D. Salas is supported by COLCIENCIAS – Grant for National Doctorates 617-2 and partially funded by the Humboldt University of Berlin IRTG 1740. The work of G. Poveda and O. J. Mesa is supported by Universidad Nacional de Colombia at Medellin. N.Boers acknowledges funding by the Alexander von Humboldt Foundation, the German Federal Ministry for Education and Research, and the German Science Foundation (DFG, Reference BO 4455/1-1). The work by J. Kurths is supported by PIK. We thank Profs. Brian Mapes (University of Miami) and David J. Raymond (New Mexico Tech) for their insightful comments and discussions. Thanks to: U.S. Geological Survey (USGS HydroSHEDS) for the Digital Elevation Models, NOAA for the ENSO index data and, A. F. Hurtado for reanalysis data of precipitation over Colombia.

3. Regional rainfall anomalies in Colombia and their association with ENSO: A phase synchronization approach

Hernán D. Salas, Germán Poveda, Óscar J. Mesa, and Jürgen Kurths

3.1. Abstract

We investigate Phase Synchronization (PS) between the El Niño - Southern Oscillation (ENSO) signal and the (inter-annual and annual) cycles of rainfall in Colombia. To that end, we carry out a detailed data analysis in order to define the annual cycle (AC), eliminating the seasonal residual frequencies in hydro-climatic anomalies (HyAns), assessing the statistical significance of PS metrics, and checking the sensitivity of the PS metrics in relation to diverse HyAns estimation methods. Then, we characterize the seasonal regional patterns of rainfall anomalies in relation to the ENSO's states. We find that the positive (negative) HyAns experienced in the Pacific, Caribbean and Andean regions of Colombia, during La Niña (El Niño), are phase-locked with the ENSO signal in the tropical Pacific Ocean, whereas the negative (positive) HyAns experienced in the Orinoco and Amazon regions, during La Niña (El Niño), do not show such phase-locking. Moreover, we provide evidence that the ENSO signal is phase-locked with the AC of rainfall in some regions of Colombia, which suggest that the AC plays an important role in the influence of ENSO on Colombian climatology and opens new paths towards the understanding of non-linear feedbacks between hydro-climatic processes. Our results show that, at inter-annual timescales, ENSO exhibits the strongest phase-locking with the annual and inter-annual cycles of rainfall throughout Colombia, although other macro-climatic processes also show significant PS such as the Pacific Decadal Oscillation (PDO) and the North Atlantic Oscillation (NAO). Moreover, we show that the highest positive (negative) rainfall anomalies over western Colombia coincide with the strong (weak) PS between the ENSO and the PDO signals. This work provides new evidence on the non-linear interactions between hydro-climatic processes in Colombia and

ENSO, and constitute an unexplored approach to the understanding of climatic anomalies in tropical South America.

3.2. Introduction

The hydro-climatic variability of Colombia is influenced by a suit of periodic and quasi-periodic processes acting on a wide range of time scales such as: the diurnal cycle of solar radiation and temperature (DC), tropical easterly waves (TEW), the Madden-Julian Oscillation (MJO), the annual cycle of solar radiation (AC), the Quasi-Biennal Oscillation (QBO), the El Niño-Southern Oscillation (ENSO), the Pacific Decadal Oscillation (PDO), the North-Atlantic Oscillation (NAO) and, the Atlantic Multidecadal Oscillation (AMO) [*Poveda and Mesa*(1997), *Poveda et al.*(2001), *Poveda et al.*(2002), *Poveda et al.*(2004), *Poveda et al.*(2005), *Poveda et al.*(2011)]. In this work, we aim to explore the non-linear interactions between the occurrence of ENSO over the tropical Pacific Ocean and the AC and rainfall anomalies (HyAns) in Colombia based upon the following arguments and observations.

First, there is a tendency in the scientific literature to disregard the importance of the annual cycle inherent in monthly the hydro-climate records, given that it explains the largest amount of variability. The AC is taken for granted and therefore most analysis are focused on the study of anomalies with respect to the annual cycle [*Wu et al.*(2008)]. Such an approach assumes that the hydro-climate variables have a constant response to the periodic incoming solar radiation (SR), disregarding the non-linear interactions of the Earth's climate system, while at the same time overlooking important interactions between the AC of hydro-climatic processes and other climatic processes at inter-annual timescales.

Second, in Chapter 2 was evidenced that HyAns can be defined through different methods, among them: *(i)* the Traditional Annual Cycle or constant climatology (HyAns–TAC), *(ii)* **F**-filtering of the Annual cycle by moving average (HyAns–FAC), *(iii)* Annual cycle extracted by Singular Spectrum Analysis (HyAns–SSAC) and, *(iv)* the Modulated Annual Cycle, which is based on the EEMD technique. Furthermore, the quantification of interdependence between climate time series during ENSO, at inter-annual timescales, can be biased due to: (i) the presence of a seasonal significant residual in time series of anomalies, (ii) the definition of constant or non-constant annual cycle, and (iii) the presence of high-frequencies (intra-annual variability and noise) in HyAns time series (see Chapter 2). Moreover, HyAns estimation techniques affect interdependence quantification, which leaves room for ambiguity in the physical interpretation of results (see Chapter 2). Hence, we point out the need to study the sensitivity of the linear and non-linear interdependence quantification techniques in relation to diverse HyAns methods.

Third, ENSO is one of the main controlling mechanisms of Earth's climate at inter-annual time scales. It is a conjoint process between *El Niño* (EN, oceanic component) and the *Southern Oscillation* (SO, atmospheric component). El Niño refers to the anomalous warming of the central and eastern waters of the tropical Pacific Ocean, which produces a deepening of

the oceanic's thermocline, concomitant with the weakening and (sometimes) reversal of the trade winds and the displacement of the core of convection from the western to the central and eastern regions of the tropical Pacific. The SO is a stationary wave that produces an atmospheric pressure see-saw between the western and eastern equatorial Pacific [*Sarachik and Cane*(2010)]. Recent works by [*Stein et al.*(2011), *Stein et al.*(2014)] have provided evidence of phase-locking between the AC of SSTs and the ENSO signal in the tropical Pacific Ocean using synchronization techniques. However, no study has used a similar approach to investigate the interrelations between ENSO and the AC of hydro-climatic variables in other regions. i.e northern South America. In particular, during the ENSO cold (warm) state, positive (negative) anomalies in rainfall and streamflows are experienced overall in Colombia, those causing extreme hydro-climatic events with important socio-economical, environmental and ecological impacts. Therefore, a better understanding of the influence of ENSO on Colombian hydro-climatic variability is fundamental to improve the diagnosis, modeling and forecasting of extreme hydro-climatic events [*Poveda and Mesa*(1997), *Poveda et al.*(2001), *Poveda et al.*(2011)].

Fourth, solar radiation (SR) is a periodic forcing on the Earth's non-linear climate system. In response to such periodic forcing the hydro-climatic variables contain a strong annual cycle (AC) signature which represents a high percentage of their variance. In the case of rainfall in Colombia, the AC exhibits an uni-modal and bi-modal behavior depending on the location in the country. For the most part, a bimodal annual cycle of rainfall is restricted to the Andean region of Colombia, while unimodality is witnessed off the Andes, with maximum rainfall associated with a shift of the ITCZ over Colombia [*Poveda et al.*(2015), *Urrea et al.*(2018)]. Bi-modality can be explained by the periodic forcing of the incoming SR which occurs twice each year, but uni-modality is observed also in areas where the periodic forcing of SR occurs twice each year. According to [*Hoyos et al.*(2017)], the Intertropical Convergence Zone (ITCZ) over the Orinoco and Amazon regions advances slower than over the rest of the country producing a unimodal convergence of moisture which contributes to explain the unimodaly in precipitation. Notwithstanding, physical processes involved in the AC of rainfall have not been satisfactory explained [*Urrea et al.*(2018)].

Finally, there is evidence of the interdependence between hydro-climatic variables of Colombia and the Pacific ocean-atmospheric dynamics at ENSO timescales [*Poveda et al.*(2001), *Waylen and Poveda*(2002), *Poveda et al.*(2011), *Bedoya-Soto and Poveda*(2017), *Bedoya-Soto et. al.*(2018)]. However, such interdependence has been studied by means of linear or non-linear statistical tools, while ignoring *the interaction between the oscillations* under the assumption that physical phenomena are generated by multiple oscillatory interacting systems or *synchronization* in the sense of [*Pikovsky et al.*(2001)]. Diverse types of synchronization are known, such as frequency synchronization (FS), phase synchronization (PS), identical synchronization (IS), generalized synchronization (GS) and lag synchronization (LS) [*Brown and Kocarev*(2000)]. In particular, for two oscillatory systems X and Y, PS (or phase-locking) means that the instantaneous phases of X, $\phi_x(t)$, are related to the instantaneous

phases of Y, $\phi_y(t)$. If $|n_x\phi_x - m_y\phi_y| < c$, where n_x and m_y are natural integers, and c is a constant, both systems are in $n_x : m_y$ PS. In contrast, FS means a link between the frequencies such that if $|n_x\omega_x - m_y\omega_y| < c$, where n_x and m_y are natural integers and, c is a constant, both systems are in FS. Thereafter, PS implies FS but FS does not imply PS. In addition, the PS approach does not include either the interrelation between the amplitudes or control mechanisms such as Amplitude Modulation (AM), but the adequate characterization, quantification and explanation of the phases is valuable even if the amplitude interrelations are not well known [*Von Storch et al.*(1995)].

Hence, we aim to investigate the characteristics of PS between ENSO (system 1) and the (annual and inter-annual) cycles of rainfall in Colombia (system 2). Our goal is to characterize and quantify temporal and spatial PS patterns between both systems during La Niña and El Niño. Hypothetically, we consider that ENSO is the driver system and that rainfall in Colombia is the response system (the influenced system). To those ends, we use a set of non-linear and non-stationary data analysis techniques such as Ensemble Empirical Mode Decomposition (EEMD), Generalized Phase Difference (GPD), diverse HyAns estimation methods and an index that provides a measure of the strength of phase synchronization (SPS) between both systems. The existence of a phase relation implies the possibility to predict the phases of the Colombian hydrology through ENSO [*Shiff et al.*(1996)].

The purpose of this study is manifold, in particular: (i) to characterize the seasonal regional patterns of hydro-climatic anomalies in Colombia during El Niño and La Niña, (ii) to provide evidence of PS between the ENSO signal in the tropical Pacific Ocean and the annual and inter-annual variability of rainfall in the Colombia and, (iii) to investigate PS features between diverse macro-climatic processes and rainfall in Colombia during ENSO. This will allow improvements in diagnosis, understanding and management of water resources for socio-economical, environmental and ecological purposes in Colombia.

This work is organized as follows: section 3.3 presents the region of study; the hydro-climatic data sets are described in section 3.4, while the EEMD, GPD, SPS, and HyAns methods are presented in section 4.4. Finally, our results are discussed in section 4.5 and the conclusions are drawn in section 3.7.

3.3. Region of study

3.3.1. Natural regions of Colombia

As explained in Chapter 1, the continental territory of Colombia can be divided into five main natural regions (Fig. **3-1**) with different hydro-climatological, geomorphological and bio-ecological characteristics due to the influence of diverse geographical features and processes at different spatial and temporal scales.

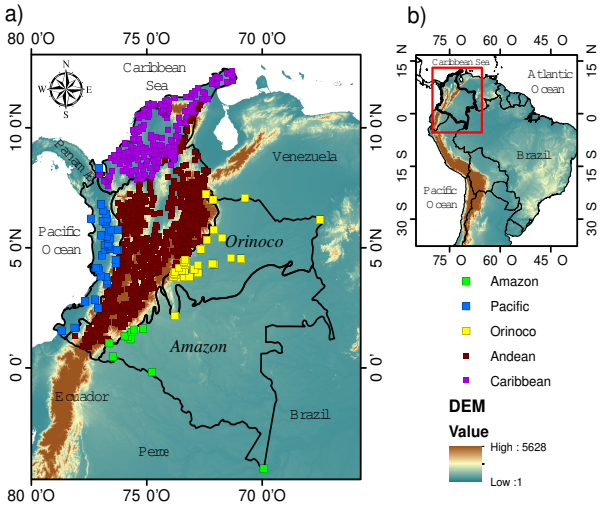

Figures 3-1.: Location of the region of study. (a) National context including the Colombian Natural Regions [IGAC, 2002] and rain gauges from IDEAM. (b) Continental context.

3.4. Data sets

3.4.1. SSTs in the tropical Pacific Ocean and the ENSO signal

We use the monthly Extended Reconstructed Sea Surface Temperatures (ERSSTv5) in the Niño 3.4 region (5^o N–5^o S and 170–120^o W) as well as Extreme Eastern Tropical Pacific SST or the Nino 1+2 zone (0^o–10^oS and 90^oW–80^oW). Details in https://www.cpc.ncep.noaa.gov. In addition, we use the monthly multivariate ENSO index (MEI) to classify the ENSO events, as explained in Chapter 2. Precipitation records were classified according to El Niño and La Niña months, as per the MEI definition. See details in Tables B-1 and B-2 (Suppl. Info.).

3.4.2. Colombian Precipitation datasets

*Dataset 1:*We use data from a reanalysis performed by [*Hurtado and Mesa*(2014)], which produced monthly precipitation fields for Colombia, spanning the period from 1975 to 2006, at a spatial resolution of 5 minutes of arc, in the region 5^oS–15^oN and 80^oW–65^oW. [*Hurtado and Mesa*(2014)] by using a set of 2270 rain gauges from diverse institutions including Instituto de Hidrología, Meteorología y Estudios Ambientales de Colombia (IDEAM), Empresas Públicas de Medellín (EPM), Centro Nacional de Investigaciones del Café (CENICAFE) and The Global Historical Climatology Network (GHCN). In addition, they also used satellite images from the Global Precipitation Climatology Project(GPCP)-V2, National Centers for Environmental Prediction (NCEP)/National Center for Atmospheric Research (NCAR), Tropical Rainfall Measuring Mission (TRMM), and the Geostationary Satellite System (GOES). Finally, the monthly precipitation fields resulted from a combination of the available data and

the implementation of the PRISM model in the Colombian territory (see details in [*Hurtado and Mesa*(2014)]).

Dataset 2: We use a set of 937 rain gauges from IDEAM, at monthly timescale, having record lengths of 40 years, for the period 1976-2015, with less than 10% missing values. The geographical distribution of this data set is as follows: 38 time series for the Pacific, 631 in the Andean, 228 in the Caribbean, 30 in the Orinoco, and 10 in the Amazon region.

3.4.3. Other Macro-climatic Indices

We included further macro-climatic indices data, which are related to processes different from the ENSO system, namely: the `Tropical Northern Atlantic Index` (TNA), which consist of anomaly of the average of the monthly SST from 5.5^{o}N to 23.5^{o}N and 15^{o}W to 57.5^{o}W [*Enfield, et al.*(1999)], the `Tropical Southern Atlantic Index` (TSA) that contains the monthly average SST anomaly from Eq-20^{o}S and 10^{o}E-30^{o}W [*Enfield, et al.*(1999)], `North Atlantic Oscillation` (NAO) from NOAA Climate Prediction Center (CPC), available in https://www.cpc.ncep.noaa.gov. `Pacific Decadal Oscillation` (PDO), which is the leading PC of monthly SST anomalies in the North Pacific Ocean [*Zhang et al.*(1997),*Mantua*(2002)], `Atlantic multidecadal Oscillation` (AMO), which is calculated using is the Kalplan SST over the northern Atlantic, 0 to 70^{o}N [*Enfield, et al.*(2001)], and `Atlantic Meridional Mode` (AMM), which is defined via applying the Maximum Covariance Analysis to SST and the zonal and meridional components of the 10m wind field over the region (21^{o}S-32^{o}N, 74^{o}W-15^{o}E) [*Chiang and Vimont*(2004)].

These macro-climatic indices data were provided by NOAA Earth System Research Laboratory, freely available on https://www.esrl.noaa.gov/psd/data/climateindices/list/.

3.4.4. Reanalysis

We use data from the ERA5 atmospheric reanalysis [*Hersbach et al.*(2019)], which provides estimates of a large number of atmospheric, land and oceanic climate variables. The ERA5 data covers the Earth on a 30km grid and resolve the atmosphere using 137 levels from the surface up to a height of 80km. In particular, we use a spatial domain over Colombia (10^{o}S–20^{o}N and 85^{o}W–50^{o}W) for variables such as: monthly wind speed at pressure levels from 925hPa, vertically integrated moisture divergence, specific humidity, and vertical integrated water vapour fluxes (northward/eastward).

3.5. Methods

3.5.1. Generalized Phase Difference (GPD)

Theoretically, the GPD method was derived basing on physical properties of coupled oscillatory systems [*Rosenblum et al.*(2001)] (details in Appendix A). In practice, according to [*Pikovsky et al.*(2001)], the presence of a horizontal plateau in the phase difference vs. time diagram is the simplest way to evidence synchronization. In general, for two time series $x(t)$ and $y(t)$, their instantaneous phases $\phi_x(t)$ and $\phi_y(t)$, can be estimated using the analytic signal method expressed as [$Gabor(1946), Panter(1965)$],

$$Z_x(t) = x(t) + i\tilde{x}(t) = A_x^H e^{i\phi_x^H(t)} \tag{3-1}$$

where $\tilde{x}$ is the Hilbert transform (HT) of $x(t)$ defined as,

$$\tilde{x}(t) = \frac{1}{\pi}\text{p.v.}\int_{-\infty}^{\infty}\frac{x(t')}{t-t'}dt' \tag{3-2}$$

where p.v denotes the Cauchy's principal value.
From $Z_x(t)$ it is possible to calculate the instantaneous phase $\phi_x(t)$ as,

$$\phi_x^H(t) = \arctan\frac{Im(Z_x)}{Re(Z_x)}; \tag{3-3}$$

The instantaneous phase of $y(t)$, $\phi_y(t)$, can be calculated using a similar procedure. It is worth noting that HT is a non-parametric method and that the estimation of $\phi_x(t)$ and $\phi_y(t)$ based on the analytic signal (Eq. 3-1) is comparable with a technique based on wavelets [*Le Van Quyen et al.*(2001)].
Finally, denoting $\phi_x^H(t) = \phi_x$ and $\phi_y^H(t) = \phi_y$, the GPD can be expressed as,

$$\phi_{n,m} = n\phi_x - m\phi_y, \tag{3-4}$$

which in turn allows defining that $n : m$ *phase locking* appears if,

$$|\phi_{n,m} - s| < c, \tag{3-5}$$

where $c < 2\pi$ and s is the average phase between the two time series $x(t)$ and $y(t)$ [*Rosenblum et al.*(2001)]. However, for noisy oscillators or time series with oscillations at several frequency bands, the phase difference $\phi_{n,m}$ is unbounded due to phase jumps and the condition (Eq. 3-5) is not valid anymore. Nevertheless, the probability mass distribution of the *cyclic relative phase*

$$\Phi_{n,m} = \phi_{n,m}\texttt{mod}(2\pi) \tag{3-6}$$

has a dominating peak around a preferential value indicating phase synchronization in a statistical sense [*Rosenblum et al.*(2001)]. A stable phase locking in a ratio $n : m$ means n cycles of the oscillator x and m cycles of the oscillator y.
Hence, on the one hand, the GPD method has advantages such as: *(1)* the phase analysis allows, by means of $\phi_{n,m}$ plots, to trace transitions between qualitatively different regimes that are due to nonstationarity in the parameters of interacting systems and/or coupling and, *(2)* it is possible to apply this method even to very short records. On the other hand, the method has disadvantages such as: *(1)* the synchronous regimes of order different from $n : m$ shows nonsynchrony, *(2)* there are no straightforward methods to determine the integers n and m, so that they need to be identified by trial and error and, *(3)* if noise is relatively strong, this method becomes ineffective and may even be misleading [*Pikovsky et al.*(2001)].

3.5.2. Synchronization metrics

Strength of Phase Synchronization (SPS)

Although several *n:m synchronization indices* have been proposed in the literature (e.g. [*Rosenblum et al.*(2001)]), we use an index as measure of phase synchronization defined as,

$$\chi_t = \left|\left\langle e^{i(n\phi_x - m\phi_y)}\right\rangle_t\right| \tag{3-7}$$

The notation $\langle\cdot\rangle$ indicates temporal averaging. The index χ_t varies from 0 to 1, $\chi = 0$ indicates that the phases of the two time series are completely independent, while $\chi = 1$ indicates perfect phase synchronization [*Rosenblum et al.*(2001), *Stein et al.*(2014)].
In order to analyze the evolution of χ throughout the year, we calculate the long-term average of χ for each quarter.

3.5.3. Phase-Lag estimator

In classical time series analysis, the cross-correlation function is a well known linear technique to quantify the time-lag association between two time series. In phase synchronization analysis, lag synchronization occurs, when the phases of two interacting systems nearly coincide if one is shifted in time. To quantify the *lag*, we propose a function based on SPS as,

$$\chi(\tau) = \left|\left\langle e^{i\phi_{n,m}(\tau)}\right\rangle\right|, \tag{3-8}$$

where τ is the time-lag and $\phi_{n,m}\,(\tau)$ is the phase difference between the instantaneous phases $\phi_x(t-\tau)$ and $\phi_y(t)$, i.e. the GPD defined as $\phi_{n,m}(\tau) = n\phi_x(t-\tau) - m\phi_y(t)$, being x the ENSO signal and y a hydrological variable. The index $\chi(\tau)$ also varies from 0 to 1, with $\chi(\tau) = 0$ indicating non-synchronization and $\chi(\tau) = 1$ perfect phase synchronization.

3.5.4. Decomposition method

In the literature have been reported diverse techniques to decompose time series into its elementary patterns of behavior such as trends, oscillatory patterns, and noise [*Ghil et al.*(2001)]. In Chapter 2 was heightened the need for appropriate procedures of deseasonalization of time series. In such a work, the authors propose the F-filtering of the annual cycle (FAC) by moving averages (hereafter HyAns–FAC) as an adequate method to filter out the seasonal frequencies and their harmonics from the original climatic time series. Notwithstanding, the HyAns–FAC method allows decomposing a time series into two frequency bands: *(i)* noise, intra-annual and seasonal components and *(ii)* inter-annual frequencies. Here, we require a technique that allow us to decompose climate time series, at least, into three frequency bands: *(i)* seasonal components (or annual cycle), *(ii)* inter-annual variability, and *(iii)* intra-annual variability (high-frequency band) and noise. Hence, the EEMD method meets mentioned requirements and furthermore it has four similar properties to the HyAns–FAC method (see Chapter 2): *(i)* non-constant annual cycle, *(ii)* adequate separation of high and inter-annual frequencies, *(iii)* no-significant residual seasonal frequencies in anomalies and, *(iv)* the magnitude of extreme values of anomalies in a middle range compared with the other HyAns methods.
The EMD method has become a common and powerful tool in geophysical time series analysis [*Huang et al.*(1998), *Wu et al.*(2008), *Huang and Wu*(2008), *Wang et al.*(2015)]. EMD is useful to decompose non-linear and non-stationary time series into a set of Intrinsic Mode Functions (IMFs), which are extracted through an iterative, adaptive and temporally local procedure that does not force the data $x(t)$ to prescribed waves as traditional decomposition methods (e.i. sinusoidal waves or wavelets) [*Ghil et al.*(2001)]. However, the EMD method has a problem, it is not easy to associate physical variability modes to the IMFs because each IMF contains information in different frequency bands [*Wu et al.*(2008), *Rato et al.*(2008)]. To face up this "mode mixing" problem, [*Wu and Huang*(2005), *Wu and Huang*(2009)] proposed the EEMD allowing to decompose the original time series data, $x(t)$, into a set of IMFs exhibiting scale-consistent oscillation features. A brief summary of EMD and EEMD is presented in Appendix B.

3.5.5. Significance Tests

In this study, we apply two different statistical significance tests. The first significance test was proposed by [*Ahdesmäki, et al.*(2005)] as a robust method for detection of periodicities in time series. In our case, such a method allows us to guarantee that after decomposing of the hydrological time series into different frequency bands using EEMD: *(i)* the frequency band containing information at inter-annual timescales (hydro-climatic anomalies or HyAns) has no-significant seasonal residual and, *(ii)* the frequency band containing information at seasonal timescales (annual cycle) is adequately separated from the noise and inter-annual frequency bands. This procedure is necessary because the PS technique can be highly biased

by the presence of seasonal residual frequencies in anomalies (not shown here).
The second significance test is necessary to determine if the synchronization metrics are statistically significant. That means, we need to check if the strength of phase synchronization (see section 3.5.2) between X (the ENSO signal) and Y (the hydrological variable in Colombia) is a robust result. Hence, we develop a significance test for Phase Synchronization based on permutations, which is presented next.

Significance test for Phase Synchronization

Our study requires implementing a statistical test for the hypothesis of Phase Synchronization (PS) between the systems X and Y. In our case, X represents the ENSO system and $Y(\tau)$ denotes the hydro-climatic variables in Colombia, at defined time lags, τ. Then, we consider the original system X and a representative number of possible states of the system Y, which represent independent copies of the underlying system, so-called here synthetic time series (STS). For the construction of the STS from the system Y, we use permutations of the data points of the original time series Y but being careful to preserve the seasonality of the time series. That is, we permute data points in separate subsets for each month. e.g. we took all data points for January and put them randomly, after doing that for all months, we reconstruct a synthetic time series.
The null hypothesis is that each STS is an independent realization of the system Y, corresponding to a different initial condition or to a possible time series of the same system. To test the statistical significance of the strength of PS, $\chi(\tau)$, among X and $Y(\tau)$, we generate such 500 STSs of the Y system and obtain a test distribution of $\chi(\tau)$ calculated with the observations of the system X and each one of the STS of Y. Finally, we construct the upper 95% confidence interval (CI) based on the respective 95th percentile of the test distribution. The lags at which values fall outside the confidence band represent the ones where the null hypothesis is rejected, or that the system X is in PS with the system Y, i.e. they are phase dependent at that particular lag τ.

3.5.6. On the sensitivity of PS metrics in relation to diverse HyAns methods

Methods to estimate hydro-climatic anomalies (HyAns) have differences among them and therefore induce high-biases and error sources toward the interdependence analysis and modeling of climate time series. Moreover, such differences could generate ambiguities for the physical interpretation of results (see Chapter 2). Hence, we verify the sensitivity of PS metrics using the four HyAns methods assessed in Chapter 2, namely: *(i)* the Traditional Annual Cycle or constant climatology (HyAns–TAC), *(ii)* **F**-filtering of the Annual cycle by moving average (HyAns–FAC), *(iii)* Annual cycle extracted by Singular Spectrum Analysis or Singular-Spectrum Annual Cycle (HyAns–SSAC) and, *(iv)* the Modulated Annual Cycle

or variable climatology, which is based on the EEMD technique. This PS analysis allows us to assess how sensitive or robust is our PS approach in relation to diverse methods to estimate HyAns.

3.5.7. PS between other Macro-climatic Indices and hydro-climatic anomalies in Colombia

Colombia's hydro-climatology can be influenced by processes that occur in other zones of the tropical Pacific Ocean (e.g. Nino 1+2) or low-frequency processes such as PDO. Likewise, Colombia's hydro-climatic variability is also influenced by macro-climatic processes that occur in the Atlantic Ocean, different from the ENSO system [*Poveda and Mesa*(1997), *Poveda et al.*(2001), *Poveda et al.*(2002), *Poveda et al.*(2004), *Poveda et al.*(2005), *Poveda et al.*(2011)]. Hence, we quantify PS using other macro-climatic indices such as TNA, TSA, NAO, AMO, AMM, and CAR. These cited works argue that such processes are related to hydro-climatic variability of Colombia, although such interdependence is still far from being understood in terms how the other macro-climatic processes influence anomalies over Colombia during ENSO. In this work, we quantify PS between HyAns in Colombia and other macro-climatic indices considering La Niña and El Niño epochs in order to shed light on non-linear spatio-temporal patterns of interdependence and their relationship with HyAns over Colombia.

3.6. Results and Discussion

3.6.1. PS between SST3.4 and rainfall in Colombia using raw data

We start analyzing phase relationships between SST in the tropical Pacific Ocean (ERSST3.4 containing its annual cycle) and the precipitation over Colombia (containing its annual cycle). The time series of precipitation are obtained by spatially averaging the monthly precipitation fields (Data set No. 1) separately for the five geographical regions of Colombia as shown in the Fig. **3-1**. With the purpose of comparing the original data, without extracting frequency bands, time series are standardized by subtracting the long-term average (grand-mean) and dividing by the long-term standard deviation (grand-standard deviation). Note that this standardization does not remove the annual cycle (AC).
Therefore, we use GPD and SPS to quantify PS between SST3.4 and precipitation over Colombia. Figure **3-2** (panel a) shows the time series of the MEI index and its periodogram (panel b) with different colors denoting the occurrence of El Niño and La Niña events during the period 1975-2006. In addition, Fig. **3-2** (panel c) shows the standardized time series and their periodograms (panel d) to visualize the spectral composition of both signals. Finally, Fig. **3-2** (panel e) evidence the presence of preferential values in the phase difference vs. time diagram, $\Phi_{1,1}(t)$, while Fig. **3-2** (panel f) evidences that the probability mass distribution

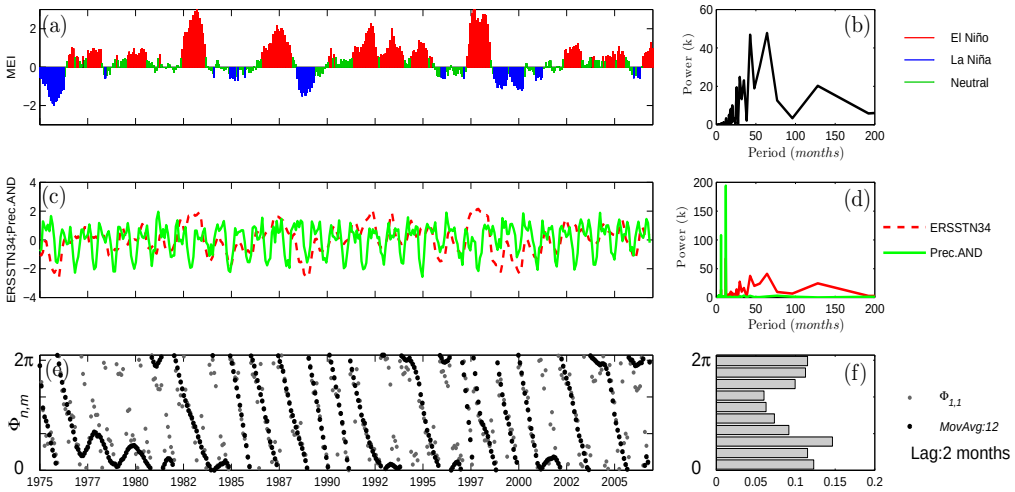

Figures 3-2.: Results of Phase difference $\Phi_{1,1}$ between SST3.4 (including its AC) and the long-term mean monthly precipitation (including its AC) for the Andean region of Colombia using the data set No. 1. (a) MEI index. (b) Periodogram of the MEI index (original time series). (c) Standardized time-series (without removing the annual cycle). (d) Periodograms of the time series. (e) Cylindrical representation of $\Phi_{1,1}$. (f) relative frequency distribution of $\Phi_{1,1}$.

of the cyclic relative phases has preferential values around $\Phi_{1,1} \sim 1.5\pi$ to 2π (September to February), indicating PS in a statistical sense, as we explained in section 3.5.1.

In general, Figure **3-3** shows the strength of PS, χ, between SST3.4 in the tropical Pacific and average precipitation for the five regions of Colombia, with a phase ratio 1:1 given that the predominant signal in both time series is the AC. Fig **3-3** (a-e) demonstrates χ as a function of time-lag $\tau = 1, 2, ..., 12$ months, where $\chi(\tau)$ is calculated using $\phi_{n,m}(\tau) = n\phi_x(t-\tau) - m\phi_y(t)$, being x the SST3.4 and y the precipitation time series (Details in 3.5.3). Our results evidence that PS is weak ($\chi < 0.40$) when the data are not classified according to the regimes of ENSO (El Niño and La Niña). In contrast, rainfall in the Pacific, Caribbean, Andean, and Orinoco regions exhibit stronger PS during La Niña than during El Niño. During La Niña, PS uncover a 2 months-lag, whereas during El Niño such time lag between the signals is not evident. Moreover, the Amazon region evidences a slightly stronger PS during La Niña than during El Niño, with 2 months-lag, which is not so clear as in the other regions. Figure **3-4** (Data set No. 1) shows the strength of PS, χ, as a moving-PS index between SST3.4 and average rainfall throughout each region (including their ACs). Our results evidence that the strongest El Niño events (1982-1983;1987-1988;1991-1992;1997-1998) exhibit weak PS, whereas La Niña events (1975-1976;1984-1985;1988-1989;1995-1996;1998-1999) exhibit strong PS. Analogous results were found for the rainfall dataset No. 2 (see the Suppl.

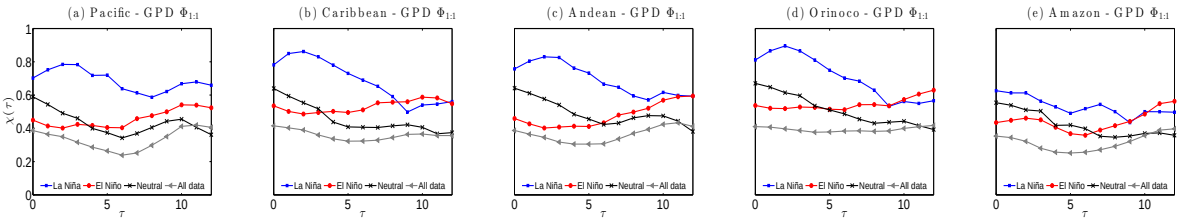

Figures 3-3.: Strength of phase synchronization, χ, between ERSST3.4 and long-term mean regional precipitation (both time series containing their annual cycles), using the Data set No. 1, with $\Phi_{1,1}$. (a-e) χ as a function of lag τ (in months) for El Niño and La Niña. (f-j) [right axis] χ for El Niño and La Niña with $\tau = 2$. [left axis] Average precipitation.

Info.). However, at this point, it is not possible to differentiate PS features between the El Niño events occurred in Eastern Pacific, Central Pacific or Mixed events, following the classification used by [Andreoli et al.(2017)].

Our analysis using raw data indicate three main results: *(i)* PS is weak, $\chi < 0.40$, when the data are not classified according to the states of ENSO (Niña and El Niño) for $\tau = 1, ..., 12$ months-lag, *(ii)* PS is strong during La Niña, $\chi \sim 0.80$, for $\tau = 2, ..., 4$ months-lag, exhibiting higher values for the Pacific, Caribbean, Andean, and, Orinoco regions, whereas the Amazon region exhibits moderate PS, $\chi \sim 0.60$, for $\tau = 1, 2$ months-lag, which suggest a lag-synchronization during La Niña, and *(iii)* during El Niño, the phase-lag function does not show a clear time-lag between the signals and there is no clear evidence of PS.

It is worth noticing that the PS results in Fig. **3-3** are calculated by spatially averaging of the monthly rainfall fields (Data set No. 1) for the five geographical regions of Colombia. Hence, the spatial averaging smooths the data and might hide slight phase differences among time series into the same natural region. Notwithstanding, we show clear differences in PS results regarding the states of ENSO although, at this point, it is hard to link such results with the annual cycle of rainfall in Colombia, the influence of ENSO on hydrological variables or the physical mechanisms behind PS. However, from our results discussed some remarkable questions arise:

- How significant is the ENSO signal in the original (raw) time series (which contain their annual cycles) regarding the states of ENSO (La Niña and El Niño)?

- Results indicate differences between data depending on whether they are classified by the states of ENSO. Is there PS between ENSO variability and rainfall anomalies over Colombia during all the ENSO states?

- Is there PS between the annual cycle of the hydrological variables in Colombia and the ENSO signal?

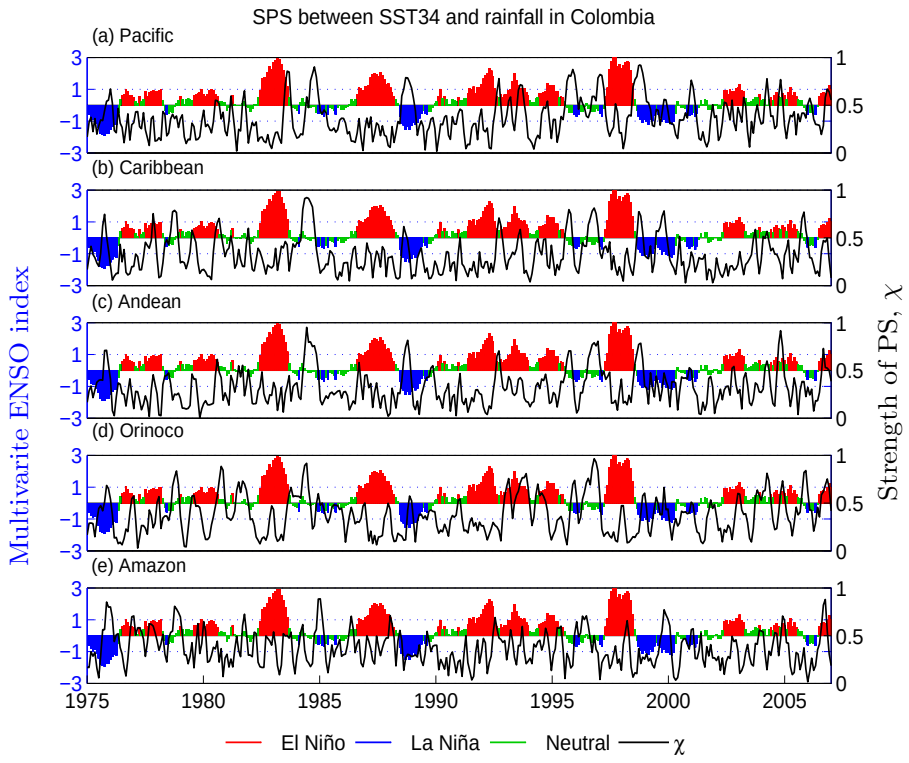

Figures 3-4.: Strength of phase synchronization between ERSST3.4 and long-term mean regional precipitation (both time series containing their annual cycles), using the Data set No. 1, with $\Phi_{1,1}$. [left axis] Multivariate ENSO index indicating periods El Niño, La Niña, and Neutral. [right axis] Strength of PS, χ.

- Is there any relationship between the Colombian zones that exhibit PS and the sign and magnitude of hydro-climatic anomalies?

In the next sections, we face up the above-mentioned questions and discuss our results in relation to physical mechanisms that control the annual cycle of rainfall and their anomalies during the warm and cold states of ENSO.

3.6.2. PS between SST3.4 and HyAns in Colombia at inter-annual timescales

Data pre-processing

In general, to quantify PS between the ENSO signal and the AC and HyAns in Colombia requires the following series of steps: *(i)* to define representative time series for the regions of Colombia, e.g. time series of rainfall or anomalies averaged over each natural region, *(ii)* to standardize the data (without subtract the seasonal variability), *(iii)* to filter out data in order to define the MAC, high-frequencies and noise of the hydro-climatic variables as well

Tables 3-1.: Percentage of the total variance, σ^2, explained by the MAC; Total Anomalies,A_T (in relation to MAC); Low-Frequency Anomalies, A_{LF}, and High-Frequency Anomalies,A_{HF}. Dataset No. 1.

Region	% σ^2 **MAC**	% σ^2 A_T	% σ^2 A_{HF}	% σ^2 A_{LF}
Andean	85.16	14.84	6.87	7.96
Caribbean	85.77	14.23	5.10	9.13
Pacific	72.63	27.37	16.27	11.10
Orinoco	92.66	7.34	1.59	5.74
Amazon	72.82	27.18	8.67	18.52

as their anomalies in relation to the MAC as explained by [*Wu et al.*(2008)], *(iv)* to test the significance of frequencies at seasonal timescales in the anomaly time series as stated by [*Ahdesmäki, et al.*(2005)] and, *(v)* to test the significance of the PS metrics (see section 3.5.5). The detailed steps behind our PS analysis are described in Suppl. Info (Section B.1).

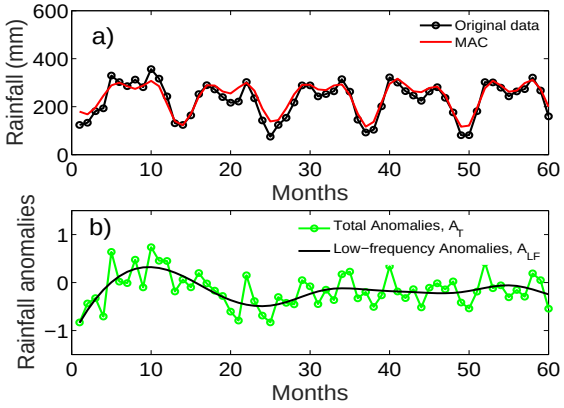

Figures 3-5.: Time series of rainfall and its standardized anomalies in the Andean region (Data set No. 1), example for a 5 years record length. a) Original averaged time series and its MAC. b) Rainfall anomalies after subtracting MAC or total anomalies, A_T and low-frequency anomalies or anomalies at inter-annual scales, A_{LF}.

Herein, we define high-frequency anomalies, A_{HF} as anomalies in frequency bands below 12 months, and low-frequency anomalies, A_{LF} that corresponds to anomalies in frequency bands above 12 months. In turn, the total anomalies A_T which are defined as the sum of A_{HF} and A_{LF}. Fig. **B-2** illustrates the difference between the original time series and MAC as well as the difference between A_T and A_{LF}. Furthermore, we verify the spectral characteristics of the original data, MAC, and A_{LF} for the time series of rainfall over each region (see Suppl. Info., Figs. B-1 to B-3)

In general, the MAC in relation to the total variance, σ_T, constitutes $\langle 82.0\% \rangle$ $[72.0\% - 93.0\%]$

and A_T constitutes $\langle 18.0\% \rangle$ $[7.3\% - 27.4\%]$. In turn, A_{HF} constitutes $\langle 8.0\% \rangle$ $[1.6\% - 16.3\%]$, whereas A_{LF} represents $\langle 10\% \rangle$ $[5.7\% - 18.5\%]$ (see details in Table **B-2**). Hereafter, we study the regional behavior of A_{LF} in Colombia and their association with ENSO.

Regional rainfall anomaly patterns

In Chapter 2 we show rainfall anomalies throughout Colombia considering the states of ENSO and using diverse methods to estimate hydro-climatic anomalies (HyAns). In general, Chapter 2 confirms that the Pacific, Andean and Caribbean regions exhibit negative (positive) rainfall anomalies during El Niño (La Niña) [*Poveda and Mesa*(1997), *Poveda et al.*(2001), *Poveda et al.*(2011), *Bedoya-Soto et. al.*(2018)]. Additionally, that work shows that Orinoco and Amazon regions exhibit positive (negative) rainfall anomalies during El Niño (La Niña). Hence, rainfall anomalies in the Pacific, Andean and Caribbean regions are opposite to those experienced in the Orinoco and Amazon regions during the warm and cold states of ENSO.

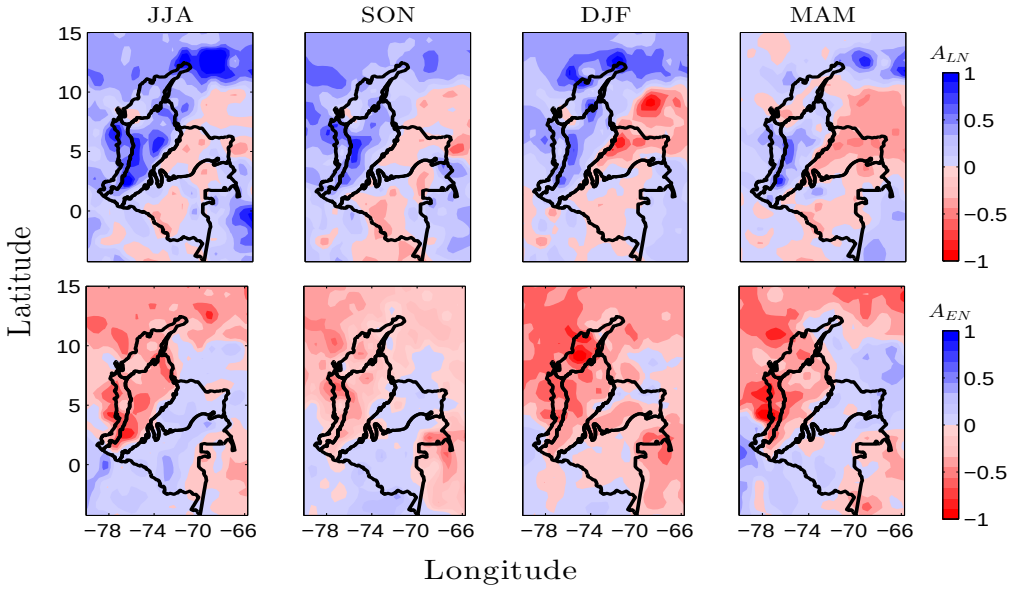

Figures 3-6.: Seasonal average composite rainfall anomalies (HyAns) over Colombia, during ENSO (Data set No. 1). (Top panels) HyAns during La Niña (A_{LN}). (Bottom panels) HyAns during El Niño (A_{EN}).

Here, we present the seasonal rainfall anomaly patterns in relation to ENSO. During La Niña, Fig. **3-6** (top row) evidences that the Pacific, Andean and Caribbean regions exhibit their highest positive rainfall anomalies during JJA and SON, whereas the Orinoco and Amazon regions exhibit their highest negative rainfall anomalies during DJF. During El Niño, Fig. **3-6** (bottom row) negative rainfall anomalies predominate throughout the year in the Pacific, Andean and Caribbean regions showing their maxima during DJF, which is the

unique quarter where the complete continental territory of Colombia experiences negative rainfall anomalies. On the other hand, the Orinoco and Amazon regions exhibit positive rainfall anomalies during JJA, SON and MAM. Quarters that exhibit less impact by ENSO are MAM (SON) during La Niña (El Niño). Analogous results were found using the rainfall Data set No. 2 (see Fig. B-8 in Suppl. Info.).

During La Niña (El Niño), positive (negative) rainfall anomalies in the **Pacific** region can be explained in terms of the increasing (decreasing) moisture advection of the CHOCO jet as a result of increase (decrease) of the temperature gradient between surface air temperatures over the Pacific coast off Colombia and El Niño 1+2 zone during JJA and SON [*Poveda and Mesa*(2000), *Rueda and Poveda*(2006)]. Analogously, in the **Caribbean** region, positive (negative) rainfall anomalies could be explained through the influence of the CLLJ wind anomalies during ENSO. [*Wang*(2007)] and [*Martin and Schumacher*(2011)] showed that during JJA, rainfall in the Caribbean (including the Caribbean region of Colombia) exhibits significant correlations with the CLLJ index. Moreover, it is postulated that the CLLJ induces changes in moisture flux divergence in the Caribbean, which enhance convection and increase rainfall [*Martin and Schumacher*(2011)]. Furthermore, during La Niña, the easterly CLLJ winds are weak (strong) in JJA (DJF), whereas during El Niño, the easterly CLLJ winds are strong (weak) in JJA (DJF) [*Wang*(2007)]. [*Arias et al.*(2015)] mentioned that the weakening (strengthening) of the CLLJ winds is associated with increasing (decreasing) rainfall anomalies over northern Colombia. Hence, based on Gill's theory the weakening (strengthening) of the CLLJ winds is related to the increase (decrease) of the SST temperature in the Caribbean sea that subsequently increase (decrease) evaporation, increase (decrease) moisture convergence, and increase (decrease) rainfall in that zone [*Wang*(2007), *Martin and Schumacher*(2011), *Arias et al.*(2015)]. On the other hand, rainfall anomalies in the **Andean** region can be explained by the conjoint influence hydro-climatic processes of the Pacific and Caribbean regions, as well as by the land-surface atmosphere feedback, which manifest themselves in the fundamental role of local recycling moisture processes in the Magdalena and Cauca river basins [*Poveda et al.*(2014), *Arias et al.*(2015)]. In the **Orinoco** and **Amazon** regions, rainfall anomalies could obey to anomalies in the Orinoco LLJ which transport moisture from the Atlantic Ocean and subsequently, to induced-changes in local hydrological processes and terrestrial recycling from Amazon and Orinoco river basins [*Spracklen et al.*(2012), *Poveda et al.*(2014), *Arias et al.*(2015), *Hoyos et al.*(2017), *Jiménez-Sánchez*(2019)]. However, the dynamics of the Orinoco LLJ at interannual timescales and its influence on HyAns of the Orinoco and Amazon regions during ENSO constitutes an understudied topic, which is necessary to improve our knowledge on the HyAns of these regions under the ENSO influence. It is worth remarking that low-level jet anomalies are not the unique mechanisms influencing HyAns over Colombia but constitute an important mechanism of moisture transport and flux moisture divergence dynamics. Finally, HyAns in the Orinoco and Amazon also are influenced by the Cross-Equatorial winds [*Wang and Fu*(2002)] during ENSO, which also needs further research in order to

advance in the understanding of HyAns of these regions.

3.6.3. Composites of hydro-climatic variables from ERA5 during ENSO

We carry out a composite analysis using ERA5 data, at a monthly resolution for the period 1979-2018, in order to verify the atmospheric conditions over northern South America and their relationships with rainfall anomalies over Colombia during the states of ENSO. In general, it is possible to confirm some aspects previously mentioned in section 3.6.2. During El Niño (La Niño) the SSTs over the far-eastern tropical Pacific are warmer (colder), Suppl. Info. Figures **B-9** and **B-10**, while surface winds are weaker (stronger) (see Fig. **3-7**).

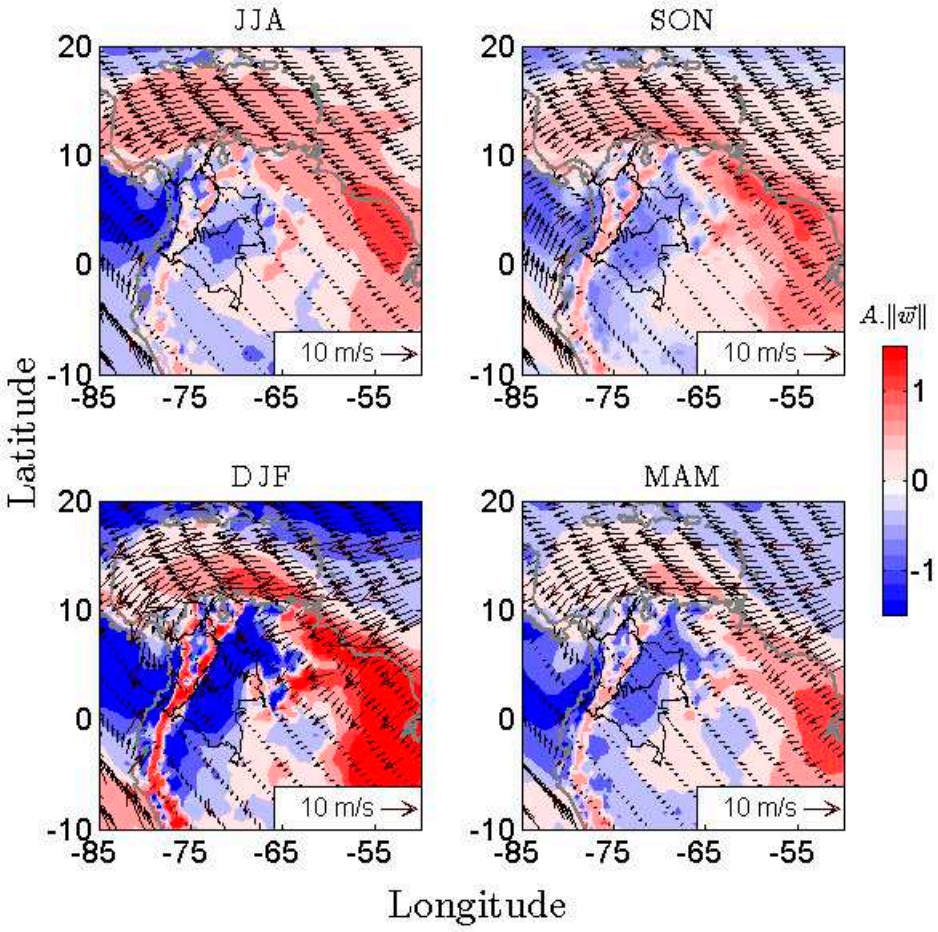

Figures 3-7.: Composite of anomalies of the surface winds magnitude at 100m ($A \cdot \|\overrightarrow{w}\|$) during El Niño. (arrows) climatology of winds during El Niño for the period 1979-2018 using ERA5.

Furthermore, during mentioned warm (cold) states of ENSO, the mean vertical integrated moisture divergences (mvimd) exhibit positive (negative) anomalies (see Fig. **3-8**), which

coincide with negative (positive) rainfall anomalies over the Andean, Pacific, and Caribbean regions of Colombia as well as over the Caribbean sea (northern Colombia) as shown in Fig. **3-9**. During El Niño (La Niña), DJF (SON) experiences the highest negative (positive) rainfall anomalies.

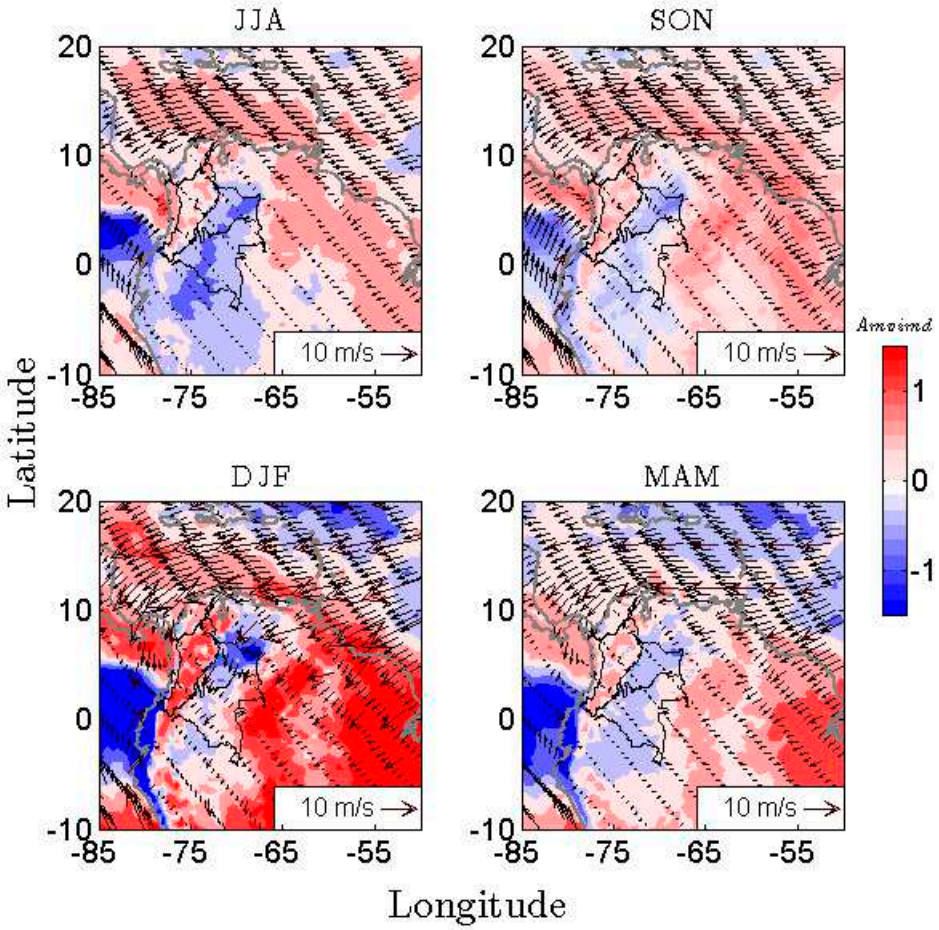

Figures 3-8.: Composite of mean vertical integrated moisture divergence (*Amvimd*) during El Niño. (arrows) climatology of winds during El Niño for the period 1979-2018 using ERA5.

Moreover, we analyze the volumetric soil water anomalies (VSW) during the states of ENSO. Our results evidence that during El Niño (La Niña), the VSW experiences negative (positive) anomalies. Those results confirm that ENSO impacts the soil water dynamics, which is a key component to advance in the understanding of land-atmosphere interactions over northern South America [*Cai et al.(2020)*, *Poveda and Mesa*(2000), *Bedoya-Soto and Poveda*(2017), *Bedoya-Soto et. al.*(2018), *Poveda et al.(2020)*].

Figures **3-7**, **3-8**, **3-9**, and **3-10** show only the results during El Niño. An analogous analysis was done for La Niña, which is can be seen in the Supp. Info. Figures **B-11**, **B-12**, **B-13**,

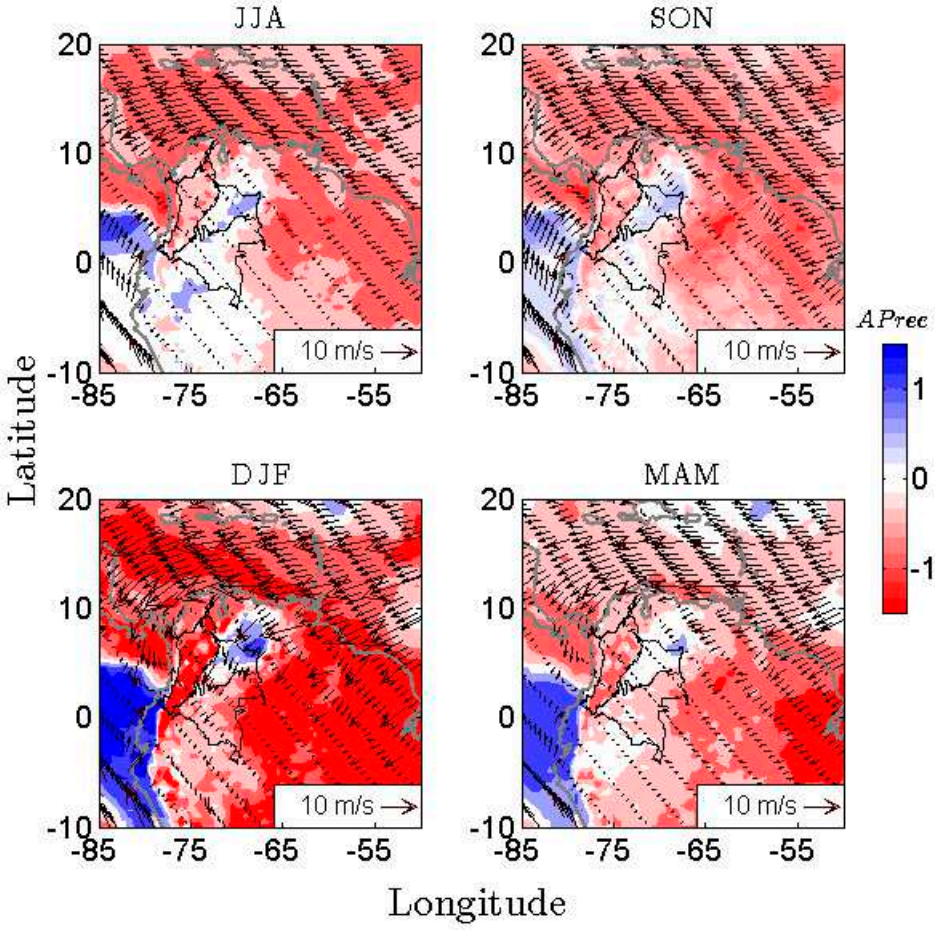

Figures 3-9.: Composite of rainfall anomalies (*APrec*) during El Niño. (arrows) climatology of winds during El Niño for the period 1979-2018 using ERA5.

and **B-14**.

PS between the ENSO signal and rainfall anomalies over Colombia

In this section, we quantify PS between SST3.4 anomalies and rainfall anomalies in Colombia. In addition, we calculate Pearson correlations between ENSO and HyAns in order to revise the ability of linear (Pearson) and non-linear techniques (PS) to capture spatio-temporal patterns of interdependence. This approach will allow us *(i)* reviewing possible physical mechanisms reported in the literature, (ii) comparing linear and non-linear quantifiers of interdependence, and *(iii)* hypothesize other possible processes that influence positive (negative) rainfall anomalies during La Niña (El Niño) in the regions of Colombia.
Fig. **3-11** (a-e) shows the strength of PS between SST3.4 anomalies in the tropical Pacific and rainfall anomalies in Colombia, as a function of time-lag τ, $\chi(\tau)$, using a phase ratio 1:1 (Data set No. 1). In this case, we use the time series of rainfall anomalies based on average

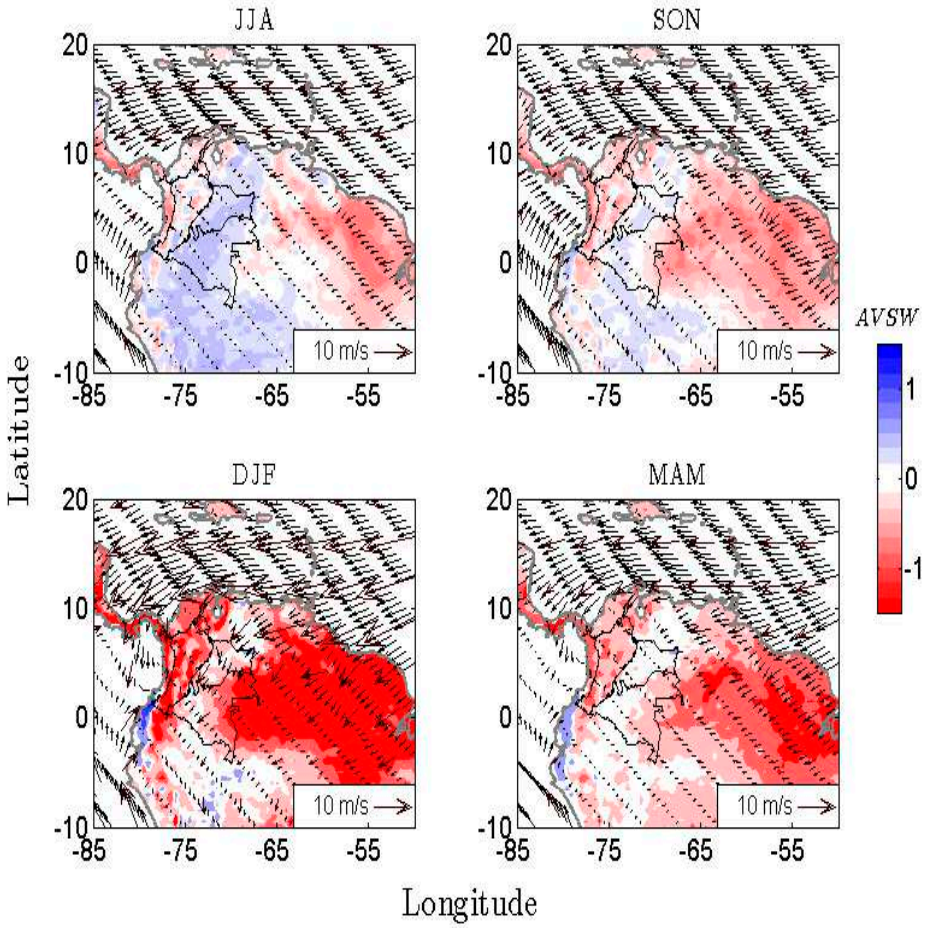

Figures 3-10.: Composite of volumetric soil water anomalies (AVSW) during El Niño. (arrows) climatology of winds during El Niño for the period 1979-2018 using ERA5.

rainfall over each Colombian region. Our results uncover strong PS (highly statistically significant) in the Pacific, Andean and Caribbean regions, whereas the Orinoco and Amazon regions do not exhibit clear PS (PS is not statistically significant). Furthermore, regions with significant values show stronger PS during La Niña than during El Niño. Moreover, during El Niño, we find lag-synchronization with 2-5 months-lag whereas during La Niña lag-synchronization is not evidenced. Similar results were found for the rainfall data set No. 2 (see Suppl. Info., Fig. B-15).

In addition, Fig. **3-12** shows the seasonal strength of PS, χ, between SST3.4 anomalies and HyAns in Colombia during the cold (top row) and warm (bottom row) ENSO's states. our results reveal that, during La Niña, the Pacific and Andean regions as well as a vast area over the Caribbean sea exhibit the strongest PS in JJA and SON, with geographic areas of significant PS that coincide with the seasons and localities of maximal positive rainfall

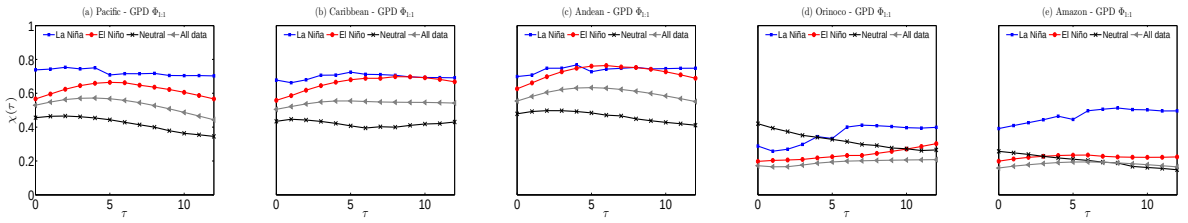

Figures 3-11.: Strength of phase synchronization, χ, between the SST3.4 anomalies and the standardized rainfall anomalies, A_{LF}. (Data set No. 1; 1976-2006) with $\Phi_{1,1}$. (a-e) χ as a function of lag τ (in months) during El Niño and La Niña for each region of Colombia.

anomalies. During El Niño, the Pacific, Caribbean, and Andean regions as well as the Caribbean sea show moderate PS, with the largest geographic area of significant PS during DJF, which coincide with the season and localities of maxim negative rainfall anomalies. The Orinoco and Amazon regions show non-significant PS during ENSO.

As a complement, Fig. **3-13** shows the seasonal Pearson correlations, r, between SST3.4 anomalies and HyAns during La Niña (top row) and El Niño (bottom row). Our results evidence that the r-values exhibit patterns of linear interdependence, which are not in agreement with the spatial patterns of seasonal rainfall anomalies over Colombia. To illustrate this, please see the spatial patterns of r during El Niño (Fig. **3-13**, bottom row) in relation to rainfall anomalies over Colombia (Fig. **3-6**, bottom row). It is worth to remark that, for the case of Colombia, the spatial patterns of Pearson correlation are highly sensitive to the method used to define Hyans in relation to the ENSO's states (see Chapter 2).

On the other hand, as explained in previous sections, the strength of PS, χ, exhibits high values when the phase differences, $\Phi_{n,m}$, between two time series have a dominating peak around a preferential value in the relative frequency distribution of $\Phi_{n,m}$. Then, only if $\chi_{n,m}$ has significant values it makes sense to interpret the mean value of $\Phi_{n,m}$, which can be understood as a time-lag between time series. Hence, Fig. **3-14** shows the average $\langle\Phi_{1,1}\rangle$ with overlapped hatched contours where $\langle\chi_{1,1}\rangle$ is statistically significant. In our case, a phase difference of $\frac{\pi}{3}$ approximates to 1 month lag. Then, Fig. **3-14** (top row) evidences that, at inter-annual time scales, during La Niña, for all quarters, SST3.4 anomalies in the tropical Pacific Ocean lead rainfall anomalies in the Pacific, Caribbean and Andean regions from 1 to 3 months lag. In contrast, during El Niño, JJA and SON, SST3.4 anomalies lead rainfall anomalies from 3 to 5 months lag. These results show that, during El Niño, rainfall anomalies exhibit a time-lag longer than during La Niña in relation to anomalies in the tropical Pacific ocean.

Summarizing, we found the following remarkable results: *(i)* strong (moderate) PS patterns in the Pacific, Caribbean and Andean regions were observed since the raw PS analysis (section 3.6.1, Fig. **3-3**), which was done using rainfall time series averaged over each

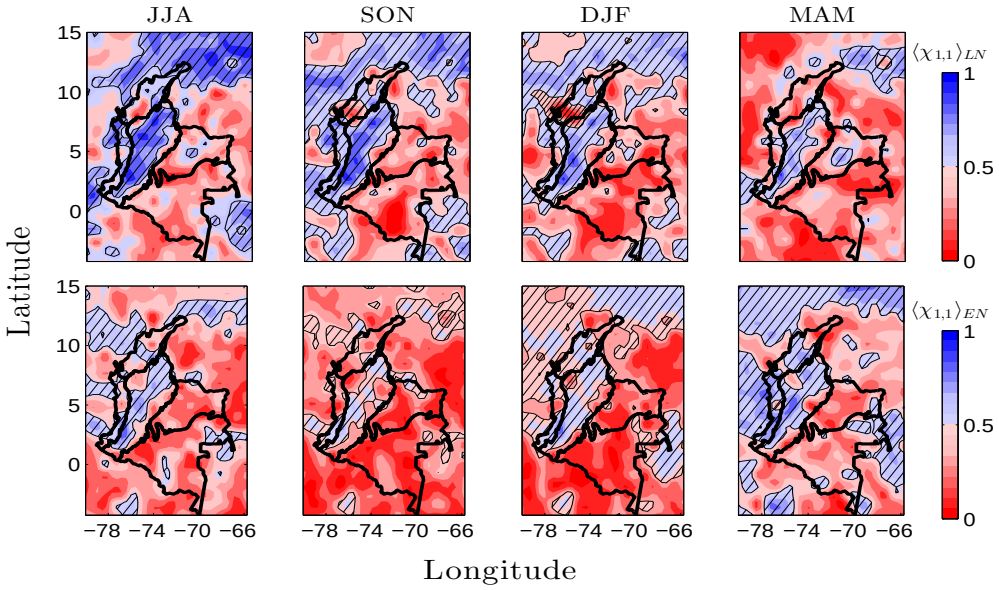

Figures 3-12.: Strength of phase synchronization between the standardized rainfall anomalies over Colombia (Data set No.1) and SST3.4 anomalies during ENSO. (top row) La Niña, $\langle\chi\rangle_{LN}$. (bottom row) El Niño, $\langle\chi\rangle_{EN}$. Phase ratio $\Phi_{1,1}$. The hatching contour lines indicate zones where χ is significant at 5%.

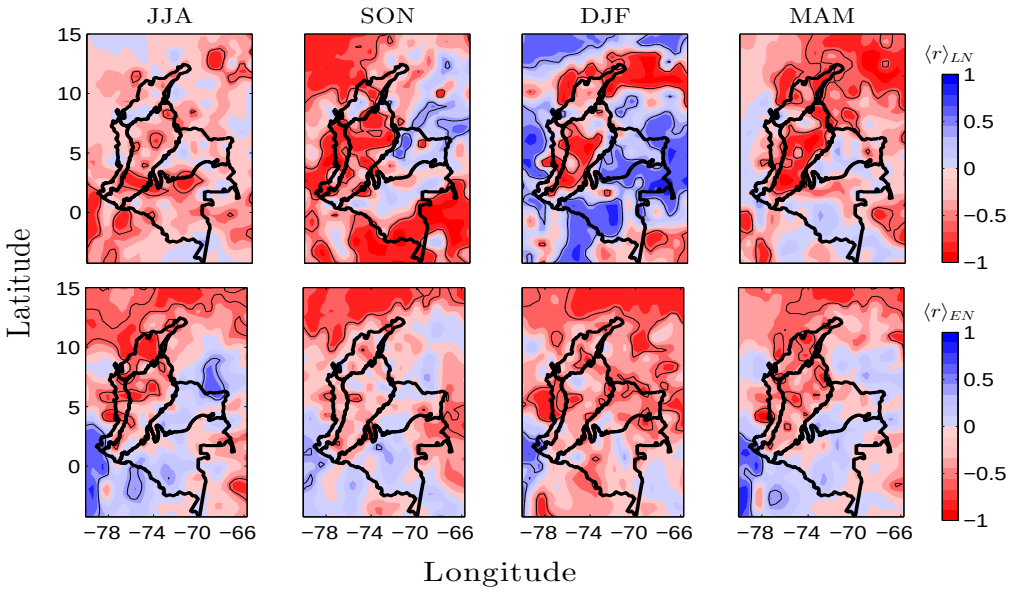

Figures 3-13.: Pearson correlations, r, between the standardized rainfall anomalies over Colombia and SST3.4 anomalies during ENSO. (top row) La Niña, $\langle r\rangle_{LN}$. (bottom row) El Niño, $\langle r\rangle_{EN}$. Contour lines denote zones where r is significant at 5%.

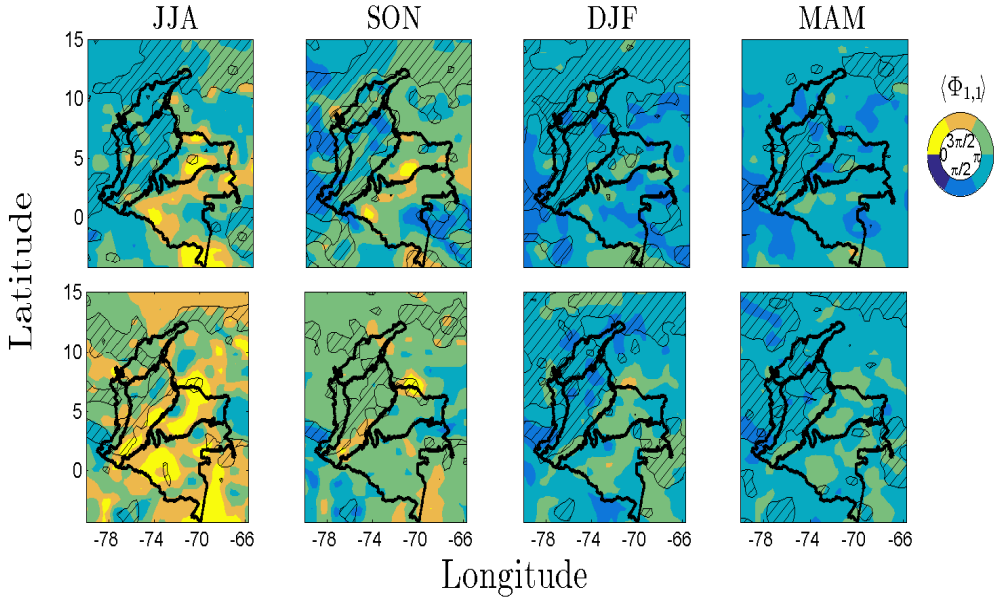

Figures 3-14.: Composite of average Phase Differences, $\langle \Phi_{1,1} \rangle$, between rainfall anomalies over Colombia and SST3.4 anomalies (Data set No. 1). (top row) La Niña. (bottom row) El Niño. A phase difference $\langle \Phi_{1,1} \rangle \approx \frac{\pi}{3}$ approximates to 1 month-lag. The hatched contours indicate zones where $\chi_{1,1}$ is significant at 5%.

region, *(ii)* the Generalized Phase Difference (GPD) technique helps to identify the spatial seasonal patterns of hydrological anomalies in Colombia in relation to the states of ENSO (La Niña and El Niño), whereas the linear Pearson correlation is not able to capture such patterns, and *(iii)* the Pacific, Andean and Caribbean regions are strongly (moderately) phase-locked with the tropical Pacific dynamics during La Niña (El Niño) in coherence with positive (negative) rainfall anomalies experienced in these regions. Hence, our PS results support the hypothesis of coupling between Colombian's climatology and the tropical Pacific Ocean dynamics in the mentioned regions, whereas the Orinoco and Amazon regions do not show PS with tropical Pacific Ocean variability. As discussed in section 3.6.2, PS results can be explained by a reduction (increase) of moisture advection from the CHOCO jet influencing the Pacific region [*Poveda and Mesa*(2000), *Rueda and Poveda*(2006), *Poveda et al.*(2014)] and by the strengthening (weakening) of CLLJ winds [*Wang*(2007)], which could inhibit (intensify) convection and rainfall in the Caribbean region [*Arias et al.*(2015)]. In the Andean region, the influence of the Caribbean and Pacific regions together with to the local hydrological processes enhanced by the large scale rivers basins and the orography of the Andean mountains helps to explain PS results associated to ENSO [*Poveda and Mesa*(1997), *Poveda et al.*(2001), *Poveda et al.*(2011), *Poveda et al.*(2014), *Arias et al.*(2015)]. Moreover, our results do not contradict the hypothesis that in the Orinoco and Amazon regions, the inter-annual dynamics of climate processes during ENSO are controlled by the

Atlantic Ocean dynamics [*Poveda et al.*(2014), *Arias et al.*(2015), *Hoyos et al.*(2017)]. Finally, our results uncover a link between the spatial PS patterns and rainfall anomalies during ENSO. Furthermore, it is well known that PS in non-linear oscillatory systems is defined as the appearance of a certain relation between the phases of interacting systems (or between the phase of a system and that of an external force), while the amplitudes can remain non-correlated [*Rosenblum et al.*(2001)]. On the other hand, generalized synchronization (GS) emerges when the state of the driven system is completely determined by the state of the driving system, i.e. the phases and amplitudes of both systems are correlated [*Pikovsky et al.*(2001)]. Hence, GS between ENSO and HyAns in Colombian regions that exhibit statistically significant PS is an open topic for further research.

Assessing PS between ENSO and rainfall anomalies in Colombia using diverse HyAns methods

We quantify PS using the four HyAns methods explained in Chapter 2, named: HyAns–TAC, HyAns–FAC, HyAns–SSAC, and HyAns–MAC (see section 3.5.6). The main objective is verifying how sensitive is the *Generalized Phase Difference* technique and the *Strength of Phase Synchronization* metric (hereafter PS metrics) in relation to diverse HyAns methods. To that end, we select the quarters that exhibit the strongest PS between SST3.4 and HyAns in Colombia, during La Niña and El Niño (i.e. JJA and DJF, respectively). Fig. **3-15** shows the PS in relation to the HyAns methods mentioned. Our results evidence that the strength of PS for the HyAns–FAC and HyAns–MAC methods are analogous, both methods exhibiting strong (moderate) PS during La Niña (El Niño) in JJA (DJF). PS metrics show similar results for HyAns–FAC and HyAns–MAC methods, for all quarters during La Niña and El Niño epochs. In contrast, PS metrics using the HyAns–TAC and HyAns–SSAC methods show significant differences with HyAns–FAC and HyAns–MAC. According to Chapter 2, HyAns–FAC and HyAns–MAC have some common properties, among them: *(i)* non-constant annual cycle, *(ii)* adequate separation of high and inter-annual frequencies, *(iii)* non-significant residual seasonal frequencies in anomalies and, *(iv)* the magnitude of extreme values of anomalies in a middle range compared with the other HyAns methods. On the other hand, HyAns–TAC and HyAns–SSAC do not meet the previously mentioned requirements for the case of rainfall anomalies over Colombia, which induce biases to results for quantification of interdependence by means linear and non-linear techniques.

3.6.4. PS analysis between ENSO and the AC of rainfall in Colombia

We quantify the strength of PS between the MEI signal (having only inter-annual frequency components) and the modulated annual cycle (MAC) of precipitation throughout Colombia. Fig. **3-16**a shows the MEI index and the states of ENSO (El Niño, La Niña, and Neutral). Fig. **3-16**b gives the cylindrical representation of the phase differences between the time series, $\Phi_{1,2}$. In this case, we do not classify data according to the states of ENSO then,

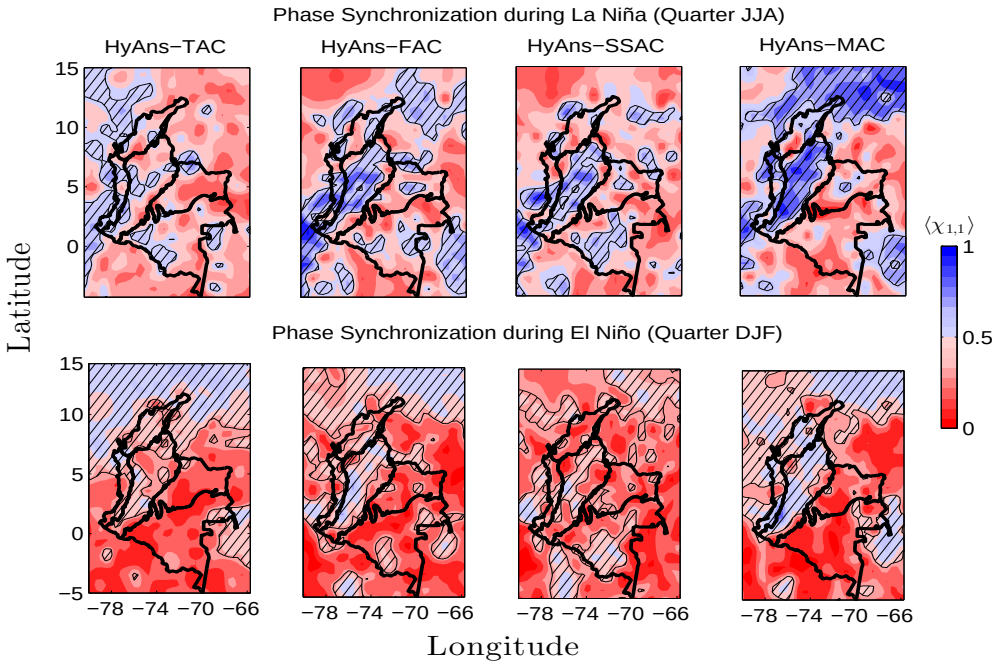

Figures 3-15.: Strength of Phase Synchronization, χ, between the SST3.4 anomalies and rainfall anomalies throughout Colombia, using the HyAns methods: HyAns–TAC, HyAns–FAC, HyAns–SSAC, HyAns–MAC for the quarters that exhibit the strongest PS during ENSO. Data set No. 1, period 1976-2006, phase ratio $\Phi_{1,1}$. (top row) χ for JJA during La Niña. (bottom row) χ for DJF during El Niño.

the almost uniform relative frequency distribution of $\Phi_{1,2}$ can be explained by the presence of data from the diverse states of ENSO. However, Figure **3-16** (panels c and d) evidences that the probability mass distribution of $\Phi_{1:2}$ is not perfectly phase-locked during El Niño (Fig. **3-16**c) and La Niña (Fig. **3-16**d) but certain phase differences are more probable than others. This behavior suggest some synchrony between the ENSO events and the AC of rainfall in Colombia.

Fig. **3-17**(a-e) shows the strength of PS between ENSO (SST3.4 anomalies) and the AC of rainfall throughout Colombia (Data set No. 1). We use as time series the monthly precipitation fields (and time series from rain gauges) spatially averaged over each region. Then, it is possible that such procedure smoothes the data and hides slight phase differences among time series. In general, PS is stronger during La Niña and El Niño than during the neutral ENSO's state. Furthermore, PS during El Niño is stronger than during La Niña. Moreover, our results suggest a non-lagged synchronization because the PS-function, $\chi(\tau)$, does not show prominent peaks for a specific time-lag $\tau \neq 0$. These results provide evidence that the inter-annual variability of ENSO is strongly phase-locked with the AC of rainfall over Colombia, particularly during El Niño and La Niña. Analogous results were found using the Data set No. 2 (not shown).

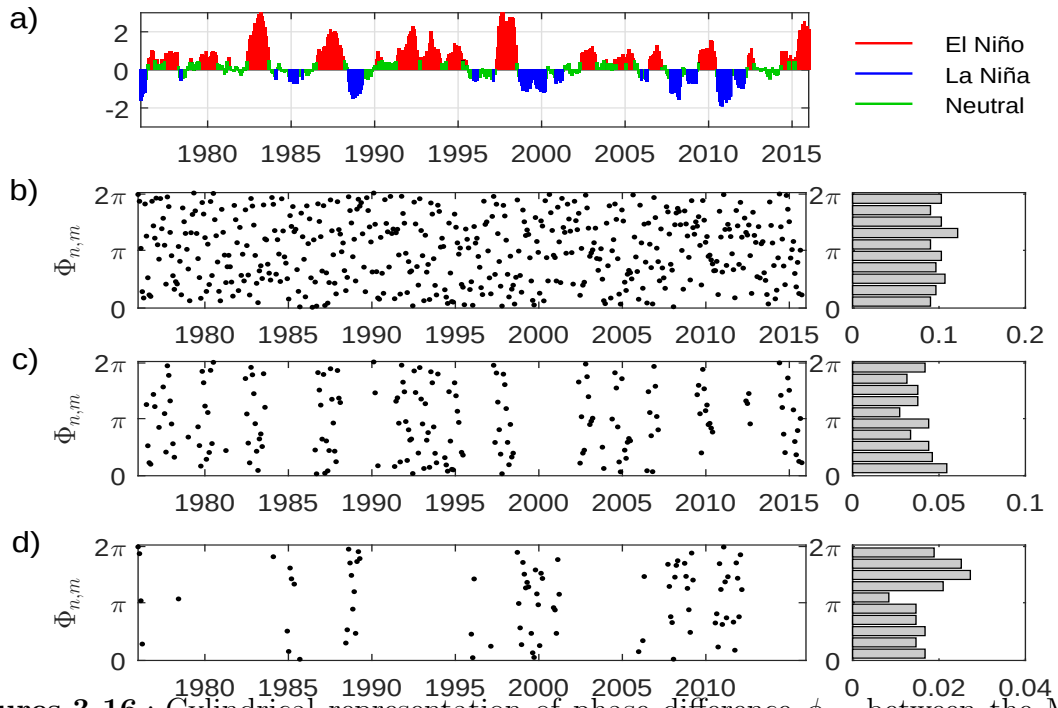

Figures 3-16.: Cylindrical representation of phase difference $\phi_{1,2}$ between the MEI index and the annual cycle of rainfall in the Andean region (Data set No. 2). (a) MEI index. (b) [left] $\phi_{1,2}$ using all record length data and [right] relative frequency distribution (c) [left] $\phi_{1,2}$ for El Niño state and [right] relative frequency distribution. (d)[left] $\phi_{1,2}$ for La Niña state and [right] relative frequency distribution.

Furthermore, we calculate the strength of PS, χ, between ENSO and the AC of rainfall using the two datasets available over Colombia in order to investigate spatial patterns of PS during La Niña and El Niño states. In general, Fig. **3-18** shows that in vast areas of the Colombian territory, the MAC of rainfall is strongly phase-locked with ENSO. Furthermore, the phase-locking patterns change depending on the season and the state of ENSO. **During La Niña**, Fig. **3-18** (top row) demonstrates strong PS, throughout the year, over the Caribbean sea, and the **Caribbean** and **Orinoco** regions. The northern **Andean** region exhibits significant PS during SON and DJF, whereas the southern Andean does not exhibit PS along the year. The central **Pacific** region exhibit PS in SON and DJF, while the Pacific region exhibit strong-PS during SON and the north Pacific coast of western Colombia shows strong-PS in DJF and MAM. Finally, a vast area in the **Amazon** region shows strong-PS during MAM and JJA. **During El Niño**, Fig. **3-18** (bottom row) shows strong PS in most of the Colombia territory along the year, except in southern Amazon and the south-western Colombian frontier with Ecuador in SON and DJF. During JJA a distinctive feature of non-PS crosses Colombian territory from the north-eastern Caribbean coast to the southern Pacific coast of Colombia (passing by the northern Andean region and the central Pacific

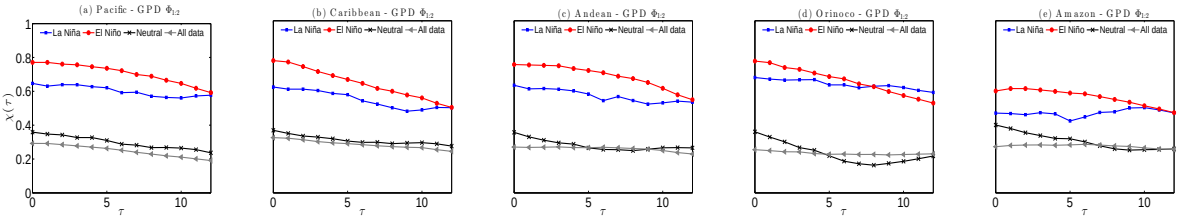

Figures 3-17.: Strength of phase synchronization, χ, between the SST3.4 anomalies and the MAC of rainfall throughout regions of Colombia (Data set No. 1; 1975-2006) with $\Phi_{1,2}$. (a-e) χ as a function of lag τ (in months) for El Niño and La Niña.

region). Further research is necessary in order to interpret these PS patterns in relation to the main mechanisms that determine the annual cycle of rainfall in such diverse regions.

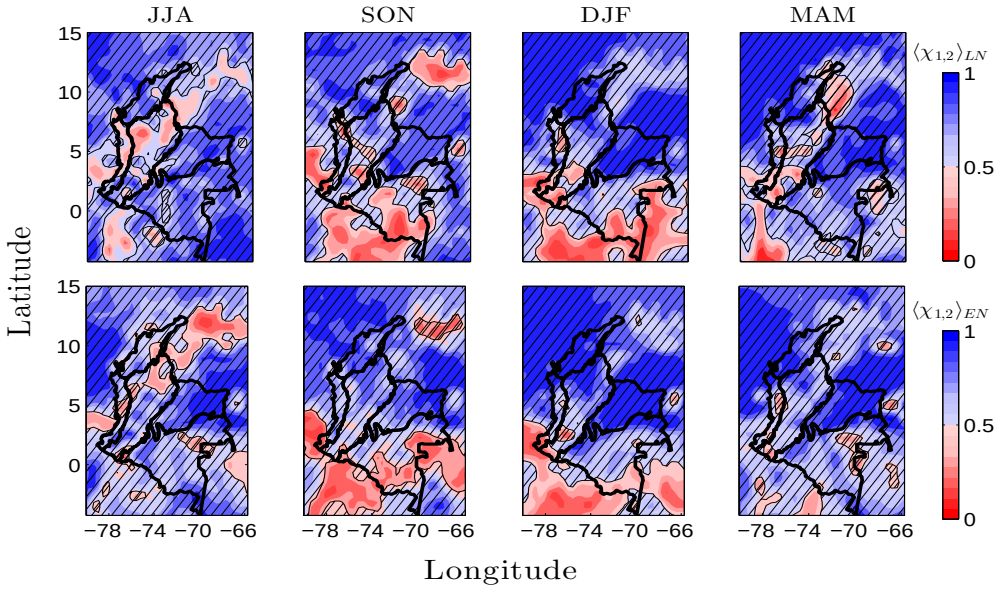

Figures 3-18.: Strength of phase synchronization, $\langle\chi\rangle$, between the SST3.4 anomalies and the modulated annual cycle (MAC) of precipitation over Colombia considering ENSO. Phase ratio $\Phi_{1,2}$, Data set No. 1. (top row) La Niña $\langle\chi\rangle_{LN}$. (bottom row) El Niño $\langle\chi\rangle_{EN}$. The hatched contours indicate zones where χ is significant at 5%.

As in section 3.6.3, the average Phase Differences, $\langle\Phi_{1,2}\rangle$, make sense only in areas where $\chi_{1,2}$ is statistically significant. Fig. **3-19** shows that although χ has similar strong-PS patterns between the ENSO signal and the AC of rainfall over most of the Colombian territory, the $\langle\Phi_{1,2}\rangle$ patterns change depending on the quarter and the ENSO state. During MAM and SON, when the ITCZ passes over central Colombia [*Hoyos et al.*(2017)], $\langle\Phi_{1,2}\rangle$ shows similar results for both La Niña and El Niño. In particular, $\langle\Phi_{1,2}\rangle$ exhibits a wave-like propagation

from the Orinoco region in direction to north and south, whose values are lower during MAM than during SON. In contrast, during La Niña and El Niño, in the boreal winter (DJF), when the ITCZ is located in its southernmost position [*Hoyos et al.*(2017)], $\langle \Phi_{1,2} \rangle$ exhibits a wave-like propagation, which increases from the Caribbean Sea to the central Orinoco region. Finally, during La Niña, in the boreal summer (JJA) when the ITCZ is located in its northernmost position, the phase differences are lower over the Caribbean Sea and higher over the northern Andean, Orinoco and Amazon regions. During El Niño, the $\langle \Phi_{1,2} \rangle$ values are higher over all Colombian territory than during La Niña.
In this sense, [*Stein et al.*(2014)] studied synchronization between ENSO and the annual cycle over the tropical Pacific Ocean. They investigated two possible mechanisms behind such synchronization feature, namely: (i) frequency locking of ENSO to periodic forcing by the annual cycle, or (ii) the effect of the seasonally varying background state of the equatorial Pacific on ENSO's coupled stability. As conclusions, their results indicated that the annual modulation of the coupled stability of the equatorial Pacific ocean-atmosphere system is by far the more likely mechanism generating the synchronization between ENSO and the annual cycle. In our case of study, at this point, PS between ENSO and the annual cycle of rainfall in Colombia cannot be associated with physical mechanisms behind the found PS patterns. However, the findings by [*Stein et al.*(2014)] allow us to hypothesize as a possible physical mechanism the annual modulation of the land-ocean-atmosphere interactions over northern tropical South America, which enhance or reduce the impact of ENSO on this regions. This hypothesis deserves further research.

3.6.5. PS between other macro-climatic indices and HyAns in Colombia

We quantify PS between rainfall anomalies throughout Colombia and other macro-climatic indices, such as: TNA, NAO, TSA, PDO, CAR, QBO, N12, AMO and AMM (see sections 3.4.3 and 3.5.7). To that end, we classify rainfall anomalies in Colombia and the macro-climatic time series, by considering La Niña and El Niño epochs as mentioned in Chapter 1. In addition, we filtered out the macro-climatic indices using EEMD in order to guarantee that time series preserve only the inter-annual frequency bands (see section B.1 and the Suppl. Info. B). Fig. **3-20** shows $\chi_{1,1}$ between the PDO index and rainfall anomalies in Colombia during ENSO (Data set No. 1). During La Niña in JJA, the PDO exhibits the strongest PS with rainfall anomalies over the Caribbean sea and the Caribbean, Andean, and Pacific regions. Furthermore, these regions coincide with zones of strong phase-locking between negative SST3.4 anomalies and rainfall anomalies (see Fig. **3-12** top row). Moreover, those areas of PS coincide with the Colombian regions that exhibit the highest positive rainfall anomalies (see Fig. **3-6** top row). During El Niño in JJA, SON, and MAM, the PDO also exhibits moderate PS with rainfall anomalies over the mentioned regions.
At this point, we hypothesize that some extreme positive (negative) anomalies over Colombia,

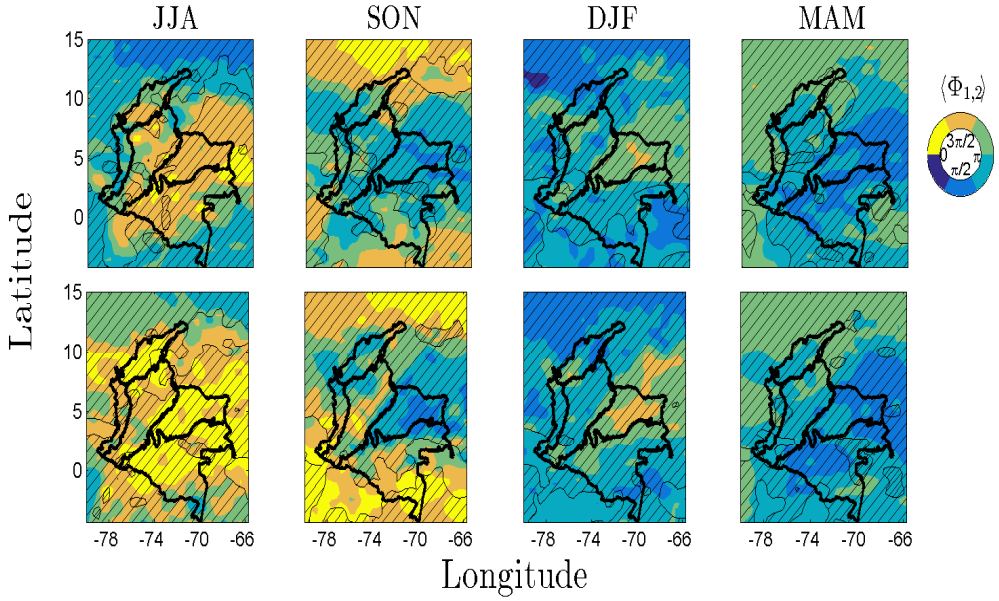

Figures 3-19.: Composite of the average Phase Differences, $\langle\Phi_{1,2}\rangle$, between SST3.4 anomalies and the MAC of rainfall over Colombia. (top row) La Niña. (bottom row) El Niño. The hatched contours indicate zones where $\chi_{1,2}$ is significant at 5%.

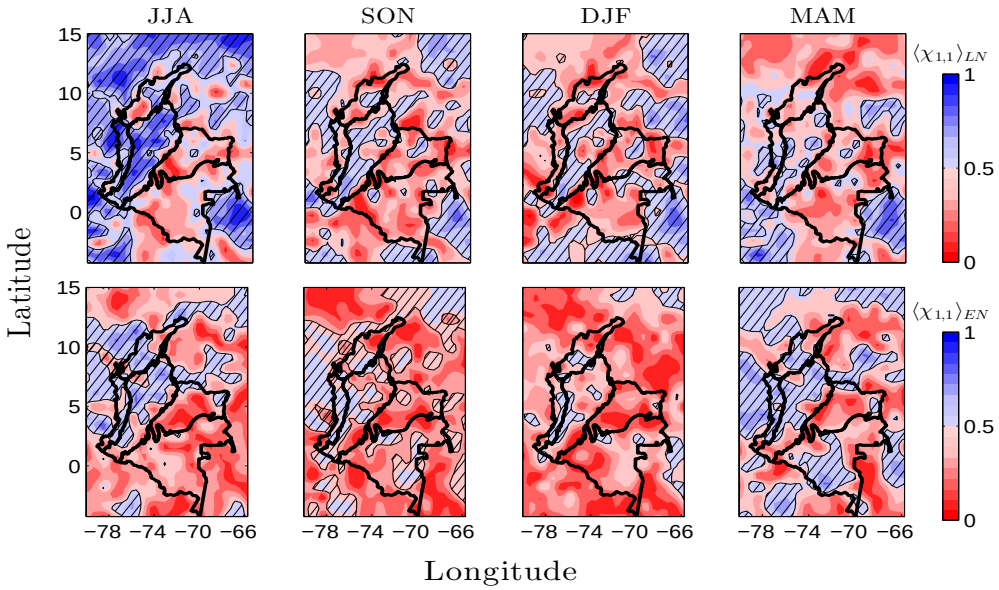

Figures 3-20.: Strength of phase synchronization, $\langle\chi\rangle$, between the PDO index and rainfall anomalies in Colombia during ENSO. Phase ratio $\Phi_{1,1}$, Data set No. 1. (top row) La Niña $\langle\chi\rangle_{LN}$. (bottom row) El Niño $\langle\chi\rangle_{EN}$. The hatched contours indicate zones where χ is significant at 5%.

during La Niña (El Niño), are enhanced by the conjoint effect of the PDO and the ENSO states. According to [*Mantua*(2001)], PDO primarily affects the North Pacific region but its effects can be felt also near the equator. Conversely, ENSO primarily affects the climate of lower latitudes, but its secondary effects are felt in the North Pacific. Furthermore, a positive (negative), or warm (cold) state of the PDO produces climate and circulation patterns that are similar to El Niño (La Niña) [*Gershunov and Barnett*(1998)]. Moreover, the climate signal of El Niño is likely to be stronger when the PDO is highly positive and conversely, the climate signal of La Niña will be stronger when the PDO is highly negative [*Gershunov and Barnett*(1998)].

To investigate our hypothesis, we quantify the strength of PS, χ, between the PDO index and SST3.4 anomalies as a moving PS-index using a 24-months window-length. In addition, we compare such moving PS-index with the rainfall anomalies averaged over each Colombian region in relation to the ENSO states according to the MEI index. For the **Pacific region**, Fig **3-21**a shows the MEI index and the ENSO states: La Niña, El Niño and Neutral. Fig **3-21**b gives the PDO index and the SST3.4 anomalies. Fig **3-21**c (right axis) shows the moving PS-index between PDO and SST3.4 anomalies whereas Fig **3-21**c (left axis) shows the rainfall anomalies. Note that during El Niño events (1982-1983, 1987-1988, and 1997-1998) the PDO-index exhibits positive values, while SST3.4 shows warm anomalies. At the same time, the moving PS-index exhibits weak PS, while Colombian Pacific rainfall experiments negative anomalies. Conversely, during La Niña events (1988-1989, 1998-1999, and 1999-2000) the PDO-index exhibits negative values while SST3.4 shows cold anomalies. At the same time, the moving PS-index shows strong PS while Colombian Pacific rainfall experiments positive anomalies.

Analogously, we quantify PS between rainfall anomalies in Colombia and NAO during ENSO (see Fig. **3-22**). Our results suggest that, during La Niña in JJA, NAO is strongly phase-locked with anomalies over the Andean and Caribbean regions. In this sense, [*Wang*(2007)] statedthat the Caribbean LLJ is phase-locked with the NAO. In addition, he argued that both the CLLJ and NAO are related to the NASH [*Wang*(2007)]. Hence, a strong (weak) NASH is associated with strengthening (weakening) of the easterly CLLJ and also corresponds to the positive (negative) phase of the NAO [*Wang*(2007)]. As a complement, the work by [*Arias et al.*(2015)] showed a significant linear correlation between the CLLJ and rainfall anomalies in Colombia. Neither [*Wang*(2007)] nor [*Arias et al.*(2015)] discussed differences of phase-locking and correlations in relation to the states of ENSO, which deserve future research. Notwithstanding, these results support the hypothesis that CLLJ wind anomalies during La Niña could contribute to explain positive rainfall anomalies over the Andean and Caribbean regions of Colombia.

Finally, the macro-climatic indices TNA, TSA, CAR, QBO, AMO, and AMM also exhibit areas of significant-PS with rainfall anomalies over Colombia (see Suppl. Info., Figs. B-17 and B-22). In particular, AMO is phase-locked with rainfall anomalies over the Amazon and Orinoco regions during El Niño and La Niña (see Suppl. Info., Fig. B-16). Also, TNA

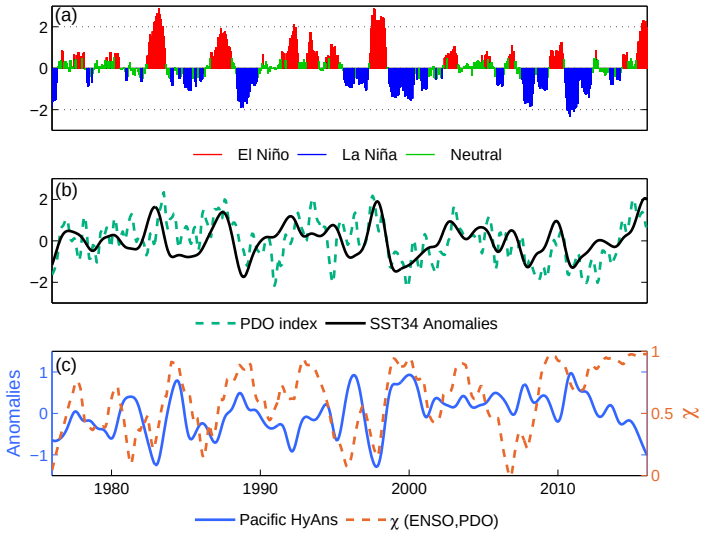

Figures 3-21.: Strength of phase synchronization, $\langle\chi\rangle$, between the PDO index and SST3.4 anomalies in relation to rainfall anomalies in the Pacific region of Colombia during ENSO. Phase ratio $\Phi_{1,1}$, Data set No. 2. (a) MEI index. (b) PDO index and SST3.4 anomalies. (c) Rainfall anomalies in the Pacific region of Colombia in relation to $\langle\chi\rangle$ between the PDO index and SST3.4 anomalies.

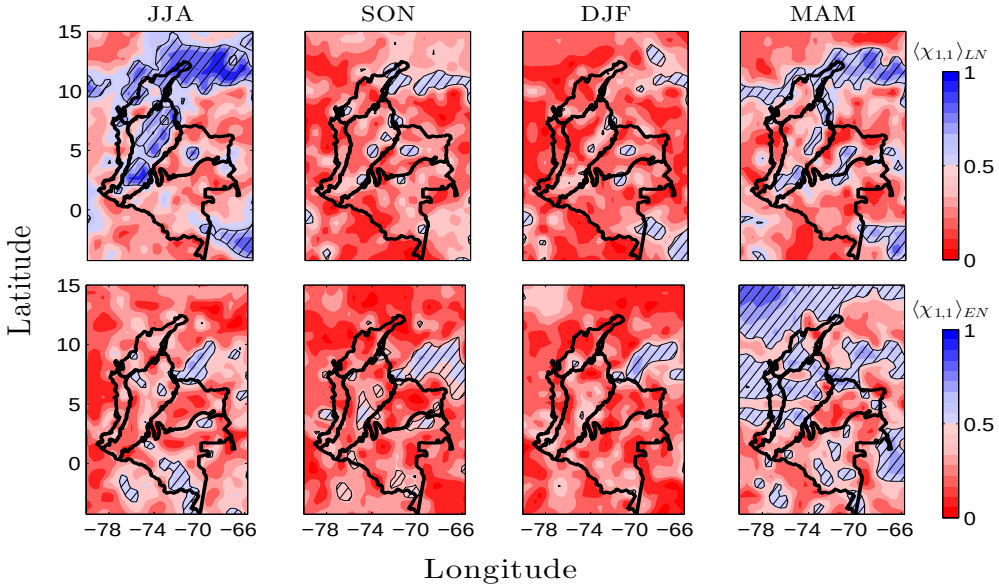

Figures 3-22.: Strength of phase synchronization, $\langle\chi\rangle$, between the NAO index and rainfall anomalies in Colombia during ENSO. Phase ratio $\Phi_{1,1}$, Data set No. 1. (top row) La Niña $\langle\chi\rangle_{LN}$. (bottom row) El Niño $\langle\chi\rangle_{EN}$. The hatched contours indicate zones where χ is significant at 5%.

shows phase-locking with rainfall anomalies over vast Colombian areas (see Suppl. Info., Fig. B-17). For the other macro-climatic indices, PS areas are smaller than those found for SST3.4 anomalies, the PDO and, the NAO signal. Furthermore, PS between HyAns and SST anomalies in the N12 zone as well as PS between HyAns and the MEI index provide similar results to those found for PS between HyAns and SST3.4 (see Suppl. Info., Figs. B-19).

3.7. Conclusions and future work

In this study, we have found five main results:
First, we present an unexplored approach based on Phase Synchronization (PS) techniques in order to investigate non-linear interactions between the ENSO signal in the tropical Pacific Ocean and the (annual and inter-annual) variability of rainfall over Colombia. To that end, we use the Generalized Phase Difference (GPD) technique as well as an index that provides a measure of the strength of PS. Our results show that the PS technique allows identifying seasonal spatial patterns of interdependence in relation to the extreme states of ENSO. However, for climate research purposes, the PS analysis must be accompanied by a rigorous data analysis in order to define adequately the annual cycle (AC), eliminate the seasonal residual frequencies in hydro-climatic anomalies, and assess the statistical significance of PS metrics. Moreover, we show that the PS technique is a robust method in relation to the different HyAns estimation methods, the HyAns-FAC and HyAns-MAC methods provide similar PS-results. This can be explained because the mentioned HyAns methods consider a non-constant annual cycle and it is possible to guarantee time series of anomalies with non-significant seasonal residual frequencies, which allow us avoid error sources and biases in quantification of PS.
Second, we study the seasonal regional rainfall anomaly patterns throughout Colombia during La Niña and El Niño. Our results evidence that, during La Niña (El Niño), the Pacific, Caribbean and Andean regions experiment positive (negative) rainfall anomalies, whereas the Orinoco and Amazon regions exhibit negative (positive) ones. During La Niña (El Niño), the Pacific, Caribbean, and Andean regions exhibit the highest positive (negative) anomalies in JJA (DJF) while the Orinoco and Amazon experiment the highest negative (positive) anomalies in DJF (JJA). Based on the literature, we discussed that such rainfall anomalies during ENSO can be explained by the influence of several concomitant hydro-climatic processes and mechanisms, among them: the three Low-Level jets surrounding Colombia (the Choco LLJ, the Caribbean LLJ, and the Orinoco LLJ), the Cross-Equatorial winds, land-surface atmosphere feedback (e.g. local recycling moisture in large river basins), other macro-climatic processes that are phase-locked with the ENSO signal (e.g. such as the PDO and the NAO), and the complex interactions between processes that occur at different timescales (e.g. ENSO signal in the tropical Pacific and the annual cycle of rainfall in Colombia). However, we also point out the need of further research on the LLJs anomalies and

the cross-equatorial wind anomalies during ENSO. Moreover, further research on the physical mechanisms behind the influence of other macro-climatic processes on hydro-climatic processes over Colombia is necessary.

Third, our findings reveal that the ENSO signal is strongly (moderately) phase-locked with rainfall anomalies over some Colombian regions during La Niña (El Niño). In particular, the PS analysis evidences that the significant seasonal spatial patterns of PS coincide with the seasonal spatial patterns of positive (negative) rainfall anomalies in the Pacific, Andean, and Caribbean regions during La Niña (El Niño). In the Orinoco and Amazon regions, rainfall anomalies do not exhibit significant PS with ENSO. Hence, our results support the hypothesis that rainfall anomalies in the Pacific, Andean and Caribbean regions are mainly influenced by the tropical Pacific Ocean dynamics, whereas rainfall anomalies in the Amazon and Orinoco regions are controlled by the Atlantic Ocean dynamics. Furthermore, we found that SST anomalies in the tropical Pacific ocean lead rainfall anomalies in Colombia with 3 to 5 months-lag during El Niño and 1 to 3 months-lag during La Niña. Moreover, the mentioned relationship between the PS patterns between ENSO and HyAns in Colombia point out the need of future research on the existence of Generalized Synchronization.

Fourth, we provide evidence of PS between the ENSO signal in the tropical Pacific Ocean and the modulated annual cycle (MAC) of rainfall over some regions of Colombia, which opens new paths towards the understanding of the non-linear feedback between the inter-annual variability of ENSO and the MAC of the hydro-climatic processes in Colombia. Although, at this point, it is not possible to provide a satisfactory physical explanation of such non-linear interdependence between ENSO and MAC. These results allow us hypothesizing as a possible physical mechanism, the annual modulation of the land-ocean-atmosphere interactions over northern tropical South America, which enhances or reduces the impact of ENSO on this regions. Future investigation on this topic is necessary.

Finally, we quantify PS between different macro-climatic indices and rainfall anomalies in Colombia. Our results reveal that the PDO signal and HyAns in Colombia are phase-locked. Such PS exhibits seasonal spatial patterns that are similar to those found for PS between the ENSO signal and HyAns over some regions. In this sense, we hypothesize that some extreme events of positive (negative) anomalies over Colombia, during La Niña (El Niño), are enhanced by the conjoint effect of the PDO and the ENSO states. Our analysis over the Pacific region of Colombia supports this hypothesis. In addition, we quantify PS between the NAO signal and HyAns in Colombia. In this sense, we found that during La Niña, in the boreal summer (JJA), HyAns in the Caribbean and Andean regions exhibit strong PS with NAO. Hence, a possible mechanism responsible for such phase-locking is the influence of the Caribbean LLJ winds anomalies on rainfall over the Caribbean and Andean regions of Colombia. In addition, we showed that other macro-climatic indices are phase-locked with rainfall anomalies, which suggest that several macro-climatic processes influence conjointly the hydro-climatology of Colombia. Moreover, such PS patterns from other macro-climatic indices also change depending on the ENSO's states.

3.8. Acknowledgments

The work of H.D. Salas is supported by COLCIENCIAS – Grant for National Doctorates 617-2 and partially funded by the Humboldt University of Berlin IRTG 1740. The work of G. Poveda and O. J. Mesa is supported by Universidad Nacional de Colombia at Medellin. The work by J. Kurths is supported by PIK. Thanks to: U.S. Geological Survey (USGS HydroSHEDS) for the Digital Elevation Models, NOAA for the ENSO index data, A. F. Hurtado for reanalysis data of precipitation over Colombia and, IDEAM the rain gauges records. Special thanks to J. M. Bedoya-Soto for the organized IDEAM dataset.

3.9. Appendix A:Phase Synchronization:Theoretical basis

According to [*Rosenblum et al.*(2001)], a stable limit cycle in the phase space is the main characteristic of stable periodic self-sustained oscillators. Then, the dynamics of a phase point on this cycle can be denoted as,

$$\frac{d\phi}{dt} = \omega_o \tag{3-9}$$

where $\omega_o = 2\pi/T_o$, and T_o is the period of the oscillation. On the other hand, if two oscillators are weakly coupled, it is possible to neglect variations of amplitudes to obtain equations describing their phase dynamics such as,

$$\frac{d\phi_1}{dt} = \omega_1 + \epsilon g_1(\phi_1, \phi_2)\,; \quad \frac{d\phi_2}{dt} = \omega_2 + \epsilon g_2(\phi_2, \phi_1) \tag{3-10}$$

where the coupling terms g_1 and g_2 are 2π-periodic in both arguments, and ϵ is the coupling coefficient.
Hence, as the interaction between the oscillators essentially effects the evolution of their phases if the frequencies ω_1 and ω_2 are in resonance, i.e. if for some integers n and m, $n\omega_1 = m\omega_2$ [*Rosenblum et al.*(2001)].
Then, in the first approximation, the Fourier expansion of the functions g_1 and g_2 contains slowly varying terms $\sim n\phi_1 - m\phi_2$ and under such assumption the *generalized phase difference* can be defined as,

$$\Phi_{n,m}(t) = n\phi_1(t) - m\phi_2(t), \tag{3-11}$$

Subtracting Eq.(3-10) and keeping only the resonance terms, we get

$$\frac{d\Phi_{n,m}}{dt} = n\omega_1 - m\omega_2 + \epsilon G(\Phi_{n,m}) \tag{3-12}$$

where $G(\cdot)$ is 2π-periodic. In addition, Eq. (3-12) is a one-dimensional ordinary differential equation that admits two types of solutions: fixed points or periodic rotations of $\Phi_{n,m}$. The

stable fixed point corresponds to perfect phase locking, when $\Phi_{n,m} = const.$ The periodic rotations describe quasi-periodic motion with two incommensurate frequencies in the system presented in Eq. (3-10) [*Rosenblum et al.*(2001)].
Finally, considering a small coupling in the Eq. (3-10), it is possible neglect the non-resonant terms. With non-resonant terms, the condition of synchronization of periodic oscillators should be generally written as a phase locking condition,

$$|n\phi_1(t) - m\phi_2(t) - \delta| = const., \tag{3-13}$$

where δ is some (average) phase shift, or as a frequency entrainment condition,

$$n\Omega_1 = m\Omega_2, \tag{3-14}$$

where

$$\Omega_{1,2} \approx \left\langle \frac{d\phi_{1,2}}{dt} \right\rangle \tag{3-15}$$

It is worth mentioning that in the synchronized state the phase difference is generally not constant but oscillates around δ.

3.10. Appendix B: Decomposition methods based on EMD

3.10.1. Empirical Mode Decomposition (EMD)

[*Huang et al.*(1998), *Huang et al.*(1999)] proposed that a time series, $x(t)$, can be expressed as,

$$x(t) = \sum_{j}^{n} (c_j(t)) + \zeta \tag{3-16}$$

where c_j correspond to the IMFs, and ζ the residual of data. The procedure can be summarized as follows [*Huang et al.*(1998)]: (1) The extreme maximum and minimum values are identified in $x(t)$, (2) the maximal values are connected using a cubic spline to find an upper envelope, $U_{max}(t)$. A similar procedure is carried out to the minimal values to find a lower envelope, $L_{min}(t)$, (3) the mean value between $U_{max}(t)$ and $L_{min}(t)$ is estimated [$\bar{U}(t) = \frac{U_{max}(t)-L_{min}(t)}{2}$], (4) the time series $\bar{U}$ is substrated of $x(t)$ [$d(t) = x(t) - \bar{U}(t)$], (5) the time series $d(t)$ is considered as the new $x(t)$ and then steps 1–4 are repeated until finding a signal with zero mean that is the first IMF, (6) The IMF is subtracted from the original time series $x(t)$ and the procedure is repeated to obtain the next IMF, and (7) stop the iterative process when $d(t)$ has only one maximum or one minimum value, so that it is not possible to extract more IMFs using $d(t)$.

3.10.2. Ensemble EMD (EEMD)

As mentioned above, [*Wu and Huang*(2005), *Wu and Huang*(2009)] proposed the EEMD as a modified version of the EMD method to solve the "mode mixing" problem. The procedure can be summarized as follows: (1) add white noise series to the original data $x(t)$, (2) apply the EMD method to $x(t)$ with added noise to find the IMFs, (3) repeat steps (1) and (2) several times and, (4) calculate the (ensemble) mean for each IMF, until finding stable values of the IMF for a given error level ϵ.

Finally, the added noise series cancel out each other and the mean IMFs remains within the natural dyadic filter windows significantly reducing the chance of mode mixing and preserving the dyadic property [*Flandrin et al.*(2004), *Wu and Huang*(2005), *Wu and Huang*(2009), *Wu et al.*(2008)]. This method is counter-intuitive because it uses multiple noise realizations added to a single time series to mimic a scenario of multiple trials of observations which are averaged for the corresponding IMFs allowing to extract scale-consistent signals [*Wu et al.*(2008)].

4. Generalized Synchronization between ENSO and hydrological variables in Colombia: A recurrence quantification approach

Hernán D. Salas, Germán Poveda, Óscar J. Mesa, and Norbert Marwan
Published in *Frontiers in Applied Mathematics and Statistics*

4.1. Abstract

We use Recurrence Quantification Analysis (RQA) to study features of Generalized Synchronization (GS) between El Niño-Southern Oscillation (ENSO) and monthly hydrological anomalies (HyAns) of rainfall and streamflows in Colombia. To that end, we check the sensitivity of the RQA concerning diverse HyAns estimation methods, which constitutes a fundamental procedure for any climatological analysis at inter-annual timescales. In general, the GS and its sensitivity to HyAns methods are quantified by means of time-lagged joint recurrence analysis. Then, we link the GS results with the dynamics of major physical mechanisms that modulate Colombia's hydroclimatology, including the Caribbean, the CHOCO and the Orinoco Low-Level Jets (LLJs), and the Cross-Equatorial Flow (CEF) over northwestern Amazonia (southern Colombia). Our findings show that RQA exhibits significant differences depending on the HyAns methods. GS results are similar for the HyAns methods with variable annual cycle but the time-lags seem to be sensitive. On the other hand, our results make evident that HyAns in the Pacific, Caribbean and Andean regions of Colombia exhibit strong (weak) GS with the ENSO signal during La Niña (El Niño), when hydrological anomalies are positive (negative). Results from the GS analysis allow us to identify spatial patterns of non-linear dependence between ENSO and the Colombian's climatology. The mentioned moisture transport sources constitute the interdependence mechanism and contribute to explain hydrological anomalies in Colombia during the phases of ENSO. During La Niña (El Niño), GS is strong (weak) for the Caribbean and the CHOCO LLJs whereas GS is moderate (strong) for the Orinoco LLJ. Moreover, moisture advection by

the Caribbean and CHOCO LLJs exhibit synchrony with HyAns at 0 to 2 (2 to 4) month-lags over north-western Colombia and the Orinoco LLJ moisture advection synchonizes with HyAns at similar month-lags over the Amazon region of Colombia. Furthermore, our results suggest a strong (weak) GS between negative (positive) Sea Surface Temperatures (SST) anomalies in the Eastern Pacific and rainfall anomalies in Colombia. In contrast, GS is strong (weak) for positive (negative) SST anomalies in the Central Pacific. Our GS results contribute to advance our understanding on the regional effects of both phases of ENSO in Colombia, whose socio-economical, environmental and ecological impacts cannot be overstated. This work provides a novel approach that reveals new insights into the impact of ENSO on northern South America.

4.2. Introduction

Synchronization is a well-known phenomenon that occurs when different oscillatory systems adjust the time scales of their oscillations due to mutual interaction [*Pikovsky et al.*(2001), *Balanov et al.*(2009)]. Diverse types of synchronization can be determined, such as frequency synchronization (FS), phase synchronization (PS), identical synchronization (IS), generalized synchronization (GS) and lag synchronization (LS) [*Brown and Kocarev*(2000)]. Particularly, GS emerges when the state of the driven system is completely determined by the state of the driving system [*rulkov*(1995)]. Hence, for two signals x and y that have a functional link $y \simeq f(x)$, GS techniques help to identify their synchronization or interrelationships even when their amplitudes behave differently. Diverse methods have been proposed to study synchronization such as those based on recurrences [*Schiff et al.*(1996), *Arnhold et al.*(1999), *Le Van Quyen et al.*(1999), *Quiroga et al.*(2002), *Zbilut et al.*(2006), *Marwan et al.*(2007)], phase differences [*Rosenblum et al.*(1997), *Tass et al.*(1998), *Pikovsky et al.*(2001), *Rosenblum et al.*(2001)], and quasi-simultaneous appearance of events [*Stolbova et al.*(2014), *Malik et al.*(2012), *Rheinwalt et al.*(2016), *Agarwal et al.*(2017)]. In particular, the method based on recurrences (recurrence plots and RQA) is based on properties from the non-linear dynamical systems such as the Poincaré Recurrence Theorem [*Poincaré*(1890)] and the Takens' theorem regarding the artificial reconstruction of strange attractors [*Takens*(1981), *Sauer et al.*(1991)]. In the last two decades, methods based on recurrences have proven to be very useful in different areas such as earth sciences, engineering, and applied physics, among others [*Marwan et al.*(2007), *Marwan*(2008), *Webber*(2014)]. Specifically, *join recurrence plots* (JRPs) have been used to study simultaneous recurrences and the detection of generalized synchronization in different systems [*Romano et al.*(2004)]. Recently, RQA has proved to be useful in diverse areas such as economy, physiology, earth sciences, astrophysics, and engineering [*Marwan et al.*(2007), *Webber*(2014)]. In particular, RQA has been used to investigate complex synchronization scenarios between coupled chaotic oscillators [*Feldhoff et al.*(2013)], emergence of GS in networks of structurally different time-delay systems [*Senthilkumar et al.*(2013), *Suresh et al.*(2016)], and precursors and synchronization of components of the tectonic system [*Hobbs*

and Ord(2018)], among others. The oscillatory nature of diverse hydroclimate phenomena is well known, such as those associated with the annual cycle of insolation (12 months), and the quasi-periodic El Niño-Southern Oscillation (3-4 years), which constitutes the most important modulator of interannual climate variability worldwide [*Sarachik and Cane*(2010)]. In turn, ENSO itself exhibits phase-locking with the annual cycle [*Stein et al.*(2011)], and affects the annual cycle of hydroclimatic variability in tropical South America and elsewhere [*Sarachik and Cane*(2010)]. Thus, GS and RQA provide powerful theoretical and quantitative frameworks to understand the non-linear interaction between ENSO and hydroclimatic processes in the region.

As far as we know, RQA has not been used to test the sensitivity of different methods to estimate hydro-climatic anomalies at interannual timescales (hereafter HyAns). In Chapter 2, we demonstrated that HyAns exhibit significant differences in terms of magnitude, timing, and sign, depending on the estimation method. Furthermore, we also demonstrated that linear and non-linear quantifiers of dependence can be significantly affected by how HyAns are defined (see Chapters 2 and 3). Then, in this work, we test the sensitivity of the GS metrics using the four HyAns methods assessed in Chapters 2 and 3, namely: *(i)* the Traditional Annual Cycle or constant climatology (HyAns–TAC), *(ii)* F-filtering of the Annual cycle by moving averages (HyAns–FAC), *(iii)* Annual cycle extracted by Singular Spectrum Analysis or Singular-Spectrum Annual Cycle (HyAns–SSAC) and, *(iv)* the Modulated Annual Cycle or variable climatology (HyAns–MAC). We also aim to provide advances regarding the robustness of the GS quantifiers based on recurrences for climate analysis at inter-annual timescales.

4.2.1. ENSO effects on hydro-climatology of Colombia

Colombia experiences positive (negative) anomalies in rainfall and streamflows, during the cold (warm) phase of ENSO, whose magnitude and timing vary across the main geographic regions of the country (Caribbean, Andes, Pacific, Orinoco and Amazon) [*Arias et al.*(2015), *Poveda and Mesa*(1997), *Poveda et al.*(2001), *Waylen and Poveda*(2002), *Poveda et al.*(2010), *Bedoya-Soto and Poveda*(2017), *Bedoya-Soto et. al.*(2018)]. Associated with those anomalies, there are extreme hydro-meteorological events of important socio-economical, environmental and ecological impacts. As such, the GS provides a new framework to further understand the impacts on ENSO on the hydroclimatology of Colombia, and the physical mechanisms responsible for such anomalies using a non-linear dynamical systems approach based on recurrences [*Marwan et al.*(2007)]. In general, we investigate GS between hydrological records of monthly series of rainfall and streamflows in Colombia and diverse variables related to moisture transport mechanisms influencing the Colombian hydrology during the extreme phases of ENSO. In particular, our GS-analysis is carried out at inter-annual timescales

considering the extreme phases of ENSO (La Niña and El Niño) separately. Three main moisture-ladden Low-Level Jets are considered as major mechanisms associated with hydroclimatic anomalies in Colombia, namely: *(i)* the Caribbean LLJ [*Wang*(2007)], *(ii)* the **Ch**orro del **O**ccidente **Co**lombiano (hereafter CHOCO LLJ) [*Poveda and Mesa*(2000), *Yepes et al.*(2019)], and *(iii)* the Orinoco LLJ [*Jiménez-Sánchez*(2019)] also known as the Eastern Andean LLJ or Corriente de los Andes Orientales (CAO) [*Montoya*(2001), *Torrealba and Amador*(2010)] (hereafter Orinoco LLJ). Furthermore, we also consider *(iv)* the Cross-Equatorial Flow (CEF) [*Wang and Fu*(2002)] as a possible mechanism of meridional moisture transport from the Amazon River basin to the Colombian territory. Additionally, in order to contrast our analysis with the available literature, we consider the SST gradient between the Pacific Ocean off the Colombian coast and the El Niño 1+2 zone, which makes part of the physical mechanism behind the CHOCO LLJ dynamics [*Poveda and Mesa*(2000)].
Also, we study the emergence of GS between two different types of ENSO and the Colombian hydrology, given that several recent works have shown that major SST warming has occurred frequently in the central Pacific (hereinafter CP El Niño), notably different from the eastern Pacific warming pattern during canonical El Niño events [*Sullivan et al.*(2016), Andreoli et al.(2017), Ashok and Yamagata (2007), Ashok and Yamagata (2009)] (hereinafter EP El Niño). Moreover, the CP El Niño exerts distinct socio-economical, environmental and ecological impacts around the globe [*Sullivan et al.*(2016), Andreoli et al.(2017), Ashok and Yamagata (2007), Ashok and Yamagata (2009)]. [Andreoli et al.(2017)] stated that the different SST anomaly patterns in the tropical Pacific affect the large-scale (Walker circulation and troposferic Rossby waves) and local atmospheric circulation patterns over northern South America producing different anomaly precipitation patterns. In particular, few works have studied the influence of the different types of El Niño events on Colombian's hydroclimatology [*Córdoba-Machado et al.*(2015), *Córdoba-Machado et al.*(2014), *Navarro-Monterroza et al.* (2019), *Serna et al.* (2018)]. Those works indicate that SST anomalies on the Eastern Pacific (EP) and the Central Pacific (CP) ocean are related with positive or negative hydrologic anomalies in the country depending on the location. At this point, there is not a clear consensus on the relationship between the different SST anomalies in the tropical Pacific and its influence on the hydrologic response in Colombia. Recently, [*Sullivan et al.*(2016)] proposed robusts indices for the EP El Niño, CP El Niño, and the Mixed-type El Niño, which are based on the normalized SST anomalies in the Niño3, Niño4, and Niño3.4 areas of the tropical Pacific Ocean, respectively. Therefore, we aim to quantify GS using those indices to infer clues on the influence of the different types of ENSO on Colombia hydrology.

4.2.2. Objectives

The objectives of this work are manifold: (i) To quantify non-linear inter-dependencies between the ENSO signal and the anomalies of hydrological variables in Colombia using the GS approach based on RQA; (ii) To assess the sensitivity of the GS-metrics based on

RQA using diverse methods used to define hydro-climatic anomalies; (iii) To evaluate the impact of ENSO on the Colombian hydrology though its effect on the sources of moisture that feed the water cycle dynamics over Colombia; (iv) To calculate GS between different types of El Niño indices (Central Pacific, Eastern Pacific, and Mixed) and the Colombian hydrology; and (v) To examine by means of GS metrics the propagation of the ENSO signals over Colombia.

To achieve the mentioned objectives we revise and characterize hydrological anomalies over Colombia during the phases of ENSO. Besides, a quantification of the linear and non-linear associations among the different variables seems necessary to elucidate new insights and explanations. In particular, we look for evidences about the influence of the aforementioned moisture sources on Colombian hydrology during ENSO. To that end, we consider the behavior of the moisture advection through the Caribbean, CHOCO, and Orinoco LLJs as well as the CEF during the phases of ENSO. Furthermore, our physical interpretation of GS results are based on Gill's theory [Gill (1980)] that states that weakening (strengthening) of the low-level winds is related to the increase (decrease) of the SSTs, which subsequently increase (decrease) of evaporation, increase (decrease) of moisture convergence, and increase (decrease) of rainfall in some regions [*Wang*(2007), *Martin and Schumacher*(2011), *Arias et al.*(2015)].

This work is outlined as follows: Section 4.3 describes the datasets and the region of study. Section 4.4 presents the RQA, the GS-index, the statistical tests for RQA. Results are discussed in Section 4.5 and the final remarks are drawn in Section 4.6.

4.3. Data and region of study

We use monthly rainfall and streamflows series from the five major regions of Colombia: Caribbean, Andes, Pacific, Orinoco and Amazon. Fig. **4-1** shows six macro-climatic zones, namely: Nino3.4 and Nino1+2 in the tropical Pacific Ocean, as well as the zones related to the Caribbean, CHOCO, and Orinoco LLJs, and the Cross Equatorial Flow (CEF). Details are provided in sections 4.3.1, 4.3.3, and 4.3.4.

4.3.1. The ENSO signal

Classification of the ENSO events

To classify the ENSO events, we use the monthly Multivariate ENSO Index (MEI) [*Wolter and Timlin (1998)*], which is based on six variables over the tropical Pacific: sea-level pressure, zonal and meridional surface wind components, sea and air surface temperatures, and

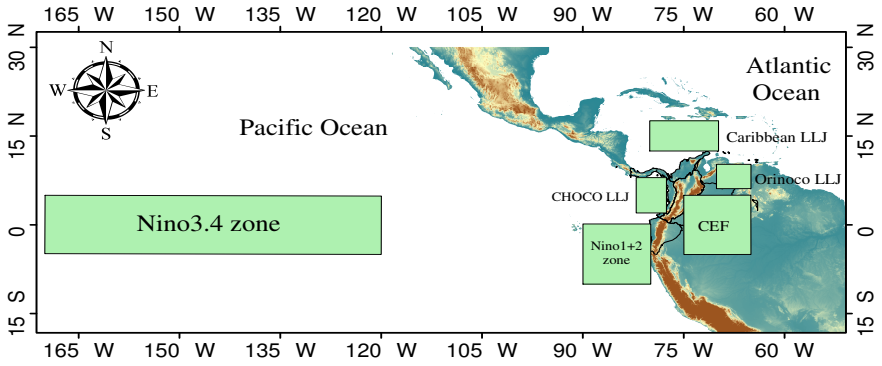

Figures 4-1.: Macro-climatic zones associated with the Colombian hydrology.

total cloud fraction. It is considered to be a more reliable estimator of the ENSO state compared to other indexes such as Nino3.4 (based solely on sea surface temperatures) or the Southern Oscillation Index (SOI), which is based on sea-level pressures [Rasmusson and Carpener (1982), Trenberth and Stepaniak (2001)]. Values of the MEI index greater (lesser) than +0.5 (-0.5) define the occurrence of El Niño (La Niña) events, whereas the remaining periods will be referred to as neutral. The information of precipitation and streamflows was classified according to El Niño and La Niña months, following the classification previously described.

Sea Surface Temperatures in the tropical Pacific Ocean – El Niño 3.4 zone (SST3.4)

We use the monthly Extended Reconstructed Sea Surface Temperatures (ERSSTv5) in the El Niño 3.4 region (hereafter SST3.4), in the area 5^o N–5^o S and 170–120^o W. Details in https://www.cpc.ncep.noaa.gov. The mentioned SST3.4 time series was filtered using a 12-month moving average filter to extract the inter-annual variability. Then, we calculate the GS index between SST3.4 and rainfall and streamflows series in Colombia.

Indices for different types of El Niño

A recent study proposed three simple indices to represent the EP El Niño, CP El Niño, and the mixed type of El Niño (Mixed-type), which can be used for understanding, prediction, and impact assessment [*Sullivan et al.*(2016)]. In general, those indices are based on the SST in the Niño3 and Niño 4 regions, which coincide with the areas that exhibit maximum SST warm anomalies of the EP and CP El Niño, respectively [*Sullivan et al.*(2016)]. Indices for EP type, CP type, and Mixed-type El Niño are calculated as [*Sullivan et al.*(2016)]:

- EP = Niño3normalized - 0.5 * Niño4normalized,
- CP = Niño4normalized - 0.5 * Niño3normalized,

- Mixed-type = EP + CP $\simeq$ Niño3.4normalized,

where Niño3normalized, Niño4normalized, and Niño3.4normalized denote the normalized SSTs anomalies in the Niño3 (5^{o}S–5^{o}N, 150^{o}W–90^{o}W), Niño4 (5^{o}S–5^{o}N, 160^{o}W–150^{o}W), and Niño3.4 (5^{o}S–5^{o}N, 170^{o}W–120^{o}W) regions, respectively [*Sullivan et al.*(2016)].
Fig. **4-2** shows the MEI index and its classification in La Niña, El Niño, and Neutral as explained in section 4.3.1. Furthermore, Fig. **4-2**a shows the EP El Niño index, Fig. **4-2**b shows the CP El Niño index and, Fig. **4-2**c shows the Mixed-type El Niño as defined by [*Sullivan et al.*(2016)].

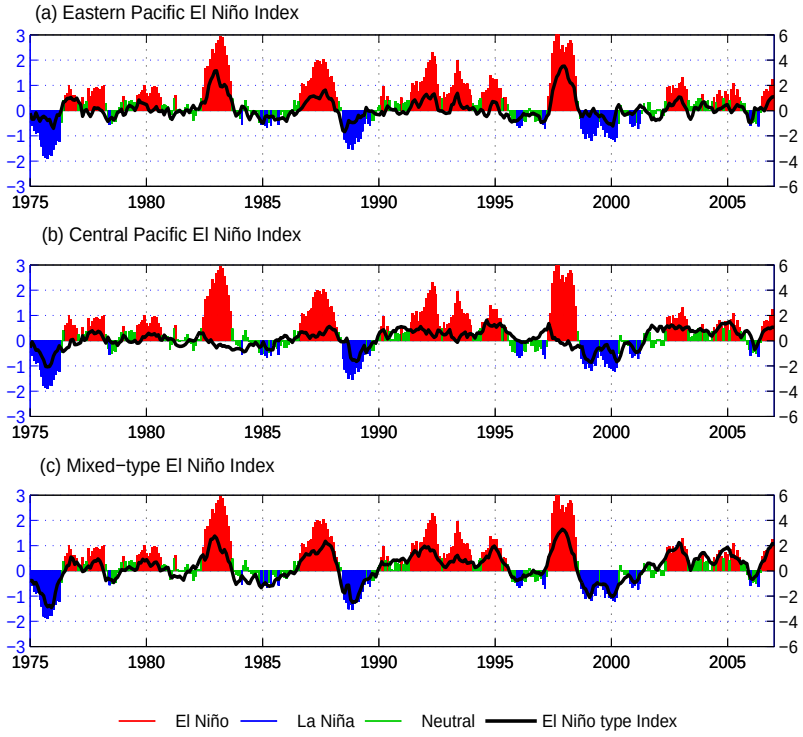

Figures 4-2.: Indices for different types of El Niño in the period 1975-2006: (left axis) MEI index denoting La Niña (blue), El Niño (red) and Neutral (green) phases of ENSO. (right axis- black line) Eastern Pacific (EP) type (top row), Central Pacific (CP) type (middle row), and Mixed-type(bottom row).

4.3.2. Colombian hydrology

Precipitation

- Dataset 1: We use data from a reanalysis of Colombian rainfall performed by [*Hurtado and Mesa*(2014)], which produced monthly precipitation fields, spanning the period

from 1975 to 2006, at a spatial resolution of 5 minutes of arc, in the region 5^{o}S-15^{o}N and 80^{o}W-65^{o}W. Those authors used a set of 2270 rain gauges from diverse institutions including Instituto de Hidrología, Meteorología y Estudios Ambientales de Colombia (IDEAM), Empresas Públicas de Medellín (EPM), Centro Nacional de Investigaciones del Café (CENICAFE) and The Global Historical Climatology Network (GHCN). In addition, they also used satellite information from the Global Precipitation Climatology Project(GPCP)-V2, National Centers for Environmental Prediction (NCEP)/National Center for Atmospheric Research (NCAR), Tropical Rainfall Measuring Mission (TRMM), and the Geostationary Satellite System (GOES). Finally, the monthly precipitation fields resulted from a combination of the available data and the implementation of the PRISM model over the Colombian territory. The resulting data set is freely available upon request to one the authors (O. J. M) [*Hurtado and Mesa*(2014)].

- Dataset 2: We also use data from a set of 937 rain gauges from IDEAM, at monthly resolution, having record lengths of 40 years, for the period 1976-2015, with less than 10% missing records. The geographical distribution of this data set is as follows: 38 time series in the Pacific, 631 in the Andes, 228 in the Caribbean, 30 in the Orinoco, and 10 in the Amazon region. See Fig. **4-3**b.

Streamflows

We use monthly average streamflows data from seven IDEAM's river gauging stations having common record lengths of 38 years, from 1976 to 2013 (see Table S1 in the Supp. Info). Furthermore, we use a set of 18 time series from XM (url: www.xm.com.co), at monthly time-scale, with record lengths 40 years from 1976-2015 (see Table S2 in the Supp. Info). Most river gauging stations are located in the Andean region, whereas long-term data in the Orinoco and Amazon regions are not available. See Fig. **4-3**a.
Table **B-1** details the sample size used to quantify dependency among diverse variables for each dataset. The samples were defined once each month is classified as El Niño, La Niña, and Neutral according to the MEI index (details in section 4.3.1).

Tables 4-1.: Sample size of monthly anomalies according to the phases of ENSO for each dataset.

		Total monthly data points		
Datasets	**Period**	**El Niño**	**La Niña**	**Neutral**
Hurtado & Mesa (2014)	1975-2006	158	65	161
IDEAM–Precipitation	1976-2015	193	85	202
IDEAM–Streamflows	1976-2013	176	85	195
XM–Streamflows	1976-2015	193	85	202

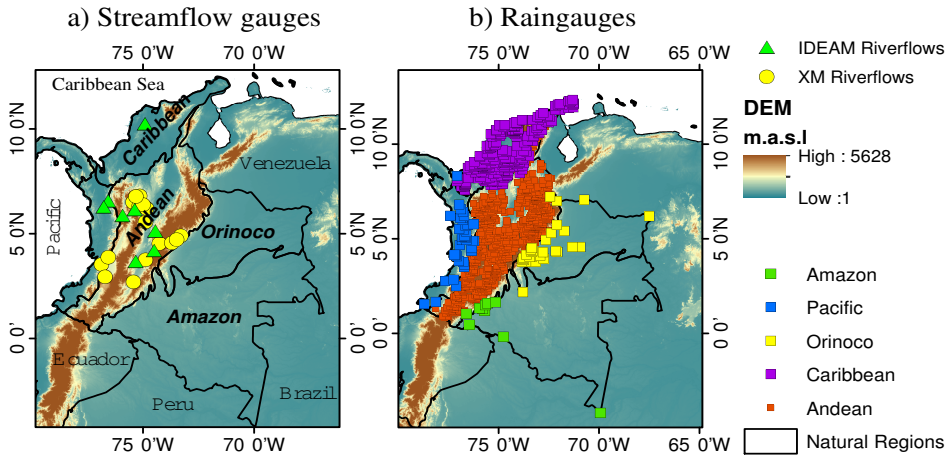

Figures 4-3.: National context including the Colombian Natural Regions as well as the streamflows and rainfall gauges. a) Streamflow gauges. b) Raingauges.

4.3.3. Moisture Advection through Low-Level Jets

In order to investigate the influence of the Low Levels Jets (LLJs) as rainfall-generating moisture transport mechanisms and therefore as physical mechanisms behind the emergence of GS, we use data from the NCEP/NCAR Reanalysis Project [*Kalnay et al.*(1996)]. Moisture advection is calculated as the product between the monthly mean zonal winds and the monthly mean specific humidity at 925 hPa. In particular, moisture advection is calculated over the following geographic zones, which are associated with the three LLJs surrounding Colombia, namely: (i) The Caribbean LLJ moisture advection is calculated over the region 12.5^{o}N–17.5^{o}N, 80^{o}W–70^{o}W. This region is selected based on the work by [*Wang*(2007)], who studied the variability of the Caribbean LLJ; (ii) The CHOCO LLJ moisture advection is quantified over the region 2^{o}N–8^{o}N, 82^{o}W–77.5^{o}W. This region was used in study [*Poveda and Mesa*(2000)], which deals with the characterization and influence of the CHOCO LLJ on ocean-land-atmosphere interactions over the far eastern Pacific; and (iii) The Orinoco LLJ moisture advection is calculated over the region 6^{o}N–10^{o}N, 70^{o}W–65^{o}W. This region is located over the vast Llanos (plains) region over the Colombia-Venezuela border and, selected according to previous works [*Montoya*(2001), *Jiménez-Sánchez*(2019), *Torrealba and Amador*(2010)].

In particular, the CHOCO LLJ dynamics is related to the SST gradient in the far eastern tropical Pacific. That is, the surface air temperature gradient between the Pacific Ocean off the Colombian coast (2^{o}N–8^{o}N, 77.5^{o}W–82^{o}W) and the El Niño 1+2 region (10^{o}S–0^o, 90^{o}W–80^{o}W) from the sea level to 925 hPa [*Poveda and Mesa*(2000)]. Hence, we calculate the SST gradient between both zones and its association with rainfall and streamflows in Colombia using the GS metrics. We will contrast the GS results obtained between ENSO and the Colombian hydrology (rainfall and streamflows) with those obtained between LLJs

and the Colombian hydrology to infer similarities and differences.

4.3.4. The Amazonian Cross-Equatorial Flow

The Cross-Equatorial Flow can be related to the hydrological dynamics over eastern and southeastern Colombia (Orinoco and Amazon regions) and the northern-most Amazon basin [*Wang and Fu*(2002)]. Hence, as in the previous section, we estimate the moisture advection as the product between the mean meridional winds and the mean specific humidity at 925 hPa, using data from the NCEP/NCAR Reanalysis Project [*Kalnay et al.*(1996)], over the region 5^oS–5^oN, 65^oW–75^oW [*Wang and Fu*(2002)].

4.4. Methods

4.4.1. Generalized synchronization using the Recurrence Quantification Analysis

Recurrence in phase space is a fundamental property of diverse types of dynamical systems [*Marwan et al.*(2007)]. This recurrence behavior can be characterized and quantified by means of the so-called Recurrence Plot (RP), which is a modern tool of non-linear data analysis that allows to visualise and quantify properties of higher-dimensional phase space trajectories [*Eckmann et al.*(1987)]. The construction of the RP from a time series, x_i, requires the representation of the m-dimensional phase space of the system X. For single time series, x_i, it is necessary to reconstruct the dynamics using the time delay embedding technique as [*Packard et al.*(1980), *Takens*(1981)],

$$\vec{x_i} = \left(x_i, x_{i+\omega}, ..., x_{i+\omega(m-1)}\right), \qquad \vec{x_i} \in R^m \tag{4-1}$$

where m is the embedding dimension and ω is the time delay. The false nearest neighbors (FNN) is the most used method to quantify m, whereas the Auto- Information Function (AIF) is commonly used to quantify the time-delay [*Marwan et al.*(2007), *Fraser and Swinney*(1986), *Kantz and Schreiber*(2004), *Marwan*(2011)]. Once m and ω have been estimated, the RP is calculated using the pair-wise proximity test to obtain the recurrence of X for the times i and j as,

$$R_{ij}^X = \Theta(\epsilon - ||\vec{x_i} - \vec{x_j}||), \qquad i, j = 1, ..., N' \tag{4-2}$$

where N is the number of data points, $N' = N - (m-1)\omega$ is the dimension of phase space vectors, ϵ is the threshold to the proximity between the phase space vectors. According to the literature, ϵ must be selected as a few percent (not larger than 10 %) of the maximum

phase space diameter [*Webber*(2014), *Mindlin and Gilmore*(1992), *Zbilut and Webber*(1992)]. $||\vec{x_i} - \vec{x_j}||$ is the spatial distance between vectors in phase space. $||\cdot||$ denotes any norm in phase space (e.g., Manhattan, Euclidean, or maximum norm) [*Webber*(2014)], and $\Theta(\cdot)$ is the Heaviside function such as $\Theta(x) = \{1 \mid x > 0; 0 \mid x \leq 0\}$ [*Marwan et al.*(2007)]. The plot of the recurrence binary matrix R^X provides the RP. Then, the probability that one system recurs to a certain state $\vec{x}_i$ is equal to the column-average of the recurrence matrix [*Marwan et al.*(2007)].

$$p(\vec{x}_i) = \frac{1}{N'} \sum_{j=1}^{N'} R^X_{i,j} \tag{4-3}$$

On the other hand, the Joint Recurrence plot (JRP) is used to study the possible influence between two different physical systems, constituting a measure of their simultaneous recurrence. The *joint recurrence matrix* is defined as the Hadamard product of the RPs of the single RPs of systems X and Y [*Marwan et al.*(2007), *Romano et al.*(2004), *Marwan et al.*(2013)],

$$JR^{X,Y}_{i,j} = \Theta(\epsilon - ||\vec{x}_i - \vec{x}_j||) \times \Theta(\epsilon - ||\vec{y}_i - \vec{y}_j||) \tag{4-4}$$

Hence, the probability of finding a simultaneous recurrence at time i in both systems X and Y is equal to the column-average of the JR^{XY} matrix [*Marwan et al.*(2013)],

$$p(\vec{x}_i, \vec{y}_i) = \frac{1}{N'} \sum_{j=1}^{N'} JR^{X,Y}_{i,j} \tag{4-5}$$

The same procedure can be carried out considering the relationship between the system X and the time lagged system $Y(\tau)$. Then, if both systems X and the time lagged $Y(\tau)$ are independent, $p(\vec{x}_i, \vec{y}_{i+\tau}) = p(\vec{x}_i)p(\vec{y}_{i+\tau})$. In contrast, if both systems are in GS, we expect approximately the same recurrences, $p(\vec{x}_i, \vec{y}_{i+\tau}) \approx p(\vec{x}_i) \approx p(\vec{y}_{i+\tau})$.
The computation of the recurrence matrices is most appropriate using a fixed amount of nearest neighbors, N_n, for each column in the matrix than a fixed threshold [*Marwan et al.*(2007), *Arnhold et al.*(1999)]. This corresponds to the original definition of RP [*Eckmann et al.*(1987)]. Therefore, according to [*Marwan et al.*(2007)], $p(\vec{x}_i)$ and $p(\vec{y}_{i+\tau})$ are equal and fixed by N_n. i.e. $p(\vec{x}_i) = p(\vec{y}_{i+\tau}) = N_n/N$. Taking the *recurrence rate* (RR) as $RR = N_n/N$,

$$S(\tau) = \frac{p(\vec{x}_i, \vec{y}_{i+\tau})}{RR} \tag{4-6}$$

where $S(\tau)$ is a time series with values ranging between 0.0 and 1.0, and τ is a time-lag between timeseries x_i and $y_{i+\tau}$ [*Marwan et al.*(2007)]. Consequently, it is possible to define a

global index for GS based on the average *joint probability of recurrence* (hereafter GS-index) by choosing the maximum value of $S(\tau)$ and normalizing it [*Marwan et al.*(2007)],

$$GS = max_{\tau} \frac{S(\tau) - RR}{1 - RR} \tag{4-7}$$

where GS ranges from 0 (independent) to 1 (correlated). In order to avoid potential pitfalls in RQA, our procedures are based on pivotal literature on recurrences [*Marwan et al.*(2007), *Marwan*(2011), *Webber*(2014)].

4.4.2. Significance tests

The existence of GS between the systems $X(t)$ and $Y(t + \tau)$ requires a statistical test to verify the significance of the GS-index at time-lag τ. Consequently, it is possible to test the significance of the GS-index based on the joint recurrence matrix between the trajectory in phase space of the original system X (ENSO in our case) and a representative number of phase space trajectories of the system Y (precipitation and streamflows in our case), which are independent copies of the underlying system Y (also called twin surrogates –TS) [*Thiel et. al.*(2006), *Thiel et. al.*(2008)]. This ensures surrogates that are uncorrelated or not synchronized with each other. Then, TS are phase space trajectories sharing the same neighborhood up to the threshold ϵ such that $R^X_{i,k} = R^X_{j,k}$, $k = 1, ..., N'$. In this work, TS are constructed using the algorithm by [*Thiel et. al.*(2006), *Thiel et. al.*(2008)], which is included in the CRP Toolbox for MATLAB provided by TOCSY, available at http://tocsy.agnld.uni-potsdam.de [*Marwan et al.*(2007)].
The null hypothesis is that each TS is an independent trajectory of the system, corresponding to different initial conditions. In this work, we test the significance of the GS-index between X and $Y(\tau)$ using 100 TS of the Y system (hydrological variables). i.e. to calculate the GS-index for each pair of X and the TS and obtain their distribution. Finally, we compare the GS-index for the original time series $x(t)$ and $y(t)$ with the 95th percentile (95% confidence boundary) of the test distribution. The time-lags τ where the GS-index, $GS(\tau)$, takes values out the confidence band imply values for which the null hypothesis is rejected. i.e. the systems X and Y are significantly dependent. In order to test for the null hypothesis, we carry out a multiple testing procedure following the Sidák-Bonferonni equations [Holm (1979), *Abdi*(2007)], and perform 5 independent tests limiting the risk of making at least one Type I error to an overall value of $\alpha[PF] = 0.05$ (PF means *alpha per family of tests*) and then we use $\alpha[PT] \approx 0.01$ (PT means *alpha per test*).

4.4.3. Joint Probability of Recurrences during ENSO

Taking into account that precipitation and streamflows exhibit different kind of anomalies depending on the ENSO phase (warm or cold), we quantify the probability of joint recurrence,

$p(\vec{x}_i, \vec{y}_i)$, at time i (Eq. 4-5) for the cold (La Niña) and warm (El Niño) phases of ENSO separately. After that, we calculate the *joint recurrence matrix* (Eq. 4-4) and then $p(\vec{x}, \vec{y}(\tau))$, where τ is the time-lag. Then, we look for the columns in the JRP that correspond to the classification of ENSO phases as per the MEI index (section 4.3.1). Finally, we calculate $p(\vec{x}_i, \vec{y}_i)$ during La Niña and El Niño conditions.

For the different types of El Niño indices (EP, CP and Mixed-type), we carry out a similar procedure. We quantify the probability of joint recurrence, $p(\vec{x}_i, \vec{y}_i)$, for each index using all data and also periods as per the MEI classification, separately.

4.4.4. Sensitivity of the GS metrics to diverse HyAns methods

Diverse methods commonly used to estimate hydro-climatic anomalies (HyAns) exhibit differences that may induce strong biases and error sources toward the interdependence analysis and modeling of climate time series (see Chapter 2). Such differences may generate ambiguities for the physical interpretation of results (see Chapter 2), and thus the need to consider the uncertainty in HyAns estimation and its consequences for quantification of interdependence using linear and non-linear techniques. In this sense, in Chapter 3 we showed that phase synchronization metrics based on Generalized Phase Differences [*Rosenblum et al.*(2001)] are sensitive to seasonal-residual frequencies in time series of anomalies.

Hence, we verify the sensitivity of GS metrics based on RQA using the four HyAns methods assessed in Chapters 2 and 3, namely: *(i)* the Traditional Annual Cycle or constant climatology (HyAns–TAC), *(ii)* **F**-filtering of the Annual cycle by moving average (HyAns–FAC), *(iii)* Annual cycle extracted by Singular Spectrum Analysis or Singular-Spectrum Annual Cycle (HyAns–SSAC) and, *(iv)* the Modulated Annual Cycle or variable climatology. In this way, we evaluate the robustness of our GS approach in relation to the diverse HyAns estimation methods.

As mentioned in Chapter 2, the HyAns–FAC method is appropriate for climatological purposes owing to the following properties: (i) a firm mathematical foundation, (ii) a varying climatology (annual cycle), (iii) an adequate separation of noise, intra-annual, seasonal and inter-annual components, since (iv) it does not leave significant residual seasonal frequencies in HyAns, (v) its extreme values are in a middle range in comparison with the HyAns–SSAC and HyAns–MAC methods, (vi) its autocorrelation function is comparable with HyAns–SSAC and HyAns–MAC, and (vii) its computational cost is one-tenth of HyAns–SSAC and hundredths times less than HyAns–MAC.

4.5. Results and discussion

4.5.1. Rainfall anomalies in Colombia and their association with ENSO by means of Pearson correlations

First, we quantify rainfall anomalies over Colombia considering both phases of ENSO (El Niño and La Niña), as explained in section 4.3.1. Rainfall anomalies were calculated using a F-Filtering of the annual cycle by moving averages, which filters out adequately the seasonal signal [Douglass (2011), Douglass (2015)]. Fig. **C-11** shows that during La Niña, Colombia experiences wetter (drier) than normal periods in the Pacific, Andean and Caribbean (Orinoco and Amazon) regions. In contrast, during El Niño, Colombia evidences drier (wetter) than normal periods in the Pacific, Andean and Caribbean (Orinoco and Amazon) regions. On the other hand, Fig. **C-11** shows that, during La Niña (El Niño), the Orinoco and Amazon regions exhibit negative (positive) rainfall anomalies throughout the year. It is worth noting that the influence of both phases of ENSO on streamflows in the Amazon region of Colombia does not show a clear-cut pattern of positive or negative anomalies [*Arango-Ruda and Poveda*(2018)]. Hence, ENSO's influence on rainfall anomalies in Colombia depends on the phase of ENSO (La Niña or El Niño) and the region of the country.
Second, we quantify the linear association between SST anomalies in the tropical Pacific and rainfall anomalies over Colombia during ENSO using Pearson correlations, r. We calculate r using the complete monthly time series to capture the big picture. Fig. **4-5** suggests that positive (negative) rainfall anomalies over the Pacific, the Andean and the Caribbean regions are significantly correlated with negative (positive) SST anomalies in the tropical Pacific Ocean. Furthermore, the spatial patterns of statistical significance of r are in agreement with the spatial patterns of positive (negative) rainfall anomalies in Colombia during ENSO (see Fig. **C-11**). However, it is worth noting that correlation patterns between SST3.4 anomalies and rainfall anomalies could differ during the phases of ENSO, and that Pearson correlations only quantify the linear association. This points out the need to explore non-linear techniques to quantify the dependence between hydrological anomalies in Colombia and the ENSO signal considering La Niña and El Niño phases.

4.5.2. Moisture Advection Anomalies by LLJs during ENSO

Low-Level Jets (LLJs) are important rainfall-formation mechanisms and their non-linear interdependence with hydroclimatology requires an adequate characterization of moisture advection anomalies [*Bonner* (1968), *Stensrud* (1996), *Gimeno et al.* (2016), *Hoyos et al.*(2017)]. To that end, we characterize the annual cycle of moisture advection anomalies by the Caribbean LLJ, the CHOCO LLJ, and the Orinoco LLJ as well as by the Cross-Equatorial Flow (CEF) during the phases of ENSO. To this end, we use data from the NCEP/NCAR Reanalysis Project [*Kalnay et al.*(1996)] and calculate moisture advection as the product

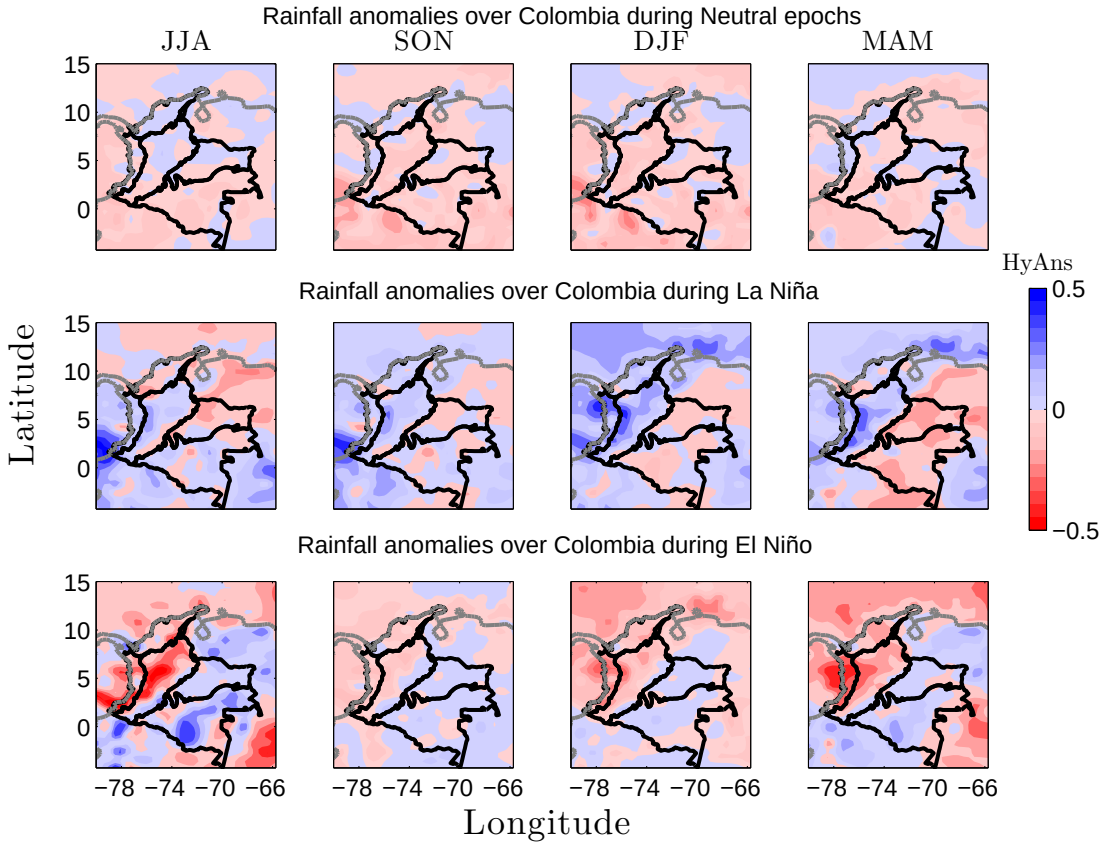

Figures 4-4.: Seasonal average rainfall anomalies (HyAns) in Colombia during ENSO. Data set No. 1. Rainfall anomalies were calculated using F-Filtering of the annual cycle by moving averages, which is previously mentioned as the HyAns–FAC method. (gray line) northern South American coast line. (black line) Borders of the Colombia's natural regions.

between the mean zonal or meridional winds and the mean specific humidity at 925 hPa averaged over the geographic areas described in section 4.3.3. We estimate moisture advection anomalies in such a way that positive or negative anomalies represent increase or decrease of moisture advection, respectively. Furthermore, after an exhaustive verification of NCEP/NCAR 925 hPa data in the period 1970-2015, the moisture advection by the Caribbean and the Orinoco LLJs have a predominant easterly direction whereas the moisture advection by the CHOCO LLJ exhibits a clear-cut westerly direction during 80% of time. Likewise, the CEF exhibits dominant northerly (southerly) moisture advection from October to March (April to September).

Fig. **4-6**a shows that the Caribbean LLJ exhibits positive (negative) zonal moisture advection anomalies during El Niño (La Niña) for the period from May to November, with a peak in July for both positive and negative cases, which coincides with the variation of Caribbean LLJ winds during June-July-August (JJA) and December-January-February

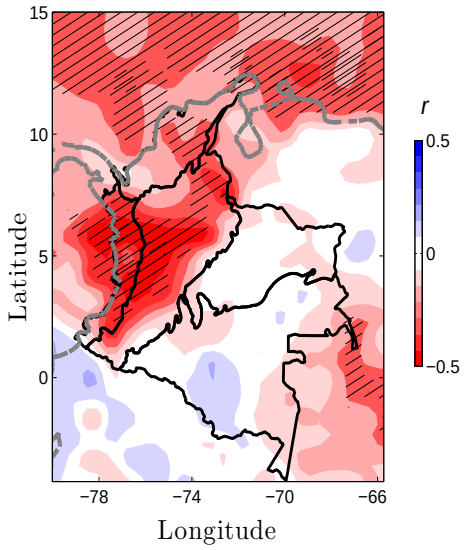

Figures 4-5.: Pearson correlation, r, between rainfall anomalies in Colombia and SST3.4 anomalies. (dashed gray line) nothern South American coast line. (black line) Borders denote Colombia's natural regions. The hatched areas indicate that r is significant at 5%. The significance levels are calculated considering the Effective Degrees of Freedom due to autocorrelation in timeseries [Afyouni et al. (2019)]

(DJF) [*Wang*(2007), *Martin and Schumacher*(2011)]. In particular, this result coincides with the observation that during La Niña, the easterly Caribbean LLJ winds are weak (strong) in JJA (DJF), whereas during El Niño, the easterly Caribbean LLJ winds are strong (weak) in JJA (DJF) [*Wang*(2007)]. Furthermore, Fig. **4-6**b shows that zonal moisture advection anomalies by the CHOCO LLJ are positive (negative) during La Niña (El Niño) from July to December. These results are consistent with those reported by [*Poveda and Mesa*(2000)]. Moreover, Fig. **4-6**c shows that moisture advection anomalies by the Orinoco LLJ are positive (negative) during El Niño (La Niña) in JJA. Finally, Fig. **4-6**d shows that the CEF exhibits positive (negative) moisture advection anomalies during La Niña (El Niño) from April to October for the southerly winds, whereas the CEF exhibits negative (positive) during La Niña (El Niño) from November to March for the northerly winds.
The annual cycles of moisture advection anomalies, as well as the annual cycle of hydrological anomalies during ENSO, are important information sources for the interpretation of results of non-linear metrics such as GS. In the following sections, we will revisit these findings in order to interpret the GS results from a physical point of view.

4.5.3. Time Delay and Embedding Dimension

Detection of GS using the recurrence quantification analysis (RQA) requires to adequately

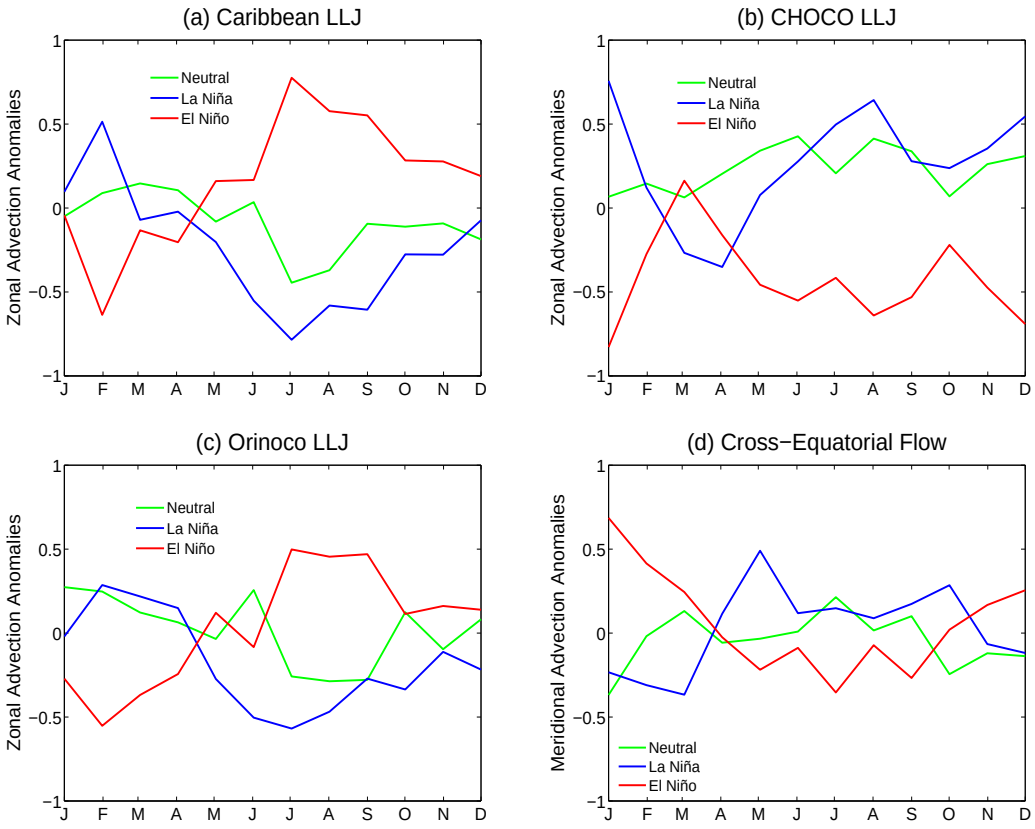

Figures 4-6.: Annual cycle of standardized moisture advection anomalies during ENSO using data from the NCEP/NCAR Reanalysis Project for the period 1970-2015. (a) Zonal moisture advection by the Caribbean LLJ. (b) Zonal moisture advection anomalies by the CHOCO LLJ. (c) Zonal moisture advection anomalies by the Orinoco LLJ. (d) Meridional moisture advection by the Cross-Equatorial Flow.

select the time delay, ω, and the embedding dimension, m. The time delay, ω, for each time series is calculated as the time that the *auto information function* (AIF) takes to decay to $1/e$ of its value at zero lag (see section 4.4.1). Figure **4-7** (panel a) shows that all the time series exhibit an exponential decay until a time delay $\omega \approx 8$ months. The embedding dimension, m, is calculated using the *false nearest neighbors* (FNN). Figure **4-7** (panel b) shows that according to FNN an appropriate embedding dimension for all time series is $m = 2$.

Hereafter, all analyses are carried out using the fixed amount of nearest neighbors (FAN) whereas the significance tests are based on 100 twin surrogates. On the other hand, in this work, the threshold of proximity between the phase space vectors was selected as $\epsilon = 10\%$ according to Refs. [*Webber*(2014), *Mindlin and Gilmore*(1992), *Zbilut and Webber*(1992)].

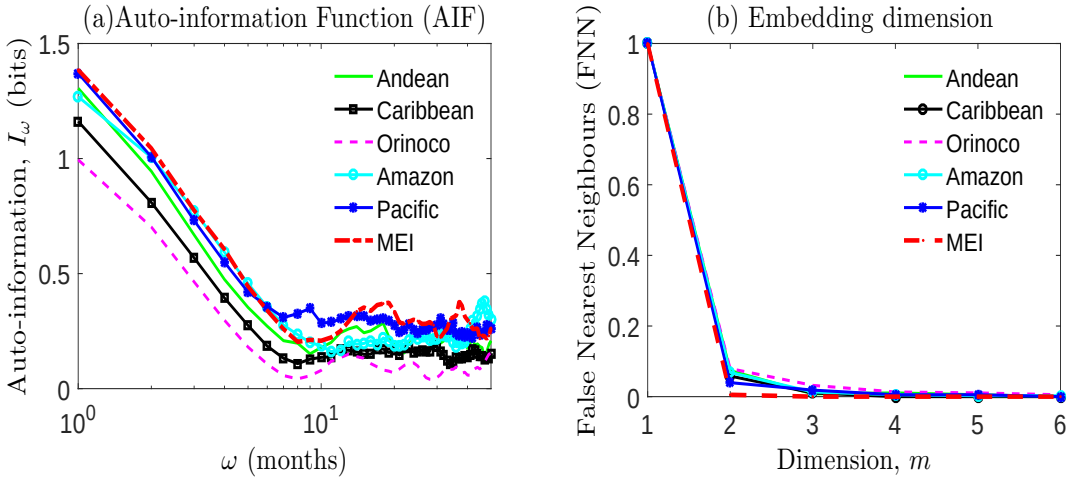

Figures 4-7.: Estimation of the time delay and the embedding dimension for monthly precipitation averaged over the natural regions of Colombia (from data set No. 1) and MEI index. (a) Time delay, ω, using the auto-information function (AIF). (b) Embedding dimension, m, using *false nearest neighbors* (FNN).

4.5.4. Sensitivity of the GS-metrics regarding diverse HyAns methods

We use a time series of rainfall anomalies for the Andean region (monthly precipitation spatially averaged over the Andean region) and quantify the GS-index using the four HyAns methods: HyAns–TAC, HyAns–FAC, HyAns–SSAC, and HyAns–MAC (see Chapter 2 and section 4.4.4). To that end, we select sample data classified according to El Niño and La Niña months, as per the MEI definition (see section 4.3.1). Fig. **4-8** shows the GS-index for the mentioned HyAns methods. In general, our findings reveal that the HyAns–TAC method exhibits the lowest GS values in relation to the other methods, during both La Niña and El Niño. This behavior can be explained by the presence of noise, intra-annual and significant-residual seasonal frequencies in anomalies, when those are estimated using HyAns–TAC (see Chapter 2). Hence, we consider that the HyAns–TAC method is not reliable for the RQA and purposes of this study.

In addition, Fig. **4-8** shows the GS-index between the ENSO signal and rainfall anomalies using diverse HyAns methods. In general, the GS-index exhibits higher values during La Niña than during El Niño, for the HyAns–FAC, HyAns–SSAC and HyAns–MAC methods. In this sense, [*Poveda and Mesa*(1996), *Poveda and Mesa*(1997)] showed that the ratio between hydrological anomalies and the long-term mean is higher during La Niña than during El Niño. In agreement with this finding, we showed in Chapter 3 that the strength of phase synchronization index between rainfall anomalies and the ENSO signal also is stronger during La Niña than during El Niño.

In terms of the time-lag between the ENSO signal and rainfall anomalies over the Andean region of Colombia, Fig. **4-8** shows that during La Niña, the HyAns–FAC, HyAns–SSAC,

and HyAns–MAC methods suggest a 2 to 4 months-lag whereas, during El Niño, the HyAns–FAC and HyAns–SSAC methods show a 4 to 6 months-lag. Furthermore, the HyAns–FAC and HyAns–MAC methods show time-lag differences during El Niño. As a conclusion, the magnitude of the GS-index is not highly sensitive to the diverse HyAns methods whereas the time-lag between time series could be affected by the HyAns methods.
Hereafter, time series are filtered using the F-filtering of the annual cycle by a moving average procedure (HyAns–FAC) in order to remove the intra-annual, semi-annual and annual frequency bands. Furthermore, we verify that the time series only contain information at inter-annual timescales using the test by [*Ahdesmäki, et al.*(2005)].

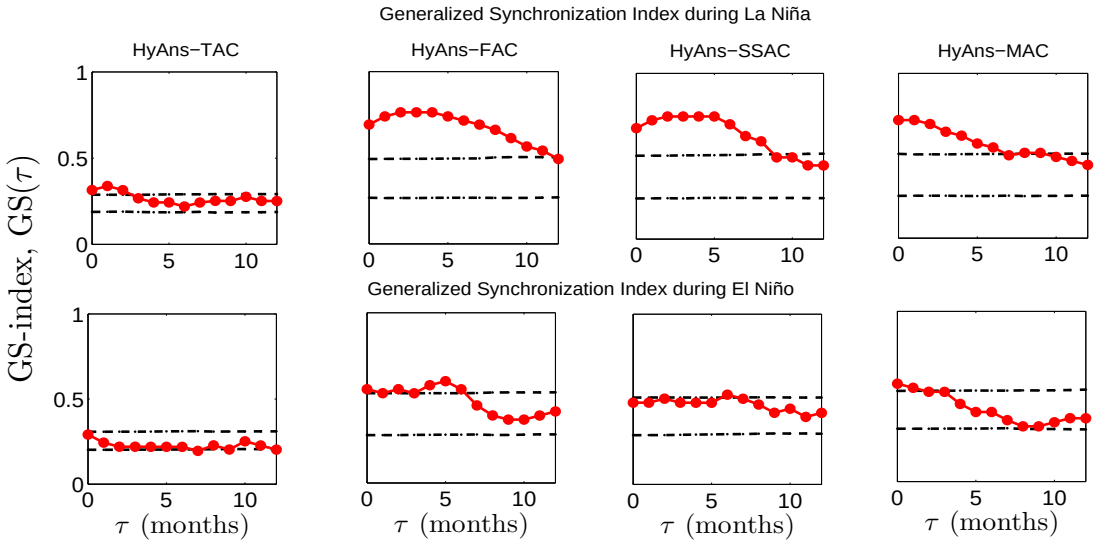

Figures 4-8.: Generalized synchronization index (GS-index) between the ENSO signal (MEI index) and monthly rainfall anomalies in the Andean region estimated using the four HyAns methods: HyAns–TAC, HyAns–FAC, HyAns–SSAC, HyAns–MAC. (top row) La Niña and (bottom row) El Niño. Period 1976-2015. τ denotes the time lag. (dashed black lines) 95% confidence boundaries.

4.5.5. GS between SST3.4 anomalies and hydrological anomalies in Colombia

As a first step, we quantify GS between SST3.4 anomalies and rainfall and streamflows anomalies over Colombia. In general, Fig. **4-9** evidences that rainfall anomalies are in GS with SST anomalies in the central tropical Pacific. In particular, the GS calculation using all data points, regardless of ENSO phases, leads to lower GS-values but whose significant values are consistent with the results considering the Neutral, La Niña, and El Niño. Furthermore, our findings show that the GS is strong (weak) during La Niña where rainfall exhibits positive

(negative) anomalies. The lowest GS values are shown in the Neutral condition. During La Niña, the GS occurs mainly over western Colombia, that is the northern and western Andean region as well as the Pacific and the Caribbean regions. In turn, mentioned regions exhibit positive rainfall anomalies. Note that the Amazon region also exhibits significant GS but, during this cold phase of ENSO, rainfall anomalies are negative. During El Niño, the GS is significant mainly over the Pacific and the Andean regions where rainfall exhibits negative anomalies. At this point, our results confirm the influence of both ENSO phases over Colombia [*Poveda and Mesa*(1997), *Poveda et al.*(2010)]. Moreover, our findings confirm that those regions exhibiting strong (weak) phase synchronization during La Niña (El Niño) also exhibit GS (see Chapter 3). Hence, the systems (ENSO and rainfall in some regions of Colombia) exhibit a functional relationship.

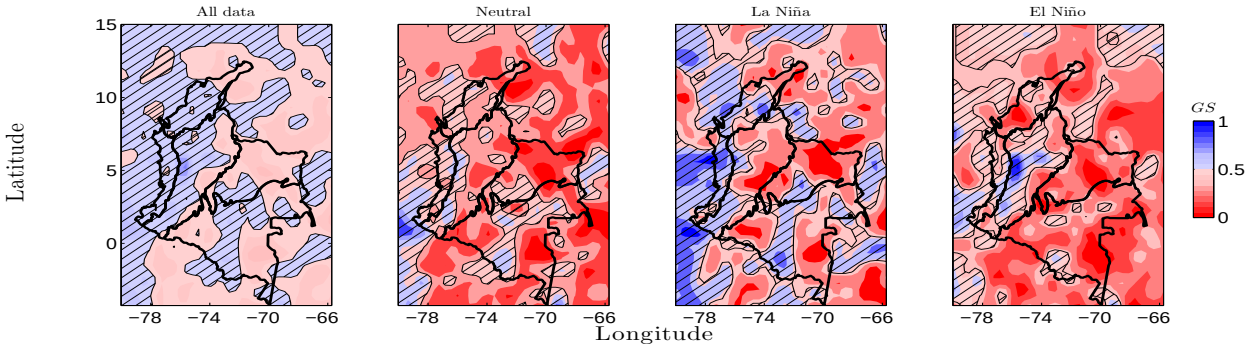

Figures 4-9.: Generalized Synchronization Index between SST3.4 anomalies and rainfall anomalies in Colombia, Data set No. 1, period 1975-2006. The hatched contours indicates zones where the GS is significant at 5%.

On the other hand, streamflows are the hydrological response to interactions, at catchment scale, between landscape characteristics (soils, vegetation, geology, the topology of drainage networks, hydraulic properties, etc) and climate and weather events [*Troch et al.*(2013)]. In addition, the catchment plays a filtering role to the high frequency nature of precipitation in association with evapotranspiration and soil moisture dynamics [*Andrés-Doménech et al.*(2015)]. In this sense, it is to be expected that marked long-term patterns of precipitation appear also in long-term characteristics of streamflows. Fig. **4-10** shows the GS index between SST3.4 anomalies and streamflow anomalies. Our results are consistent with those found for rainfall anomalies. First, our findings demonstrate that using all data points, regardless of ENSO phases, leads to lower GS-values. Furthermore, the GS index is higher during La Niña than during El Niño. In particular, streamflow anomalies exhibiting strong GS are located in the Caribbean region and the north-western Andean region. These results could be associated with the GS-patterns between rainfall anomalies and moisture advection from the Caribbean and CHOCO LLJs discussed next.

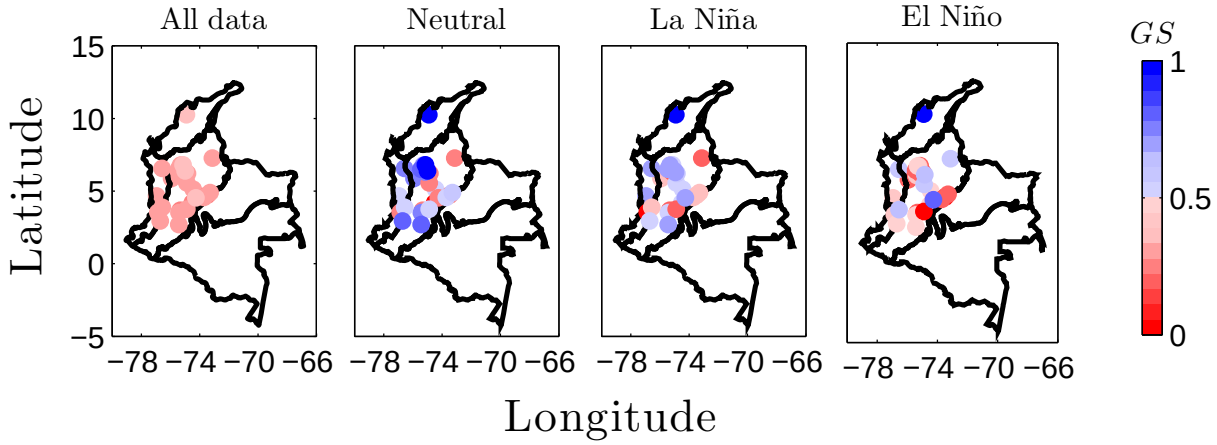

Figures 4-10.: Generalized Synchronization Index between SST3.4 anomalies and river flow anomalies from the IDEAM and XM datasets, period 1976-2013.

4.5.6. GS between the moisture advection by Low-Level Jets and rainfall in Colombia

- **GS between the Caribbean LLJ moisture advection anomalies and rainfall anomalies**

  Fig. **4-11** shows the GS-index between the moisture advection of the aforementioned low-level jets (LLJ) and rainfall anomalies throughout Colombia, the columns denote the GS-results considering all data and the different samples for the phases of ENSO (Neutral, La Niña and El Niño). Fig. **4-11** (top row) shows the GS-index between the moisture advection by the Caribbean LLJ and rainfall anomalies in Colombia. Our results reveal that rainfall anomalies over the Caribbean, the northern-Pacific, and the northern-Andean regions are related to moisture advection by the Caribbean LLJ. In particular, during La Niña, the GS-index exhibits the strongest values and the largest area, whereas during El Niño the GS-values and area of influence are smaller. These findings are in support of the Caribbean LLJ influence on the hypothesis that the Caribbean LLJ influence the hydro-climatic response over northern South America and, particularly, over northern Colombia [*Wang*(2007), *Martin and Schumacher*(2011), *Arias et al.*(2015)]. Furthermore, these results confirm the influence of the Caribbean LLJ anomalies during ENSO on the positive (negative) rainfall anomalies over northern Colombia. [*Wang*(2007)] and [*Martin and Schumacher*(2011)] showed that during JJA, rainfall in the Caribbean (including the Caribbean region of Colombia) exhibits significant correlations with the Caribbean LLJ index. Moreover, it is postulated that the Caribbean LLJ induces changes in moisture flux divergence in the Caribbean, which enhance convection and increase rainfall [*Martin*

and Schumacher(2011)]. In this sense, weakening (strengthening) of the Caribbean LLJ winds is associated with increasing (decreasing) rainfall anomalies over northern Colombia [*Arias et al.*(2015)]. Coherently, our findings reveal that positive rainfall anomalies during La Niña coincide with negative moisture advection by the Caribbean LLJ from May to November, which is evidenced as moderate GS. In contrast, our results show that negative rainfall anomalies during El Niño exhibit weak GS (see Fig. **C-11** and Fig. **4-6**a). These results can be explained because the Caribbean LLJ has an opposite relationship with ENSO in the boreal winter and summer. During the winter a weak (strong) easterly Caribbean LLJ corresponds to warm (cold) SST anomalies in the tropical Pacific, whereas during the summer a strong (weak) easterly Caribbean LLJ is associated with warm (cold) SST anomalies in the tropical Pacific [*Wang*(2007)]. Furthermore, during El Niño, the Caribbean and Central America region experiences less precipitation in July-August, suggesting that Caribbean LLJ may modulate precipitation anomalies [Muñoz et al. (2007)].

On the other hand, Fig. **4-12** (top row) shows the maximum time-lags in areas of significant GS between moisture advection anomalies by the Caribbean LLJ and rainfall anomalies during the ENSO phases. During La Niña and Neutral phases, synchrony between the Caribbean LLJ moisture anomalies and rainfall anomalies in northern Colombia corresponds to time-lags between 0 and 2 months. During El Niño, such synchrony over northern Colombia occurs at time-lags between 0 and 4 months, suggesting that during El Niño, the time-lag between the Caribbean LLJ moisture anomalies and rainfall anomalies could be longer than during La Niña.

- **GS between the CHOCO LLJ moisture advection anomalies and rainfall anomalies**

  Fig. **4-11** (middle row) shows the GS-index between moisture advection by the CHOCO LLJ and rainfall anomalies in Colombia. Results evidence that rainfall anomalies over the entire tropical Pacific, the southern Caribbean, and the western Andean regions can be associated with moisture advection by the CHOCO LLJ. During La Niña and Neutral phases, the GS values are higher than during El Niño epochs (in most of places). Furthermore, the GS-significant-areas are larger during the Neutral and El Niño than during La Niña epochs. [*Poveda et al.*(2010), *Rueda and Poveda*(2006), *Poveda and Mesa*(2000)] argue that positive (negative) rainfall anomalies in western Colombia during La Niña (El Niño) can be explained in terms of the increasing (decreasing) moisture advection of the CHOCO LLJ as a result of the increase (decrease) in the temperature gradient between surface air temperatures over the Pacific coast off Colombia and El Niño 1+2 zone during June-July-August and September-October-November. During La Niña, positive rainfall anomalies coincide with positive moisture advection anomalies by the CHOCO LLJ, both signals exhibiting prominent peaks in the same period, which is reflected as strong GS over

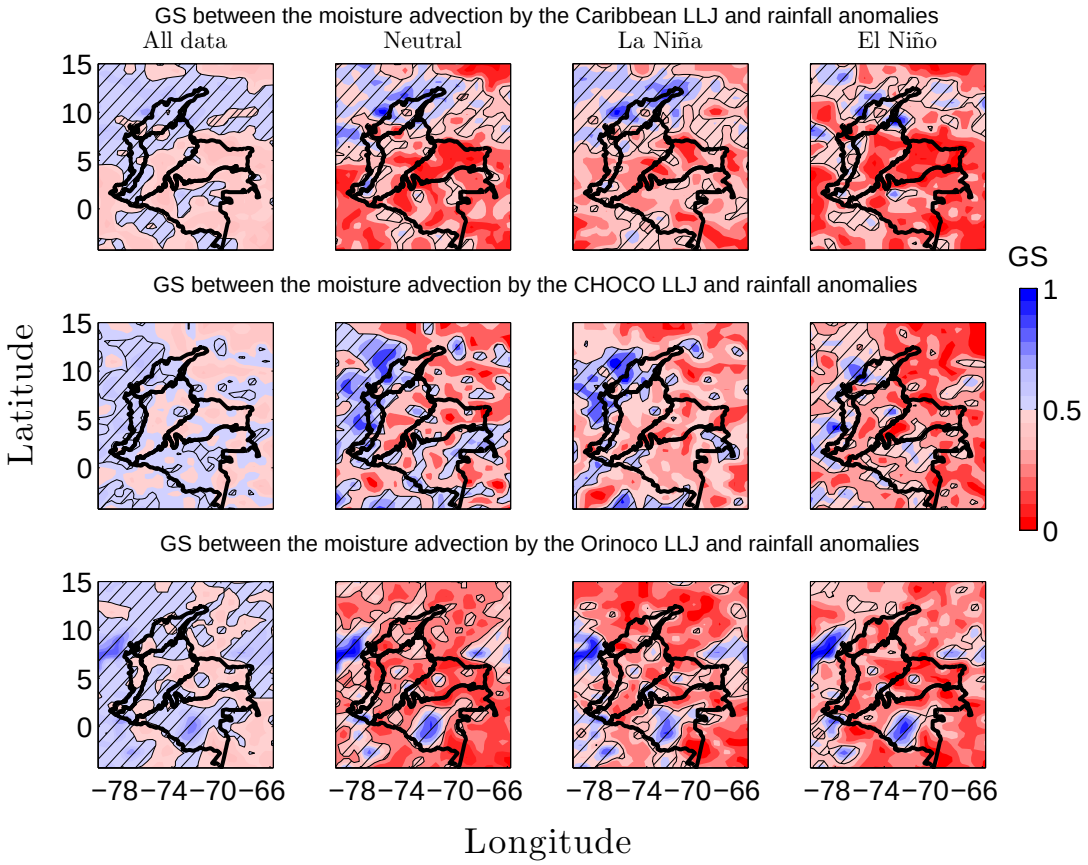

Figures 4-11.: Generalized Synchronization Index between the moisture advection of the low level jets and rainfall anomalies throughout Colombia. (top row) Caribbean LLJ. (middle row) CHOCO LLJ. (bottom row) Orinoco LLJ. Dataset No.1, period 1975-2006. The hatched contours indicates zones where the GS is significant at 5%.

northwestern Colombia (see Fig. **4-6**b; Supp. Info. Fig. C-12; Fig.**4-11**, middle row, third column, La Niña). In contrast, during El Niño, GS between negative rainfall anomalies and negative moisture advection by the CHOCO LLJ is weak, although GS is also significant (see Fig.**4-11**, middle row, last column, El Niño). Additionally, we also calculate GS between the sea surface temperature gradient in the previously mentioned regions and rainfall anomalies in Colombia. Our findings confirm the influence of the far-eastern Pacific SST gradient on rainfall anomalies on western Colombia and are consistent with those shown for GS between the CHOCO LLJ and SST3.4 (see Supp. Info. Fig. C-1).

On the other hand, Fig. **4-12** (middle row) shows the maximum time-lags in areas of significant GS between moisture advection anomalies by the CHOCO LLJ and rainfall anomalies during the ENSO phases. During La Niña and Neutral phases, synchrony

between rainfall anomalies and the CHOCO LLJ moisture anomalies in north-western Colombia corresponds to time-lags between 0 and 2 months. During El Niño, such synchrony over north-western Colombia occurs at time-lags between 2 and 6 months, suggesting that during El Niño, the time-lag between the CHOCO LLJ moisture anomalies and rainfall anomalies could be longer than during La Niña.

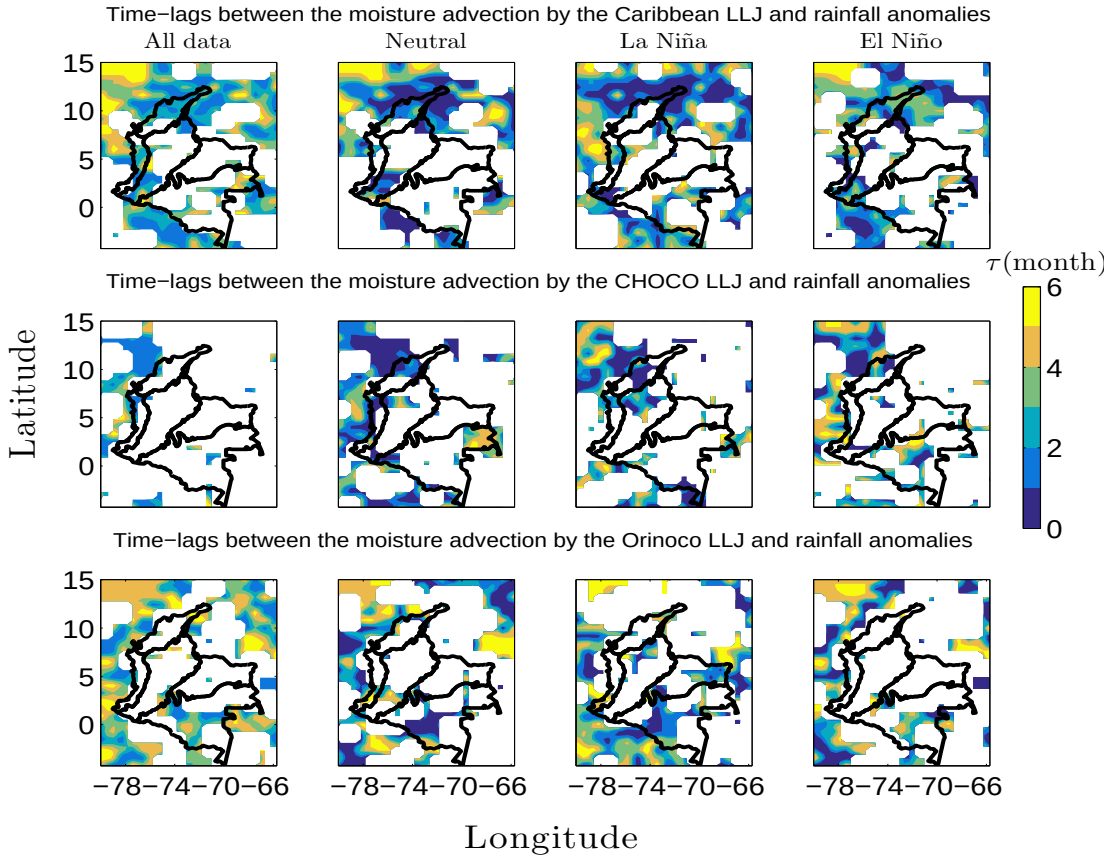

Figures 4-12.: Time-lags between the moisture advection by the low level jets and rainfall anomalies throughout Colombia. (top row) Caribbean LLJ. (middle row) CHOCO LLJ. (bottom row) Orinoco LLJ. Dataset No.1, period 1975-2006. White indicates zones where GS is not significant at 5%.

- **GS between the Orinoco LLJ moisture advection anomalies and rainfall anomalies**

Fig. **4-11** (bottom row) shows the GS-index between moisture advection anomalies by the Orinoco LLJ and rainfall anomalies in Colombia. Our GS-analysis suggests that

such positive (negative) moisture advection influences the positive (negative) hydro-climatic anomalies in the Colombian Amazon region during El Niño (La Niña), GS is moderate (strong) and the areas are larger (smaller). In contrast, these GS results can not be easily associated with rainfall anomalies in the Orinoco region (see Fig. **C-11** and Fig. **4-6**c). Hence, these findings point out the need of further research regarding the response of the Orinoco LLJ to ENSO's phases in order to advance the understanding of hydro-climatic anomalies of these regions. Note that the Pacific coast exhibits significant GS, which need to be further investigated. Fig. **4-12** (bottom row) shows the maximum time-lags in areas of significant GS between moisture advection anomalies by the Orinoco LLJ and rainfall anomalies during the ENSO phases. Results suggest a simultaneous relation between moisture by the Orinoco LLJ and rainfall anomalies over the Amazon region. During La Niña and Neutral phases, synchrony between rainfall anomalies and the Orinoco LLJ moisture anomalies in southern Colombia (Amazon region) corresponds to time-lags between 0 and 2 months. During El Niño, such synchrony occurs at time-lags between 2 and 4 months, suggesting that during El Niño, the time-lag between the Orinoco moisture anomalies and rainfall anomalies could be longer than during La Niña.

4.5.7. GS between the Cross-Equatorial Flow and rainfall in Colombia

Fig. **4-13** (top row) shows the GS-index between moisture advection by the Cross-Equatorial Flow (CEF) and rainfall anomalies in Colombia. Our results evidence that rainfall anomalies in the Amazon region are related to the meridional moisture advection by the CEF. Hence, our results support those presented by [*Wang and Fu*(2002)] regarding the influence of the CEF over hydro-climatology of the northern Amazon River basin (southern Colombia).

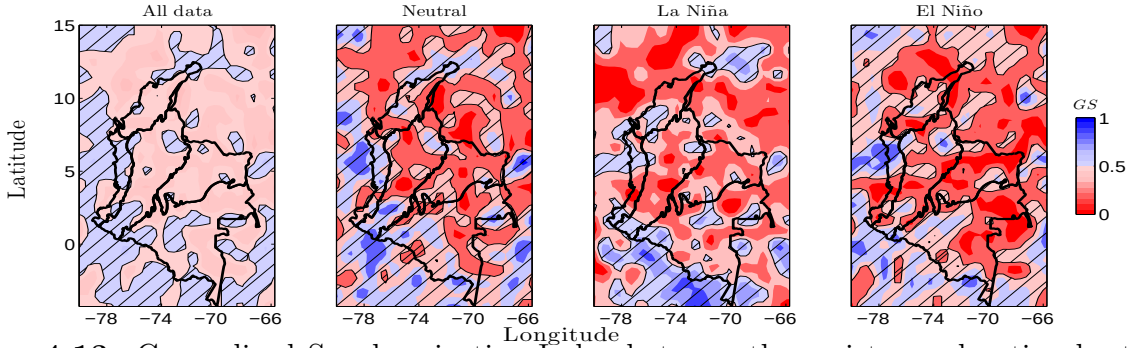

Figures 4-13.: Generalized Synchronization Index between the moisture advection by the Cross-Equatorial Flow and rainfall anomalies. Dataset No.1, period 1975-2006. The hatched contours indicate zones where the GS is significant at 5%.

In addition, our findings show that the GS-significant-areas are larger (smaller) during El Niño (La Niña) as well as the GS is strong (weak) during La Niña (El Niño). In particular, the GS results reveal a connection between the Amazon region of Colombia (north-western most Amazon River basin) and the western Colombia Pacific coast. This result supports the recent works on aerial rivers connecting Amazonia and the Colombian Pacific [*Sakamoto et al.*(2011)], as well as the existence of an Atmosphere-Land Bridge between the Pacific and the tropical North Atlantic through the Amazon River basin [*García-Serrano et al.*(2017), *Builes et al.*(2018)]. In this sense, Fig. **C-11** does not show a clear annual cycle of rainfall anomalies in these regions (see also Fig. C-12 in Supp. Info.). Nonetheless, Fig. **4-6**d evidences positive (negative) southerly moisture advection anomalies by the CEF during La Niña (El Niño) in the austral winter as well as negative (positive) northerly moisture advection anomalies by the CEF during La Niña (El Niño) in the austral summer. This results provide new insights on the influence of the Orinoco LLJ and the CEF winds over the Amazon region as modulators of rainfall anomalies during ENSO. The influence of the Orinoco LLJ seems to be stronger than the influence of the CEF over the Amazon region of Colombia (see **4-11** bottom row). Moreover, our results suggest that the influence of the CEF is stronger in the Pacific region (western Colombia) than in the Amazon region of Colombia. However, further research is needed regarding the CEF dynamics during ENSO and its influence on the Orinoco and Amazon regions of Colombia. At this point, there is not clear evidence on the influence of the CEF over the Orinoco region. Additionally, the analysis of time-lags do not show clear patterns (see Suppl. Info. Fig. C-2, top row).

4.5.8. GS between indices for different types of ENSO and hydrologic anomalies in Colombia

Fig. **4-14** (left column) shows GS between the different types of El Niño indices and rainfall anomalies in Colombia using all data. These results suggest that the three indices exhibit GS with rainfall anomalies over the Caribbean, the Pacific, and the Andean regions whereas the Orinoco and the Amazon regions do not exhibit such interdependence. Furthermore, these results agree with those shown in Chapter 3, which stated that rainfall anomalies are phase-locked with SST anomalies in the Caribbean, the Pacific, and Andean regions, whereas the Orinoco and the Amazon regions do not exhibit such phase-locking. Hence, our GS results suggest that rainfall anomalies in some regions of Colombia (the driven system) are mainly determined by ENSO (the driving system).

Additionally, we quantify GS between each index-type of ENSO and rainfall anomalies in Colombia considering the ENSO phases. We aim to characterize the GS-patterns during El Niño, La Niña and Neutral phases using the same reference periods than in previous analysis as per MEI classification (see Fig. **4-2**). Fig. **4-14** (top row) evidences that

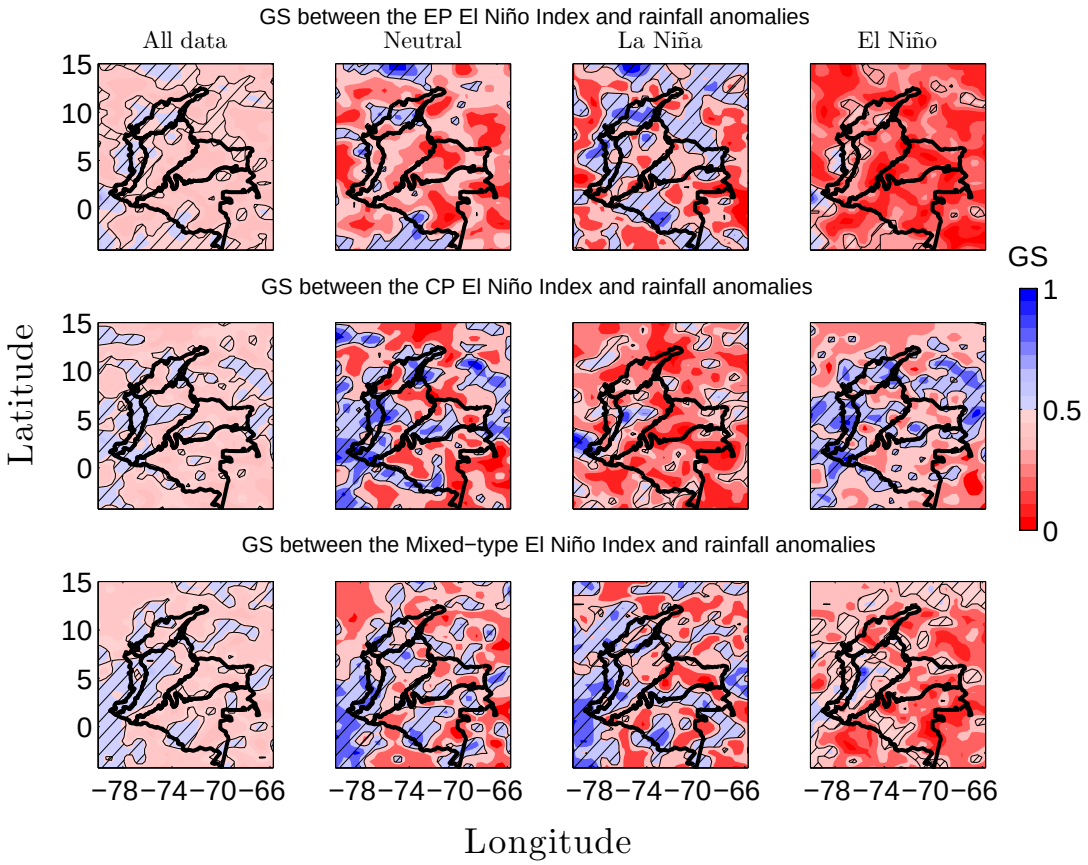

Figures 4-14.: Generalized Synchronization between indices for different types of ENSO and rainfall anomalies throughout Colombia. (top row) Eastern Pacific (EP) El Niño type. (middle row) Central Pacific (CP) El Niño type. (bottom row) Mixed El Niño type. Dataset No.1, period 1975-2006. The hatched contours indicates zones where the GS is significant at 5%.

the EP index exhibits a strong (weak) GS with rainfall anomalies in Colombia during La Niña (El Niño) over vast (small) areas of the continental Colombian territory. Fig. **4-2**a shows that during La Niña (El Niño) phase the EP index shows negative (positive) SST anomalies. This GS-result can be explained because cold (warm) SST anomalies over the Eastern Pacific produces a higher (smaller) temperature gradient between the Pacific Ocean off the Colombian coast and the El Niño 1+2 region that increase (decrease) of the moisture advection by the CHOCO LLJ [*Poveda et al.*(2010), *Poveda and Mesa*(2000)].

In contrast, Fig. **4-14** (middle row) evidences that the CP index exhibits a strong (weak) GS with rainfall anomalies during El Niño (La Niña) phase over vast areas of the continental Colombian territory. Fig. **4-2**a evidences that during El Niño (La Niña) the EP index shows positive (negative) SST anomalies that are higher (smaller) than those experienced in the Central Pacific (Fig. **4-2**a). Hence, we hypothesize that cooling (warming) of SSTs in the far eastern tropical Pacific are more associated with higher positive (negative) rainfall

anomalies in Colombia than the cooling (warming) of SSTs in the central Pacific. The cooling (warming) of SSTs in the Central Pacific seems to modulate rainfall anomalies in Colombia in different ways given that the increase (decrease) of SSTs in the central tropical Pacific are sandwiched by anomalous cooling (warming) over the eastern and western tropical Pacific, which influences the far-eastern tropical Pacific (the Pacific Ocean off the Colombian coast) and the Caribbean sea [Ashok and Yamagata (2007), Ashok and Yamagata (2009), Weng et al. (2009)]. Hence, the characteristics of such anomalous cooling (warming) over the eastern and western portions of the Central Pacific affect the SST gradients between the Pacific Ocean off the Colombian coast and the El Niño 1+2 as well as the response in the Caribbean sea, which affects the hydro-climatic response over Colombia. This result is in agreement with the study of Navarro-Monterroza et al. [*Navarro-Monterroza et al.* (2019)] regarding different effects of CP and EP El Niños on rainfall anomalies in Colombia.
A similar procedure was carried out to quantify GS between the Mixed-type El Niño indices and rainfall anomalies in Colombia. Fig. **4-14** (bottom row) evidences that the Mixed-type El Niño index exhibits strong (weak) GS with rainfall anomalies during La Niña (El Niño) in the Caribbean, the Andean and Pacific regions. These results are comparable with the GS-patterns between the SST3.4 anomalies and rainfall anomalies (see Fig. **4-9**) as expected because both, the Mixed-type El Niño Index and SST3.4 anomalies, are calculated over the same tropical Pacific zone (Niño3.4).
We analyzed time-lags between the different types of El Niño indices and hydrological (rainfall and streamflows) anomalies in Colombia but our results do not show clear evidence of synchrony or temporal propagation of spatial patterns (see Suppl. Info. Figs. C-7 to C-10).

4.6. Final remarks and future work

We use Recurrence Quantification Analysis (RQA) with the aim to study features of Generalized Synchronization (GS) between ENSO and the hydrological anomalies (rainfall and streamflows) over Colombia, taking into account the uncertainty in the non-linear recurrence metrics induced by the different methods to estimate hydro-climatic anomalies (HyAns). Our results suggest that the GS quantifier based on RQA can be significantly affected when anomalies are defined on a constant climatology (HyAns–TAC method). On the other hand, the GS-metric exhibits similar magnitude for the HyAns methods that consider a non-constant annual cycle (HyAns–FAC, HyAns–SSAC, and HyAns–MAC), whereas the time-lags between signals could be sensitive to the HyAns method used.
Our findings allow us to conclude that the hydrology of Colombia exhibits GS with ENSO. Moreover, the physical mechanisms associated with such GS could be different for each region of Colombia. Our results reveal that advection of moisture by the studied Low-Level Jets (LLJs) and the Cross-Equatorial Flow are part of the physical mechanisms influencing the hydrological anomalies in Colombia during ENSO.
We identified that GS-patterns between advection of moisture by each of the three LLJs

and hydrology change, in terms of magnitude and spatial distribution, depending on the phase of ENSO (La Niña and El Niño). In this sense, there are three main results, which advance our understanding about the hydrological anomalies in Colombia at interannual timescales: *(i)* rainfall anomalies in the Caribbean, northern-Pacific, and northern-Andean regions are mostly related with moisture advection by the Caribbean LLJ. During La Niña (El Niño), rainfall and streamflows in these regions exhibit positive (negative) anomalies, and GS is strong (weak) with the largest (smallest) areas of significant correlation; *(ii)* rainfall anomalies in the entire Pacific region, the southern Caribbean region, and the western Andean region can be associated with the advection of moisture by the CHOCO LLJ. During La Niña (El Niño), hydrological variables experiment positive (negative) anomalies and, GS is strong (weak) whereas the significant spatial GS-areas are small (large); *(iii)* rainfall anomalies in the Colombian Amazon region are correlated with the advection of moisture by the Orinoco LLJ. During La Niña (El Niño), the Amazon and Orinoco regions experience negative (positive) hydrological anomalies but only the Amazon region shows weak (strong) GS.

We provide evidence of propagation patterns over Colombia regarding the influence of the LLJs and CEF over the studied hydrological anomalies: *(i)* During La Niña, the Caribbean LLJ moisture anomalies exhibit synchrony with rainfall anomalies in northern Colombia at 0-2 months lags. During El Niño, the Caribbean LLJ moisture advection leads rainfall anomalies at 2-4 months lags. During Neutral and La Niña conditions, time-lags are similar. *(ii)* During La Niña, the CHOCO LLJ moisture anomalies exhibit synchrony with rainfall anomalies over north-western Colombia at 0-2 months lags. During El Niño, CHOCO LLJ moisture anomalies lead rainfall anomalies at 2-4 months lags. During Neutral and La Niña, time-lags are similar; *(iii)* the Orinoco LLJ exhibits synchrony with rainfall anomalies over the Amazon region (not so over the Orinoco region); *(iv)* north-western Colombia (the Caribbean region and the northern Pacific region) experiences a conjoint influence of the Caribbean LLJ and the CHOCO LLJ.

We also study the GS between the moisture advection by the Cross-Equatorial Flow (CEF) and rainfall anomalies in Colombia. Our results indicate that rainfall anomalies in the Colombian Amazon region are correlated to the CEF. During La Niña (El Niño), GS is strong (weak) whereas the GS spatial patterns are small (large). It is remarkable that our GS results reveal a connection between the Amazon region of Colombia (west-northernmost Amazon River basin) and the western Colombian Pacific coast. This result can be associated with aerial rivers connecting the Pacific and the Amazon River basin, which had been stated in several previous works [*Sakamoto et al.*(2011), *Poveda et al.*(2014), *Builes et al.*(2018)]. In particular, the Orinoco LLJ exhibits stronger GS in the Amazon region of Colombia than the CEF and the analysis of time-lags do not show clear synchronous evolution of signals, which requieres more research.

We quantify GS between three indices for the different types of El Niño (EP and CP) and hydrological variables in Colombia. Our results suggest a strong (weak) GS between negative

(positive) SST anomalies in the Eastern Pacific and rainfall anomalies in Colombia. In contrast, our results exhibit a strong (weak) GS between positive (negative) SST anomalies in the Central Pacific and rainfall anomalies. These findings evidence a different influence of the types of ENSO on hydrologic anomalies in Colombia. Further research is needed regarding the effects of the different types of El Niño on physical mechanisms influencing Colombian hydro-climatology.

This work uses a novel approach that reveals new insights regarding the impacts of ENSO given the non-linear nature of the GS method. First-order approximation of the relation between ENSO and Colombian rainfall anomalies seems to be linear, but it is hardly the whole picture. From our analysis, we can conclude that non-linearity is also important although probably there are other ways to go deeper into this relation but this first step is an important contribution. In particular, our findings contribute to explain the hydrological anomalies over Colombia in terms of diverse physical mechanisms of moisture transport during ENSO. Furthermore, we take into account the uncertainty in the analysis with respect to different ways to define anomalies, which is a fundamental procedure to avoid biases in the interpretation of results for climatological purposes at inter-annual timescales. Notwithstanding, further research is needed regarding the seasonal spatio-temporal patterns of GS at inter-annual timescales, the differences in results considering the different flavors of ENSO, and the differences in the estimation of time-lags in relation to the HyAns methods.

Further research is needed regarding the effects of the different types of El Niño on physical mechanisms influencing Colombian hydro-climatology, e.g. How do the different types of ENSO affect the dynamics of low-levels jets surrounding Colombia? How do the different types of ENSO affect the dynamics of the Cross-Equatorial Flow from the Amazon River Basin? How do the different types of ENSO affect diverse land surface-atmosphere interactions at continental, regional and local scales? How do synchronization patterns change with seasons? These topics are outside the scope of this investigation and need to be further investigated.

4.7. Acknowledgments

The work of H.D. Salas is supported by COLCIENCIAS – Grant for National Doctorates 617-2 and partially funded by the Humboldt University of Berlin IRTG 1740 and Institución Universitaria Colegio Mayor de Antioquia, Project “El Chorro de los Andes Orientales – CHAO– y su relación con la hidro-climatología de Colombia”. The work of G. Poveda and O. J. Mesa is supported by Universidad Nacional de Colombia at Medellin. The work by N. Marwan is supported by Deutsche Forschungsgemeinschaft (DFG) GRK 2043/1 “Natural risk in a changing world (NatRiskChange)”. We are grateful to: NOAA for NCEP/NCAR data, U.S. Geological Survey (USGS HydroSHEDS) for the Digital Elevation Models, A. F. Hurtado for the reanalysis data of Colombian precipitation, IDEAM for rainfall and streamflow data, XM for streamflow data. Recurrence analysis was carried out with the

CRP Toolbox for MATLAB developed by N. Marwan and available at http://tocsy.pik-potsdam.de/CRPtoolbox.

5. General conclusions and Future work

5.1. General conclusions

- The accuracy of the estimation of hydro-climatic anomalies (HyAns) is commonly taken for granted and constitutes an important source of error and bias for subsequent interdependency analysis with other time series or climatic indexes and, consequently there is room for ambiguity in the physical interpretation of results. In Chapter 2, we presented diverse methods to define anomalies and then, we quantified Pearson correlations between ENSO and rainfall anomalies in Colombia. We showed that correlation patterns can change significantly in terms of the sign, magnitude, and timing, depending on the phase of ENSO, and the location in the country. Hence, we took this result into account for subsequent non-linear interdependence analysis using synchronization techniques (Chapters 3 and 4), this in order to check the sensitivity of such synchronization techniques to the HyAns methods.

- We investigate Phase Synchronization (PS) between the El Niño - Southern Oscillation (ENSO) signal and the (inter-annual and annual) cycles of rainfall in Colombia. Our findings show that the positive (negative) HyAns experienced in the Pacific, Caribbean and Andean regions of Colombia, during La Niño (El Niño), are phase-locked with the ENSO signal in the tropical Pacific Ocean, whereas the negative (positive) HyAns experienced in the Orinoco and Amazon regions, during La Niña (El Niño), do not show such phase-locking. Moreover, our results evidence that, at inter-annual time scales, during La Niña, for all quarters, SST3.4 anomalies in the tropical Pacific Ocean lead rainfall anomalies in the Pacific, Caribbean and Andean regions from 1 to 3 months lag whereas, during El Niño, for JJA and SON, SST3.4 anomalies lead rainfall anomalies from 3 to 5 months lag. These results show that, during El Niño, rainfall anomalies exhibit a time-lag longer than during La Niña in relation to anomalies in the tropical Pacific ocean.

- We quantify Phase Synchronization (PS) between the El Niño - Southern Oscillation (ENSO) signal and the annual cycle of rainfall in Colombia. We provide evidence that the ENSO signal is phase-locked with the AC of rainfall in some regions of Colombia, which suggest that the AC plays an important role in the influence of ENSO on Colombian climatology and opens new paths towards the understanding of non-linear feedbacks between hydro-climatic processes. In particular, these links between

the inter-annual variability of ENSO and the annual cycle of rainfall over Colombia is possible because of the non-linear basis of the synchonization approach.

- At inter-annual timescales, ENSO exhibits the strongest phase-locking with the annual and inter-annual cycles of rainfall throughout Colombia, although other macro-climatic processes also show significant PS such as the Pacific Decadal Oscillation (PDO) and the North Atlantic Oscillation (NAO). Moreover, we suggest that the highest positive (negative) rainfall anomalies over western Colombia coincide with the strong (weak) PS between the ENSO and the PDO signals.

- We investigate Generalized Synchronization (GS) between the El Niño-Southern Oscillation (ENSO) signal and rainfall anomalies in Colombia. We link the GS results with the dynamics of some physical mechanisms that modulate Colombia's hydroclimatology, including the Caribbean, the CHOCO and the Orinoco Low-Level Jets (LLJs), and the Cross-Equatorial Flow (CEF). Our results confirm those results found using PS, HyAns in the Pacific, Caribbean and Andean regions of Colombia exhibit strong (weak) GS with the ENSO signal during La Niña (El Niño), where hydrological anomalies are positive (negative).

- The GS analysis allows us to identify spatial patterns of non-linear dependence between ENSO and the Colombian's climatology. The mentioned moisture transport sources (LLJs and the CEF) constitute the interdependence mechanism and contribute to explain hydrological anomalies in Colombia during the phases of ENSO. During La Niña (El Niño), GS is strong (weak) for the Caribbean and the CHOCO LLJs whereas GS is moderate (strong) for the Orinoco LLJ. Moreover, moisture advection by the Caribbean and CHOCO LLJs exhibit synchrony with HyAns at 0 to 2 (2 to 4) month-lags over north-western Colombia and the Orinoco LLJ moisture advection synchonizes with HyAns at similar month-lags over the Amazon region of Colombia.

- This work uses a novel approach that reveals new insights regarding the impacts of ENSO given the non-linear nature of the PS and GS methods. First-order approximation of the relation between ENSO and Colombian rainfall anomalies seems to be linear, but it is hardly the whole picture. From our analysis, we can conclude that non-linearity is also important although probably there are other ways to go deeper into this relation but this first step is an important contribution.

5.2. Future work

This dissertation opens important research paths that deserve to be investigated in the future, such as:

- We reviewed the concept of climatic 'anomaly' evidencing that linear and non-linear methods to quantify interdependence are affected by how we define anomalies (i.e. the method used to subtract the annual cycle signal). Hence, it is necessary to look total solutions using raw data (without extracting the annual cycle) or quantify the sensitivity and uncertainty of interdependence metrics in relation to the different ways to define anomalies. Some future applications of the uncertainty in anomalies estimation can be: (1) assessing of the false skills in forecasting models (i.e. changes in forecasting through ARIMA models in relation to diverse anomalies methods), (2) identification of general circulation models (GCMs) that show similar variability modes at annual or/and inter-annual scales (i.e. Earth's localities where a group of GCMs show analogous inter-annual variability in association to ENSO or other macroclimatic processes –in terms of sign, timing, and magnitude– for different anomaly methods).

- Our findings evidence that synchronization methods allow revealing that the links among the oscillatory processes play a fundamental role behind the complex hydroclimatic feedbacks. In this sense, it is necessary to implement synchronization techniques using time series derived from a Principal Oscillation Patterns (POPs) analysis [*Von Storch et al.*(1995)], which have a firm theoretical basis that allows reducing multiple time series into their main oscillatory signals that could be useful for prediction purposes.

- Our results show that phase and generalized synchronization techniques have a firm theoretical basis from physical properties of weakly coupled oscillators and non-linear dynamics systems, respectively. Hence, such techniques can be used to quantify non-linear interdependence between oscillatory processes that occur at different time scales (e.g. the interannual variability of ENSO and the annual cycle of Colombia's hydroclimatology). From this point of view, the synchronization framework can be useful to investigate the physical basis behind to scaling properties of hydroclimatic processes. This because synchronization can be thought as a sample space reducing process and, a process that reduces degrees of freedom is a system synchronized. Once a system is synchronized, there will not be much of scaling be visible in the statistics (pers. comm. with Thurner, S.).

- [*Bedoya-Soto et al.*(2019)] shown that the diurnal cycle of rainfall over Medellin's Valley, Central Andes of Colombia, changes with the annual cycle. It is interesting to investigate how the diurnal and annual cycles are connected. However, it is not possible to quantify the interdependence between the diurnal and the annual cycles using the synchronization techniques presented in this work. As we mentioned, phase-locking emerges if there is a relationship between oscillations with relatively small natural integers. For this case, for each annual cycle (AC) there are 365 diurnal cycles (DC), it is not possible to study this phase relationship directly using the PS

technique based on phase differences. However, it is important to investigate if there is a phase-locking scaling property that links the DC and the AC. In this sense, further research could study PS between the DC and the 5-10 day variability associated with the Tropical Easterly Waves (TEWs). Then, to explore PS between the 5-10 days and the 30-60 day variability associated with the Madden-Julian Oscillation (MJO). Finally, it is possible to look for PS features between the 30-60 day variability and the semi-annual (6 months) and annual (12 months) variability. The mentioned procedure outlines a way to address the connection between diurnal to annual variability using PS techniques.

- Until now, the literature does not provide a satisfactory explanation regarding the occurrence of different types of ENSO events. In this sense, synchronization techniques could be useful to study the synchronization patterns over the Tropical Pacific Ocean between SST anomalies and wind anomalies. This synchronization approach could provide new clues on the genesis of different flavors of ENSO.

- Synchronization techniques allow studying the non-linear interdependence between processes that occur at different time scales. Recent works by [*Stein et al.*(2011), *Stein et al.*(2014)] and this dissertation show some synchronization features between the ENSO and the annual cycle variability. Other cases deserve to be studied in the future such as (1) synchronization between the MJO and the ENSO variability over the tropical Pacific Ocean, (2) synchronization between the PDO signal and the ENSO signal and, (3) synchronization between the ENSO variability and the inter-annual variability over the Atlantic Ocean (i.e. NAO or AMO).

- This work points out the need to study the Orinoco LLJ anomalies and their relationship with the hydro-climatic response over the Orinoco and Amazon regions of Colombia during ENSO.

- During La Niña (El Niño), the Andean region does not exhibit PS between SST3.4 anomalies and the annual cycle of precipitation in this region during the boreal summer. Hence, further research is needed regarding the role of topography on the phase synchronization features.

Bibliography

Coelho, C., Uvo, C., and Ambrizzi, T. Exploring the impacts of the tropical Pacific SST on the precipitation patterns over South America during ENSO periods. Theor Appl Climatol 71, 185-197 (2002). https://doi.org/10.1007/s007040200004

Grimm, A. M., and M. T. Zilli, 2009: Interannual Variability and Seasonal Evolution of Summer Monsoon Rainfall in South America. J. Climate, 22, 2257-2275, https://doi.org/10.1175/2008JCLI2345.1.

Poveda, G., Mesa O.J. (1999) The low level westerly jet (Choco jet) and two other jets in Colombia: climatology and variability during ENSO phases (in Spanish), *Revista Academia Colombiana de Ciencias Exactas*, 23(89): 517-528.

Poveda, G., Jaramillo, L., Vallejo, L.F. (2014) Seasonal precipitation patterns along pathways of South American lowâlevel jets and aerial rivers, *Water Resources Research*, 50(1), 98-118.

Muñoz, P., Gorin, G., Parra, N., Velásquez, C., Lemus, D., Monsalve-M, C., Jojoa, M., Holocene climatic variations in the Western Cordillera of Colombia: A multiproxy high-resolution record unravels the dual influence of ENSO and ITCZ, *Quaternary Science Reviews*, 155, 159-178.

Hoyos, I., Dominguez, F., Cañón-Barriga, J., Martínez, J.A., Nieto, R., Gimeno, L., Dirmeyer, P.A. (2017) Moisture origin and transport processes in Colombia, northern South America, *Clim Dyn*, DOI 10.1007/s00382-017-3653-6.

Jaramillo, L., Poveda, G., Mejía, J.F. (2017) Mesoscale convective systems and other precipitation features over the tropical Americas and surrounding seas as seen by TRMM, *Int. J. Climatol.*, DOI: 10.1002/joc.5009

Carvajal, L.F., Salazar,J.E., Mesa, O. J., Poveda, G. (1998) Hydrological prediction in Colombia using singular spectral analysis and the maximum entropy method, Hydraulic Engineering in Mexico (in Spanish). Vol. XIII, 1, 07-16.

Poveda, G., Mesa O.J., Waylen, P. (2003) Non-linear forecasting of river flows in Colombia based upon ENSO and its associated economic value for hydropower generation, Kluwer Academic Publishers, Dordrecht, 351-371, ISBN 1-4020-1529-1, 424 p.

Hurtado, A. F., Poveda, G. (2009) Linear and global spaceâtime dependence and Taylor hypotheses for rainfall in the tropical Andes, *Journal of Geophysical Research: Atmospheres*, 114(D10).

Carmona, A.M., Poveda, G. (2014) Detection of long-term trends in monthly hydro-climatic series of Colombia through Empirical Mode Decomposition, *Climatic Change*, 123, 301-313.

Donner, R. V., Zou, Y., Donges, J. F., Marwan, N., and Kurths, J.: Recurrence networks – a novel paradigm for nonlinear time series analysis, New J. Phys., 12, 033025, https://doi.org/10.1088/1367-2630/12/3/033025, 2010.

Arnhold, J., Grassberger, P., Lehnertz, K., and Elger, C. E.: A robust method for detecting interdependences: application to intracranially recorded EEG, Physica D, 134, 419-430, 1999.

Le Van Quyen, M., Martinerie, J., Adam, C., and Varela, F. J.: Non-linear analyses of interictal EEG map the brain interdependences in human focal epilepsy, Physica D, 127, 250-266, 1999.

Schiff, S. J., So, P., Chang, T., Burke, R. E., and Sauer, T.: Detecting dynamical interdependence and generalized synchrony through mutual prediction in a neural ensemble, Phys. Rev. E, 54, 6708-6724, https://doi.org/10.1103/PhysRevE.54.6708, 1996.

Rosenblum, M. G., Pikovsky, A. S., and Kurths, J.: From phase to lag synchronization in coupled chaotic oscillators, Phys. Rev. Lett., 78, 4193-4196, https://doi.org/10.1103/PhysRevLett.78.4193, 1997.

Pikovsky, A., Rosenblum, M., Kurths, J. (2001) Synchronization: A universal concept in nonlinear sciences. *Cambridge University Press.*

Stolbova, V., Martin, P., Bookhagen, B., Marwan, N., and Kurths, J.:Topology and seasonal evolution of the network of extreme precipitation over the Indian subcontinent and Sri Lanka, Nonlinear Proc. Geoph., 21, 901-917, 2014.

Malik, N., Bookhagen, B., Marwan, N., and Kurths, J.: Analysis of spatial and temporal extreme monsoonal rainfall over South Asia using complex networks, Clim. Dynam., 39, 971-987, 2012.

Rheinwalt, A., Boers, N., Marwan, N., Kurths, J., Hoffmann, P.,Gerstengarbe, F.-W., and Werner, P.: Non-linear time series analysis of precipitation events using regional climate networks for Germany, Clim. Dynam., 46, 1065-1074, 2016.

Agarwal, A., N. Marwan, M. Rathinasamy, B. Merz, and J. Kurths, Multi-scale event synchronization analysis for unravelling climate processes: A wavelet-based approach, Nonlinear Process. Geophys., 2017.

Marwan, N., Romano, M.C., Thiel, M., & Kurths, J. (2007). Recurrence plots for the analysis of complex systems. *Physics Reports*. https://doi.org/10.1016/j.physrep.2006.11.001

Fraedrich, K., & Müller, K., Climate anomalies in Europe associated with ENSO extremes, *Int. J. Climatol.*, 12(1), 25-31 (1992).

Chandler, T. J. Teleconnections linking worldwie climate anomalies, *Dyn. Atmos. Ocean.*, 17(1), 79-81 (1992).

Mason, S.L., & Goddard, L. Probabilistic Precipitation Anomalies Associated with ENSO, *Bull. Am. Meteorol. Soc.*, 82(4), 619-638 (2001).

Hegerl, G.C., Brönnimann, S., Schurer, A., & Cowan, T. The early 20th century warming: Anomalies, causes, and consequences, *Wiley Interdiscip. Rev. Clim. Chang.*, 9(4), 1-20 (2018).

Brohan, P., Kennedy, J. J., Harris, I., Tett, S. F. B., & Jones, P. D. Uncertainty estimates in regional and global observed temperature changes: A new data set from 1850, *J. Geophys. Res.*, 111(D12), D12106 (2006).

Lange, H., Sippel, S. & Rosso, O. A. Nonlinear dynamics of river runoff elucidated by horizontal visibility graphs. *Chaos An Interdiscip. J. Nonlinear Sci.*, 28(7),075520, doi:10.1063/1.5026491 (2018).

Salas, H. D., Poveda, G., Mesa, Ó. J. & Marwan, N. Generalized Synchronization between ENSO and Hydrological variables in Colombia: A Recurrence Quantification Approach. *Front. Appl. Math. Stat.*, 6(3), DOI: 10.3389/fams.2020.00003 (2020).

Salas, J. D., Delleur, J. W., Yevjevich, V. & L.Lane, W. Applied Modeling of Hydrologic Time Series (Water Resources Publications, 1980).

Douglass, D. H. The Pacific sea surface temperature, *Phys. Lett. A*, 376(2), 128-135, 10.1016/j.physleta.2011.10.042 (2011).

Douglass, D. H., & Knox, R. S. The Sun is the climate pacemaker I. Equatorial Pacific Ocean temperatures, *Phys. Lett. A*, 379(9), 823-829 (2015).

Vautard, R., Yiou, P. & Ghil, M. Singular-spectrum analysis: A toolkit for short, noisy chaotic signals, *Phys. D Nonlinear Phenom.*, 58(1-4), 95-126 (1992).

Ghil, M. Advanced spectral methods for climatic time series, *Rev. Geophys.*, 40(1), 1003 (2002).

Huang, N. E. *et al.* The empirical mode decomposition and the Hilbert spectrum for nonlinear and non-stationary time series analysis, *Proc. R. Soc. London. Ser. A Math. Phys. Eng. Sci.*, 454(1971), 903-995 (1998).

Wu, Z. & Huang, N. E. Ensemble empirical mode decomposition: A noise-assisted data analysis method. *Adv. Adapt. Data Anal.*, DOI: 10.1142/s1793536909000047 (2008).

Cai, W. *et al.* Climate impacts of the El Niño-Southern Oscillation on South America. *Nat. Rev. Earth & Environ.*, DOI: 10.1038/s43017-020-0040-3 (2020).

Poveda, G. The hydro-climatology of Colombia: A synthesis from inter-decadal to diurnal timescales (in spanish). *Rev. Acad. Colomb. Cienc.*, 28, 201-222 (2004).

Poveda, G. & Mesa, O. J. Feedbacks between hydrological processes in tropical South America and large-scale ocean-atmospheric phenomena. *J. Clim.*, 10(10), 2690-2702, 10.1175/1520-0442(1997)0102690:FBHPIT 2.0.$CO;2$(1997).

Coelho, C. A., Uvo, C. B. & Ambrizzi, T. Exploring the impacts of the tropical Pacific SST on the precipitation patterns over South America during ENSO periods. *Theor. Appl. Climatol.*, 71(3-4), 185-197, DOI: 10.1007/s007040200004 (2002).

Grimm, A. M. & Tedeschi, R. G. ENSO and extreme rainfall events in South America. *J. Clim.*, 22(7), 1589-1609, DOI: 10.1175/2008JCLI2429.1 (2009).

Poveda, G., Álvarez, D. M. & Rueda, Ó. A. Hydro-climatic variability over the Andes of Colombia associated with ENSO: A review of climatic processes and their impact on one of the Earth's most important biodiversity hotspots, DOI:10.1007/s00382-010-0931-y (2011).

Andreoli, R. V. *et al.* The influence of different El Niño types on the South American rainfall. *Int. J. Climatol.*, 37(3), 1374-1390, DOI:10.1002/joc.4783 (2017).

Bedoya-Soto, J. M., Poveda, G., Trenberth, K. E. & VÃ©lez-Upegui, J. J. Interannual hydroclimatic variability and the 2009-2011 extreme ENSO phases in Colombia: from Andean glaciers to Caribbean lowlands, *Theor. Appl. Climatol.*, 135(3-4), 1531-1544, DOI:10.1007/s00704-018-2452-2 (2019).

Poveda, G. *et al.* High Impact Weather Events in the Andes. *Front. Earth Sci.*, DOI: 10.3389/feart.2020.00162 (2020).

Poveda, G. *et al.* The Diurnal Cycle of Precipitation in the Tropical Andes of Colombia. *Mon. Weather. Rev.*, 133 (1), 228-240, DOI:10.1175/MWR-2853.1 (2005).

Bedoya-Soto, J. M., Poveda, G. & Sauchyn, D. New insights on land surface-atmosphere feedbacks over tropical South America at interannual timescales. *Water*, 10(8), 1095, DOI: 10.3390/w10081095 (2018).

Poveda, G., Jaramillo, A., Gil, M. M., Quiceno, N. Mantilla, R. I. Seasonality in ENSO-related precipitation, river discharges, soil moisture, and vegetation index in Colombia. *Water Resour. Res.*, 37(8), 2169-2178, DOI:10.1029/2000WR900395 (2001).

Wu, Z. *et al.* The modulated annual cycle: An alternative reference frame for climate anomalies. *Clim. Dyn.*, 31 (7-8), 823-841, DOI:10.1007/s00382-008-0437-z (2008).

Fedorov, A. V. & Philander, S. G. Is El Nino changing?, *Science*, 288(5473), 1997-2002, DOI: 10.1126/science.288.5473.1997 (2000).

Thoning, K. W. & Tans, P. P. Atmospheric carbon dioxide at Mauna Loa Observatory. 2. Analysis of the NOAA GMCC data, 1974-1985. *J. Geophys. Res.*, 94(D6), 8549-8565, DOI: 10.1029/JD094iD06p08549 (1989).

Zhang, J. & Wu, Y. k-Sample tests based on the likelihood ratio. *Comput. Stat. Data Analysis*, DOI: 10.1016/j.csda.2006.08.029 (2007).

Zhang, J. Powerful goodness-of-fit tests based on the likelihood ratio. *J. Royal Stat. Soc. Ser. B: Stat. Methodol.*, 64(2), 281-294, DOI:10.1111/1467-9868.00337 (2002).

Pearson, K. Note on regression and inheritance in the case of two parents. *Proc. Royal Soc. Lond.* (1895).

Wolter, K. & Timlin, M. S. El Niño/Southern Oscillation behaviour since 1871 as diagnosed in an extended multivariate ENSO index (MEI.ext). *Int. J. Climatol.*, 31(7), 1074-1087, DOI: 10.1002/joc.2336 (2011).

Terray, P., Delecluse, P., Labattu, S. & Terray, L. Sea surface temperature associations with the late Indian summer monsoon. *Clim. Dyn.*, 21(7-8), 593-618, DOI:10.1007/s00382-003-0354-0 (2003).

Boschat, G., Simmonds, I., Purich, A., Cowan, T. & Pezza, A. B. On the use of composite analyses to form physical hypotheses: An example from heat wave - SST associations. *Sci. Reports*, 6(1), 29599, DOI: 10.1038/srep29599 (2016).

Xie, Z., Duan, A. & Tian, Q. Weighted composite analysis and its application: an example using ENSO and geopotential height. *Atmospheric Sci. Lett.*, 18(11), 435-440, DOI: 10.1002/asl.786 (2017).

Nicholls, N. The Insignificance of Significance Testing, *Bull. Am. Meteorol. Soc.*, 82(5), 981-986, DOI:10.1175/1520-0477(2001)0820981:caatio 2.3.*co*; 2(2001).

Instituto Geográfico Agustín Codazzi (IGAC), Natural regions of Colombia, https://www.igac.gov.co (2020).

Hurtado-Montoya, A. F. & Mesa-Sánchez, Ó. J. Reanalysis of monthly precipitation fields in Colombian territory. DYNA, DOI: 10.15446/dyna.v81n186.40419 (2014).

Lehner, B., Verdin, K. & Jarvis, A. New Global Hydrography Derived From Spaceborne Elevation Data, Eos, Trans. Am. Geophys. Union, 89(10), 93 (2008).

Daly, C., Neilson, R. P. & Phillips, D. L. A. Statistical-Topographic Model for Mapping Climatological Precipitation over Mountainous Terrain. *J. Appl. Meteorol.*, 33(2), 140-158, DOI: 10.1175/1520-0450(1994)0330140:astmfm 2.0.*co*; 2(2002).

Funk, C. *et al.* The climate hazards infrared precipitation with stations - A new environmental record for monitoring extremes. *Sci. Data*,2(1), 150066, DOI: 10.1038/sdata.2015.66 (2015).

Wolter, K. & Timlin, M. S. Measuring the strength of ENSO events: How does 1997/98 rank?, *Weather*, 53(9), 315-324 (1998).

Rasmusson, E. M. & Carpenter, T. H. Variations in Tropical Sea Surface Temperature and Surface Wind Fields Associated with the Southern Oscillation/El Niño. *Mon. Wea. Rev.*, 110(5): 354-384 (1982).

Trenberth, K. E. & Stepaniak, D. P. Indices of El Niño evolution. *J. Clim.*, 14(8), 1697-1701 (2001).

Kashyap, R. & Ramachandra, R. Dynamic stochastic models from empirical data (Academic press, New York, 1976).

Smith, S. W. The Scientist and Engineer's Guide to Digital Signal Processing. In The Scientist and Engineer's Guide to Digital Signal Processing, DOI: 10.1007/BF02834636 (California Technical Pub. San Diego, 1999).

Huang, N. E. & Shen, S. S. P. Hilbert-Huang Transform And Its Applications (World Scientific, 2005).

Flandrin, P., Gonçalvès, P. & Rilling, G. EMD equivalent filter banks, from interpretation to applications (World Scientific, 2005).

Wu, Z. & Huang, N. E. A study of the characteristics of white noise using the empirical mode decomposition method. *Proc. Royal Soc. A: Math. Phys. Eng. Sci.*, 460 (2046), 1597-1611 (2004).

Ahdesmäki, M., Lähdesmäki, H., Pearson, R., Huttunen, H. & Yli-Harja, O. Robust detection of periodic time series measured from biological systems. *BMC Bioinforma*. DOI: 10.1186/1471-2105-6-117 (2005).

Córdoba-Machado, S., Palomino-Lemus, R., Gámiz-Fortis, S. R., Castro-Díez, Y. & Esteban-Parra, M. J. Assessing the impact of El Niño Modoki on seasonal precipitation in Colombia. *Glob. Planet. Chang.*, DOI: 10.1016/j.gloplacha.2014.11.003 (2015).

Córdoba-Machado, S., Palomino-Lemus, R., Gámiz-Fortis, S. R., Castro-Díez, Y. & Esteban-Parra, M. J. Influence of tropical Pacific SST on seasonal precipitation in Colombia: prediction using El Niño and El Niño Modoki. *Clim. Dyn.*, 44(5-6), 1293-1310 (2015).

American Meteorological Society. AMS glossary of meteorology. http://glossary.ametsoc.org/wiki (2018).

National Oceanic and Atmospheric Administration (NOAA). Climate indices. http://www.cpc.ncep.noaa.gov/data/indices/soi (2018).

Kawale, J. *et al.* Anomaly construction in climate data: Issues and challenges. NASA Conference on Intelligent Data Understanding (CIDU) (2011).

Ahdesmäki, M., Lähdesmäki, H., Pearson, R., Huttunen, H., Yli-Harja,O. (2005) Robust detection of periodic time series measured from biological systems, *BMC Bioinformatics*, 6 (117), 1-18.

Andreoli, R. V., de Oliveira, S. S., Kayano, M. T., Viegas, J., de Souza, R. A. F., and Candido, L. A. (2017). The influence of different El Niño types on the South American rainfall. International Journal of Climatology, 37(3), 1374-1390. https://doi.org/10.1002/joc.4783

Arias, P.A., Martínez, Vieira, S.C. (2015) Moisture sources to the 2010-2012 anomalous wet season in northern South America, *Clim Dyn*, DOI 10.1007/s00382-015-2511-7.

Bedoya-Soto, J.; Poveda, G. New insights on land surface-atmosphere feedbacks over tropical South America at interannual timescales. In Proceedings of the 1st Int. Electron. Conf. Hydrol. Cycle, 12-16 November 2017; Sciforum Electronic Conference Series, Vol. 1, 2017 ; doi:10.3390/CHyCle-2017-04875

Bedoya-Soto, J. M., Poveda, G., Trenberth, K. E., and Vélez-Upegui, J. J. (2018). Interannual hydroclimatic variability and the 2009-2011 extreme ENSO phases in Colombia: from Andean glaciers to Caribbean lowlands. Theoretical and Applied Climatology, pp. 1-14. https://doi.org/10.1007/s00704-018-2452-2

Brown, R., Kocarev, L. (2000) A unifying definition of synchronization for dynamical systems, *Chaos*, 10(2), 344-349.

Córdoba-Machado, S., Palomino-Lemus, R., Gámiz-Fortis, S. R., Castro-Díez, Y., and Esteban-Parra, M. J. (2015). Assessing the impact of El Niño Modoki on seasonal precipitation in Colombia. Global and Planetary Change, 124, 41-61. https://doi.org/10.1016/j.gloplacha.2014.11.003.

Córdoba-Machado, S., Palomino-Lemus, R., Gámiz-Fortis, S. R., Castro-Díez, Y., and Esteban-Parra, M. J. (2015). Influence of tropical Pacific SST on seasonal precipitation in Colombia: prediction using El Niño and El Niño Modoki. Climate Dynamics, 44(5-6), 1293-1310. https://doi.org/10.1007/s00382-014-2232-3.

Chiang, J. C. H., and D. J. Vimont (2004) Analagous meridional modes of atmosphere-ocean variability in the tropical Pacific and tropical Atlantic. J. Climate, 17(21), 4143-4158.

Enfield, D.B., Mestas-Nuñez, A. M., Mayer, D. A., and Cid-Serrano, L. (1999) How ubiquitous is the dipole relationship in tropical Atlantic sea surface temperatures?, *J. Geophys. Res. Ocean.*, 104, 7841-7848.

Enfield, D.B., A. M. Mestas-Nuñez and P.J. Trimble (2001) The Atlantic multidecadal oscillation and it's relation to rainfall and river flows in the continental U.S., Geophysical Research Letters, 28, 2077-2080.

Flandrin, P., Rilling, G., Goncalves, P. (2004) Empirical mode decomposition as a filter bank, *IEEE signal processing letters*, 11(2), 112-114.

Gabor, D. (1946) Theory of communication, *Proc IEE London*, 93, 429-457.

Gershunov, A. and T.P. Barnett (1998) Interdecadal modulation of ENSO teleconnections. Bulletin of the American Meteorological Society, 79 (12), 2715-2725.

Ghil, M., Allen, M.R., Dettinger, M.D., Ide, K., Kondrashov, D., Mann, M. E., Robertson, A.W., Saunders, A., Tian, Y., Varadi, F., Yiou, P. (2002) Advanced spectral methods for climatic time series, *Reviews of geophysics*, 40(1), 1-41.

Hoyos, I., Dominguez, F., Cañón-Barriga, J., Martínez, J.A., Nieto, R., Gimeno, L., Dirmeyer, P.A. (2017) Moisture origin and transport processes in Colombia, northern South America, *Clim Dyn*, DOI 10.1007/s00382-017-3653-6.

Hoyos, I. (2017) Transport of atmospheric humidity in Colombia: origin, variability and coupling with global climatic phenomena (in spanish). Ph.D. dissertation, Universidad de Antioquia.

Huang, N.E., Shen, Z., Long, S.R., Wu, M.C., Shih, E.H., Zheng, Q., Tung, C.C., Liu, H.H. (1998) The empirical mode decomposition method and the Hilbert spectrum for non-stationary time series analysis, *Proc Roy Soc Lond*, 454A, 903-995.

Huang, N.E., Shen, Z., Long, S.R (1999) A new view of nonlinear water waves-the Hilbert spectrum, *Ann Rev Fluid Mech*, 31, 417-457.

Huang, N.E., Wu, Z. A review on Hilbert-Huang transform: Method and its applications to geophysical studies, *Reviews of Geophysics*, 46, 1-23.

Hurtado-Montoya, A. and Mesa, O.J. (2014) Reanalysis of monthly precipitation fields in Colombian territory, *Dyna*, 81(186), 251-258.

Instituto Geográfico Agustín Codazzi, IGAC (2002) Natural regions of Colombia.

Mantua, N.J. (2001) The Pacific Decadal Oscillation. In: Encyclopedia of Global Environmental Change, John Wiley & Sons, Inc.

Mantua, N. J. and Hare, S. R. (2002) The Pacific Decadal Oscillation, J. Oceanogr., 58, 35-44.

Martin, E. R., and Schumacher, C. (2011). The caribbean low-level jet and its relationship with precipitation in IPCC AR4 models. Journal of Climate, 24(22), 5935-5950. https://doi.org/10.1175/JCLI-D-11-00134.1

Mapes, B.E., Warner, T.T., Xu, M., Negri, A.J. (2003a). Diurnal patterns of rainfall in northwestern South America. Part I: Observations and context, *Monthly Weather Review*, 131(5), 799-812.

Warner, T.T., Mapes, B.E., Xu, M. (2003) Diurnal patterns of rainfall in northwestern South America. Part II: Model simulations, *Monthly Weather Review*, 131(5), 813-829.

Mapes, B.E., Warner, T.T., Xu, M. (2003b) Diurnal patterns of rainfall in northwestern South America. Part III: Diurnal gravity waves and nocturnal convection offshore, *Monthly Weather Review*, 131(5), 830-844.

Montoya, G., Pelkowski, J., Eslava, J.A. (2001) Sobre los alisios del nordeste y la existencia de una corriente en el Piedemonte Oriental Andino, *Rev. Acad. Colomb. Cienc.*, 25 (96), 363-370.

Muñoz, E., Busalacchi, A.J., Nigam, S. and Ruiz-Barradas, A. (2008) Winter and summer structure of the Caribbean low-level jet, J. Clim., 21, 1260-1276.

Panter, P. (1965) Modulation, Noise, and Spectral Analysis, New York, McGraw-Hill.

Pikovsky, A., Rosenblum, M., Kurths, J. (2001) Synchronization: a universal concept in nonlinear sciences, Cambridge university press.

Poveda, G., Mesa OJ. (1997) Feedbacks between hydrological processes in tropical South America and large-scale ocean-atmospheric phenomena, *Journal of climate*, 10(10), 2690-2702.

Poveda, G., Mesa O.J. (2000) On the existence of Lloro(the rainiest locality on earth): enhanced ocean-land-atmosphere interaction by a low-level jet, Geophysical research letters, 27 (11), 1675-1678.

Poveda, G., Jaramillo, A., Gíl, M.M., Quiceno, N., Mantilla, R.I. (2001) Seasonally in ENSO related precipitation, river discharges, soil moisture, and vegetation index in Colombia, *Water resources research*, 37 (8), 2169-2178.

Poveda, G., Vélez, J. I., Mesa, O. J., Hoyos, C.D., Mejía, J. F., Barco, O.J., Correa, P. (2002) The influence of macro-climatic phenomena on the annual cycle of Colombian hydrology: lineal and non-linear quantification and probabilistic percentiles (in spanish), Meteorología Colombiana, 6, 121-130, ISSN-0124-6984.

Poveda, G. (2004) The hydro-climatology of Colombia: A synthesis from inter-decadal to diurnal timescales (in spanish). Rev. Acad. Colomb. Cienc. 28(107): 201-222, 200. ISSN: 0370-3908.

Poveda, G., Mesa, O. J., Salazar, L. F., Arias, P. A., Moreno, H. A., Vieira, S. C., Agudelo, P.A., Toro, V.G., Alvarez, J. F. (2005). The Diurnal Cycle of Precipitation in the Tropical Andes of Colombia. Monthly Weather Review, 133(1), 228-240. https://doi.org/10.1175/MWR-2853.1

Poveda, G., Álvarez, D.M., Rueda, Ó.A. (2011) Hydro-climatic variability over the Andes of Colombia associated with ENSO: a review of climatic processes and their impact on one of the Earth's most important biodiversity hotspots, *Clim Dyn*, 36, 2233, doi:10.1007/s00382-010-0931-y.

Poveda, G., Jaramillo, L., and Vallejo, L. F. (2014). Seasonal precipitation patterns along pathways of South American low-level jets and aerial rivers. Water Resources Research, 50(1), 98-118. https://doi.org/10.1002/2013WR014087

Poveda, G., López, S., Isaza, A. (2015) Geographic delimitation of regions exhibiting bimodal, transitional and unimodal annual cycles of rainfall within the inter-tropics. International Conference on the *Water and Energy cycles in the Tropics*, 17-19 November 2015, Paris, France.

Le Van Quyen, M., Foucher, J., Lachaux, J., Rodriguez, E., Lutz, a, Martinerie, J., and Varela, F. J. (2001). Comparison of Hilbert transform and wavelet methods for the analysis of neuronal synchrony. Journal of Neuroscience Methods, 111(2), 83-98. https://doi.org/http://dx.doi.org/10.1016/S0165-0270(01)00372-7

Rato, R.T., Ortigueira, M.D., Batista, A.G. (2008) On the HHT, its problems, and some solutions, *Mechanical Systems and Signal Processing*, 22, 1374-1394.

Rasmusson, E., Carpenter, T. (1982) Variations in tropical sea surface temperature and surface winds fields associated with the Southern Oscillation/El Niño, Mon Weather Rev, 110, 354-384.

Rosenblum, M., Pikovsky, A., Kurths, J., Schäfer, C., Tass, P.A. (2001) Phase synchronization: from theory to data analysis, *Handbook of biological physics*, 4, 279-321.

Rueda, O. A., and G. Poveda (2006), Space-time variability of the CHOCO jet and its effect on the Colombian Pacific coast hydroclimatology [in Spanish], Meteorol. Colombiana, 10, 132-145.

Sarachik, E.S. and Cane, M.A. (2010) The El Niño - Sourthern Oscillation Phenomenon, *Cambridge University Press*.

Stein, K., Timmermann, A., Schneider (2011) Phase synchronization of the El Niño-Sourthern Oscillation with the annual cycle, *Physical review letters*, PRL 107, 128501.

Stein, K., Timmermann, A., Schneider, N., Jin, F.F., Stuecker, M.F. (2014) ENSO seasonal synchronization theory, *Journal of Climate*, 27(14), 5285-5310.

Spracklen, D. V., S. R. Arnold, and C. M. Taylor (2012), Observations of increased tropical rainfall preceded by air passage over forests, Nature, 489, 282-285, doi:10.1038/nature11390.

Schiff, S. J., So, P., Chang, T., Burke, R. E., and Sauer, T. (1996). Detecting dynamical interdependence and generalized synchrony through mutual prediction in a neural ensemble. Physical Review E - Statistical Physics, Plasmas, Fluids, and Related Interdisciplinary Topics, 54(6), 6708-6724. https://doi.org/10.1103/PhysRevE.54.6708

Torrealba, E., Amador, J. (2010) La corriente en chorro de bajo nivel de los Llanos Venezolanos de Sur América, *Revista de climatología*, 10,1-20, ISSN 1578-8768.

Tass, P., Rosenblum, M., Weule, J., Kurths, J., Pikovsky, A., Volkmann, J., Schnitzler, A., Freund, H.-J. (1998) Phys. Rev. Lett. 81, 3291-3294.

Troch, P. A., Carrillo, G., Sivapalan, M., Wagener, T., and Sawicz, K.(2013) Climate-vegetation-soil interactions and long-term hydrologic partitioning: signatures of catchment co-evolution, Hydrol. Earth Syst. Sci., 17, 2209-2217, doi:10.5194/hess-17-2209-2013.

Trenberth, K., Stepaniak, D. (2001) Indices of El Niño evolution, *J. Clim*, 14, 1697-1701.

Urrea, V., Ochoa, A., Mesa, O. Rainfall Seasonality in Colombia. *Water Resources Research* (submitted)

Vélez, J.I., Poveda, G., Mesa, O.J., (2000) Hydrological balances of Colombia (in Spanish). COLCIENCIAS-UPME, ISBN: 958-9352-25-1.

Von Storch, H. Bürger, G., Schnur, R., Von Storch, J-S (1995) Principal oscillation patterns: A review, Journal of climate, 8, 377-399.

Wang, H., Fu, R. (2002). Cross-Equatorial Flow and Seasonal Cycle of Precipitation over South America, Journal of Climate, 15, 1591-1608.

Wang, C. (2007). Variability of the Caribbean Low-Level Jet and its relations to climate. Climate Dynamics, 29(4), 411-422. https://doi.org/10.1007/s00382-007-0243-z

Wang, W.C., Chau, K.W., Xu, D.M., Chen, X.Y. (2015) Improving forecasting accuracy of annual runoff time series using ARIMA based on EEMD decomposition, *Water Resources Management*, 29(8), 2655-2675.

Waylen, P., Poveda, G. (2002) El Niño-Southern Oscillation and aspects of western South American hydro-climatology, *Hydrological Processes*, 16(6), 1247-1260.

Wu, Z., Huang, N.E. (2005) Ensemble empirical mode decomposition: a noise-assisted data analysis method, *Center for Ocean-Land-Atmosphere Studies Technical Report 193*,ftp://grads.iges.org/pub/ctr/ctr$_1$93.*pdf*.

Wu, Z., Huang, N.E. (2009) Ensemble empirical mode decomposition: a noise-assisted data analysis method, *Adv Adaptive Data Anal*, 1, 1-41.

Wu, Z., Huang, N.E., Schneider, E.K., Kirtman, B.P., Sarachik, E.S., Huang, N.E., Tucker, C.J. (2008) The modulated annual cycle: an alternative reference frame for climate anomalies, *Clim Dyn*, 31, 823-841.

Zhang, Y., J.M. Wallace and D.S. Battisti (1997) ENSO-like Interdecadal Variability: 1900-93. Journal of Climate, Vol. 10, 1004-1020.

Jiménez-Sánchez, G., , Markowski, P. M., Jewtoukoff, V., Young, G. S. and Stensrud, D. J. (2019) The Orinoco Low-Level Jet: An Investigation of Its Characteristics and Evolution Using the WRF Model, J. Geophys. Res. Atmos., 124, 10696 -10711.

Pikovsky, A., Rosenblum, M., Kurths, J. (2001) Synchronization: a universal concept in nonlinear sciences, Cambridge, UK: Cambridge University Press, pp. 432. ISBN 052153352X.

Balanov, A., Janson, N., Postnov, D., Sosnovtseva, O., Synchronization: From simple to complex. Heidelberg, Springer-Verlag Berlin, pp. 435,ISBN 978-3-540-72127-7.

Brown, R., Kocarev, L. (2000) A unifying definition of synchronization for dynamical systems, *Chaos*, 10(2), 344-349.

Rulkov, N.F., Sushchik, M. M., Tsimring, L. S. and Abarbanel, H. D. I. (1995) Generalized synchronization of chaos in directionally coupled chaotic systems, Phys. Rev. E.

Schiff, S. J., So, P., Chang, T., Burke, R. E., and Sauer, T. (1996) Detecting dynamical interdependence and generalized synchrony through mutual prediction in a neural ensemble, Phys. Rev. E, 54, 6708-6724, https://doi.org/10.1103/PhysRevE.54.6708.

Arnhold, J., Grassberger, P., Lehnertz, K., and Elger, C. E. (1999) A robust method for detecting interdependences: application to intracra- nially recorded EEG, Physica D, 134, 419-430.

Le Van Quyen, M., Martinerie, J., Adam, C., and Varela, F. J. (1999) Non-linear analyses of interictal EEG map the brain interdependences in human focal epilepsy, Physica D, 127, 250-266.

Quiroga, R. Q., Kraskov, A., Kreuz, T., and Grassberger, P. (2002) Performance of different synchronization measures in real data: a case study on electroencephalographic signals, Phys. Rev. E, 65,041903, https://doi.org/10.1103/PhysRevE.65.041903.

Zbilut, J. P., Webber, C. L. (2006) Recurrence Quantification Analysis, Wiley Encyclopedia of Biomedical Engineering, DOI: 10.1002/9780471740360.edb1355.

Marwan, N., Romano, M.C., Thiel, M., & Kurths, J. (2007). Recurrence plots for the analysis of complex systems. *Physics Reports*. https://doi.org/10.1016/j.physrep.2006.11.001

Romano, M. C., Thiel, M., Kurths, J. (2004) Generalized Synchronization Indices based on Recurrence in Phase Space, 742, 330-336.

Rosenblum, M. G., Pikovsky, A. S., and Kurths, J. (1997) From phase to lag synchronization in coupled chaotic oscillators, Phys. Rev. Lett., 78, 4193-4196, https://doi.org/10.1103/PhysRevLett.78.4193.

Tass, P., Rosenblum, M. G., Weule, J., Kurths, J., Pikovsky, A., Volkmann, J., Schnitzler, A., and Freund, H.J. (1998) Detection of n: m phase locking from noisy data: application to magnetoencephalography, Phys. Rev. Lett., 81, 3291-3294, https://doi.org/10.1103/PhysRevLett.81.329.

Rosenblum, M., Pikovsky, A., Kurths, J., Schäfer, C., Tass, P.A. (2001) Phase synchronization: from theory to data analysis, *Handbook of biological physics*, 4, 279-321.

Stolbova, V., Martin, P., Bookhagen, B., Marwan, N., and Kurths, J. (2014) Topology and seasonal evolution of the network of extreme precipitation over the Indian subcontinent and Sri Lanka, Nonlinear Proc. Geoph., 21, 901-917.

Malik, N., Bookhagen, B., Marwan, N., and Kurths, J. (2012) Analysis of spatial and temporal extreme monsoonal rainfall over South Asia using complex networks, Clim. Dynam., 39, 971-987.

Rheinwalt, A., Boers, N., Marwan, N., Kurths, J., Hoffmann, P.,Gerstengarbe, F.-W., and Werner, P.(2016) Non-linear time series analysis of precipitation events using regional climate networks for Germany, Clim. Dynam., 46, 1065-1074.

Agarwal, A., N. Marwan, M. Rathinasamy, B. Merz, and J. Kurths (2017) Multi-scale event synchronization analysis for unravelling climate processes: A wavelet-based approach, Nonlinear Process. Geophys.

Poincaré, H. (1890) Sur la probleme des trois corps et les Ã©quations de la dynamique, Acta Mathematica, 13, 1-271.

Takens, F. (1981), Detecting strange attractors in turbulence, D. Rand, L.-S. Young (Eds.), Dynamical Systems and Turbulence, Lecture Notes in Mathematics, vol. 898, Springer, Berlin, pp. 366-381.

Sauer, T., Yorke, J., Casdagli, A. M. (1991) Embedology, J. Statist. Phys. 65 (3-4), 579-616.

Marwan, N. A historical review of recurrence plots, European Physical Journal: Special Topics, 164: 3. https://doi.org/10.1140/epjst/e2008-00829-1.

Webber, C.L., Marwan, N. (2014) Recurrence quantification analysis: Theory and best practices. Springer Cham Heidelberg New York Dordrecht London, pp. 421, DOI 10.1007/978-3-319-07155-8.

Feldhoff, J. H. Donner, R. V. Donges, J.F., Marwan, N. Kurths, J. (2013) Geometric Signature of Complex Synchronisation Scenarios. EPL 102, 3, doi.org/10.1209/0295-5075/102/30007

Senthilkumar, D. V., Suresh, R., Lakshmanan, N., Kurths, J. (2013) Global Generalized Synchronization in Networks of Different Time-Delay Systems. EPL 103.5, doi: 10.1209/0295-5075/103/50010

Suresh, R., Senthilkumar, D.V., Lakshmanan, M., Kurths, J. (2016) âœEmergence of a Common Generalized Synchronization Manifold in Network Motifs of Structurally Different Time-Delay Systems. Chaos, Solitons and Fractals 93: 235-245.

Hobbs, B., Ord, A. (2018) Nonlinear Dynamical Analysis of GNSS Data: Quantification, Precursors and Synchronisation, Progress in Earth and Planetary Science (2018) 5:36,doi.org/10.1186/s40645-018-0193-6

Sarachik, E.S. and Cane, M.A. (2010) The El Niño - Sourthern Oscillation Phenomenon, Cambridge University Press.

Stein, K., Timmermann, A., Schneider (2011) Phase synchronization of the El Niño-Sourthern Oscillation with the annual cycle, Physical review letters, PRL 107, 128501.

Arias, P.A., Martínez, Vieira, S.C. (2015) Moisture sources to the 2010-2012 anomalous wet season in northern South America, *Clim Dyn*, DOI 10.1007/s00382-015-2511-7.

Poveda, G., Mesa O.J. (1997) Feedbacks between hydrological processes in tropical South America and large-scale ocean-atmospheric phenomena, *Journal of Climate*, 10(10), 2690-2702.

Poveda, G., Jaramillo, A., Gíl, M.M., Quiceno, N., Mantilla, R.I. (2001) Seasonally in ENSO related precipitation, river discharges, soil moisture, and vegetation index in Colombia, *Water Resources Research*, 37 (8), 2169-2178.

Waylen, P., Poveda, G. (2002) El Niño-Southern Oscillation and aspects of western South American hydro-climatology, *Hydrological Processes*, 16(6), 1247-1260.

Poveda, G., Álvarez, D.M., & Rueda, O.A. (2010) Hydro-climatic variability over the Andes of Colombia associated with ENSO: a review of climatic processes and their impact on one of the Earth's most important biodiversity hotspots, *Climate Dynamics*, 36, 2233, doi:10.1007/s00382-010-0931-y.

Bedoya-Soto, J.; Poveda, G. New insights on land surface-atmosphere feedbacks over tropical South America at interannual timescales. In Proceedings of the 1st Int. Electron. Conf. Hydrol. Cycle, 12-16 November 2017; *Sciforum Electronic Conference Series*, Vol. 1, 2017 ; doi:10.3390/CHyCle-2017-04875

Bedoya-Soto, J. M., Poveda, G., Trenberth, K. E., and Vélez-Upegui, J. J. (2018). Interannual hydroclimatic variability and the 2009-2011 extreme ENSO phases in Colombia: from Andean glaciers to Caribbean lowlands. *Theoretical and Applied Climatology*, pp. 1-14. https://doi.org/10.1007/s00704-018-2452-2

Wang, C. (2007). Variability of the Caribbean Low-Level Jet and its relations to climate. *Climate Dynamics*, 29(4), 411-422. https://doi.org/10.1007/s00382-007-0243-z

Poveda, G., and Mesa, O. J. (2000). On the existence of Lloró (the rainiest locality on earth): Enhanced ocean-land-atmosphere interaction by a low-level jet. *Geophysical Research Letters*, 27(11), 1675-1678. https://doi.org/10.1029/1999GL006091

Yepes, J., G. Poveda, J.F. Mejía, L. Moreno, and C. Rueda (2019) CHOCO-JEX: A Research Experiment Focused on the Chocó Low-Level Jet over the Far Eastern Pacific and Western Colombia. Bulletin of the American Meteorological Society, 100, 779-796, https://doi.org/10.1175/BAMS-D-18-0045.1.

Montoya, G., Pelkowski, J., Eslava, J.A. (2001) Sobre los alisios del nordeste y la existencia de una corriente en el Piedemonte Oriental Andino, *Rev. Acad. Colomb. Cienc.*, 25 (96), 363-370.

Jiménez-Sánchez, G., , Markowski, P. M., Jewtoukoff, V., Young, G. S. and Stensrud, D. J. (2019) The Orinoco Low-Level Jet: An Investigation of Its Characteristics and Evolution Using the WRF Model, J. Geophys. Res. Atmos., 124, 10696 -10711.

Wang, H., Fu, R. (2002). Cross-Equatorial Flow and Seasonal Cycle of Precipitation over South America, *Journal of Climate*, 15, 1591-1608.

Sullivan, A., J.-J. Luo, A. C. Hirst, D. Bi, W. Cai and He, J. (2016) Robust contribution of decadal anomalies to the frequency of central-Pacific El Niño. *Scientific Reports*, 6, 38540; doi: 10.1038/srep38540

Andreoli, R. V., de Oliveira, S. S., Kayano, M. T., Viegas, J., de Souza, R. A. F., and Candido, L. A. (2017). The influence of different El Niño types on the South American rainfall. *International Journal of Climatology*, 37(3), 1374-1390. https://doi.org/10.1002/joc.4783

Ashok, K., Behera, S. K., Rao, S. A., Weng, H., Yamagata, T. (2007). El Niño Modoki and its possible teleconnection. Journal Of Geophysical Research. 112: 1-27.

Ashok, K., Yamagata, T. (2009). The El Niño with a difference. Nature. 461: 481-484.

Córdoba-Machado, S., Palomino-Lemus, R., Gámiz-Fortis, S. R., Castro-Díez, Y., and Esteban-Parra, M. J. (2015). Assessing the impact of El Niño Modoki on seasonal precipitation in Colombia. *Global and Planetary Change*, 124, 41-61. https://doi.org/10.1016/j.gloplacha.2014.11.003.

Córdoba-Machado, S., Palomino-Lemus, R., Gámiz-Fortis, S. R., Castro-Díez, Y., and Esteban-Parra, M. J. (2015). Influence of tropical Pacific SST on seasonal precipitation in Colombia: prediction using El Niño and El Niño Modoki. *Climate Dynamics*, 44(5-6), 1293-1310. https://doi.org/10.1007/s00382-014-2232-3.

Navarro-Monterroza, E., Arias, P.A., Vieira, S.c. (2019) El Niño-Southern Oscillation Modoki and its effects on the spatiotemporal variability of precipitation in Colombia (in spanish), *Rev. Acad. Colomb. Cienc. Ex. Fis. Nat.* 43(166):120-132, doi: http://dx.doi.org/10.18257/raccefyn.704.

Serna, L.M., Arias, P.A., Vieira, S. C. (2018) The Choco and Caribbean low-level jets during El Niño and El Niño Modoki events (in spanish), *Rev. Acad. Colomb. Cienc. Ex. Fis. Nat.* 42(165):410-421, doi: http://dx.doi.org/10.18257/raccefyn.705

Gill, A. E. (1980) Some simple solutions for heat-induced tropical circulation. Quart. J .R. Met. Soc., 106:447-462

Weng, H., Behera, S. K. and Yamagata, T. (2009) Anomalous winter climate conditions in the Pacific rim during recent El Niño Modoki and El Niño events, Clim. Dyn. 32, doi:10.1007/s00382-008-0394-6 (2009).

Martin, E. R., and Schumacher, C. (2011). The caribbean low-level jet and its relationship with precipitation in IPCC AR4 models. *Journal of Climate*, 24(22), 5935-5950. https://doi.org/10.1175/JCLI-D-11-00134.1

Rasmusson, E., Carpenter, T. (1982) Variations in tropical sea surface temperature and surface winds fields associated with the Southern Oscillation/El Niño, *Mon Weather Rev*, 110, 354-384.

Trenberth, K., Stepaniak, D. (2001) Indices of El Niño evolution, *J. Clim*, 14, 1697-1701.

Hurtado-Montoya, A. and Mesa, O.J. (2014) Reanalysis of monthly precipitation fields in Colombian territory, *Dyna*, 81(186), 251-258.

Kalnay, E. et al. (1996) The NCEP/NCAR 40-Year Reanalysis Project. *Bulletin of the American Meteorological Society*, 77.3: 437-471.

Torrealba, E., Amador, J. (2010) La corriente en chorro de bajo nivel de los Llanos Venezolanos de Sur América, *Revista de climatología*, 10,1-20, ISSN 1578-8768.

Eckmann, J.-P., Kamphorst, S. O., & Ruelle, D. (1987). Recurrence Plots of Dynamical Systems. *Europhysics Letters*, 4(9), 973-977. https://doi.org/10.1209/0295-5075/4/9/004

Packard, N. H., Crutchfield, J. P., Farmer, J. D., & Shaw, R. S. (1980). Geometry from a time series. *Physical Review Letters*, 45(9), 712-716. https://doi.org/10.1103/PhysRevLett.45.712

Fraser, A. M., & Swinney, H. L. (1986). Independent coordinates for strange attractors from mutual information. *Physical Review A*, 33(2), 1134-1140. https://doi.org/10.1103/PhysRevA.33.1134

Kantz, H., & Schreiber, T. (2004). Nonlinear Time Series Analysis. Nonlinear Time Series Analysis (Vol. 47). https://doi.org/10.1198/tech.2005.s306

Marwan, N. (2011) How to avoid potential pitfalls in recurrence plot based data analysis. *Int J Bifurc Chaos*, 21:1003-1017.

Mindlin, G.M., Gilmore, R. (1992) Topological analysis and synthesis of chaotic time series. Physica D 58(1-4), 229-242.

Zbilut, J.P., Webber Jr., C.L. (1992) Embeddings and delays as derived from quantification of recurrence plots. Phys. Lett. A 171(3-4), 199-203.

Romano, M. C., Thiel, M., Kurths, J., & Von Bloh, W. (2004). Multivariate recurrence plots. *Physics Letters*, Section A: General, Atomic and Solid State Physics, 330(3-4), 214-223. https://doi.org/10.1016/j.physleta.2004.07.066

Marwan, N. Zou, Y., Wessel, N., Riedl, M. & Kurths, J. (2013) Estimating coupling directions in the cardiorespiratory system using recurrence properties, *Phil Trans R Soc A* 371:20110624. http://dx.doi.org/10.1098/rsta.2011.0624

Arnhold, J., Grassberger, P., Lehnertz, K., & Elger, C. E. (1999). A robust method for detecting interdependences: application to intracranially recorded EEG. *Physica D: Nonlinear Phenomena*, 134(4), 419-430. https://doi.org/10.1016/S0167-2789(99)00140-2

Thiel, M., Romano, M.C., Kurths, J. Rolfs, M., Kliegl, R. (2006) Twin surrogates to test for complex synchronisation. *Europhys Lett*, 75:535-541. doi:10.1209/epl/i2006-10147-0

Thiel, M., Romano, M.C., Kurths, J. Rolfs, M., Kliegl, R. (2008) Generating Surrogates from Recurrences. *Philosophical Transactions of the Royal Society A: Mathematical, Physical and Engineering Sciences*. Vol. 366. N.p., 2008. 545-557. Web.

Holm, S. (1979) A simple sequentially rejective multiple test procedure, Scand. J. Stat.

Abdi, H. (2007) The Bonferonni and Sidak Corrections for Multiple Comparisons, *Encyclopedia of Measurement and Statistics*.

Douglass, D. H. (2011). The Pacific sea surface temperature. Physics Letters, Section A: General, Atomic and Solid State Physics, 376(2), 128-135. https://doi.org/10.1016/j.physleta.2011.10.042

Douglass, D. H., and, Knox, R. S. (2015). The Sun is the climate pacemaker I. Equatorial Pacific Ocean temperatures. Physics Letters, Section A: General, Atomic and Solid State Physics, 379(9), 823-829. https://doi.org/10.1016/j.physleta.2014.10.057

Afyouni, S., Smith, S.M.,Nichols, T.E. (2019) Effective Degrees of Freedom of the Pearson's Correlation Coefficient under Autocorrelation, NeuroImage, 199, 609-625.

Bonner, W.D. (1968) Climatology of the low level jet, Mon. Weather Rev. Vol. 96 (12), 833-850.

Stensrud, D. J. (1996) Importance of low-level jets to climate: A review, J. Clim., 9, 1698-1711.

Gimeno, L., Dominguez, F., Nieto, R., Trigo, R., Drumond, A., Reason, C.J.C., Taschetto, A. S., Ramos, A.M., Kumar, R., Marengo, J. (2016) Major Mechanisms of Atmospheric Moisture Transport and Their Role in Extreme Precipitation Events, Annu. Rev. Environ. Resour., 41, 117-41.

Hoyos, I., Dominguez, F., Cañón-Barriga, J., Martínez, J.A., Nieto, R., Gimeno, L., Dirmeyer, P.A. (2017) Moisture origin and transport processes in Colombia, northern South America, *Clim Dyn*, DOI 10.1007/s00382-017-3653-6.

Poveda, G., and Mesa, O. J. (1996) The extreme phases of ENSO (El Niño and La Niña) y its influence on the Colombian hydrology (in spanish), *Ingeniería Hidráulica en México*, Vol. XI,1, 21-37.

Ahdesmäki, M., Lähdesmäki, H., Pearson, R., Huttunen, H., Yli-Harja,O. (2005) Robust detection of periodic time series measured from biological systems, *BMC Bioinformatics*, 6 (117), 1-18.

Troch, P. A., Carrillo, G., Sivapalan, M., Wagener, T., and Sawicz, K.(2013) Climate-vegetation-soil interactions and long-term hydrologic partitioning: signatures of catchment co-evolution, *Hydrol. Earth Syst. Sci.*, 17, 2209-2217, doi:10.5194/hess-17-2209-2013.

Andrés-Doménech, I., García-Bartual, R., Montanari, A., and Marco, J. B. (2015). Climate and hydrological variability: The catchment filtering role. *Hydrology and Earth System Sciences*, 19(1), 379-387. http://doi.org/10.5194/hess-19-379-2015.

Muñoz, E., Bussalacchi, A.J., Nigam, S., Ruiz-Barradas, A. (2007) Winter and Summer structure of the Caribbean Low-Level Jet, Journal of Climate, 21, 1260-1276.

Rueda, O. A., and G. Poveda (2006), Space-time variability of the CHOCO jet and its effect on the Colombian Pacific coast hydroclimatology [in Spanish], Meteorol. Colombiana, 10, 132-145.

Sakamoto, M.S., Ambrizzi, T., and Poveda, G. Moisture Sources and Life Cycle of Convective Systems over Western Colombia. *Advances in Meteorology*, 2011 (2012): 1-11.

García-Serrano, J., Cassou, C., Douville, H., Giannini, A. and Doblas-Reyes, F. J. (2017) Revisiting the ENSO teleconnection to the tropical North Atlantic, *J. Clim.*,30, 6945-6957.

Builes-Jaramillo, A., Ramos, A. M. T., Poveda, G. (2018) Atmosphere-Land Bridge between the Pacific and Tropical North Atlantic SST's through the Amazon River basin during the 2005 and 2010 droughts, *Chaos*, CHAOS 28, 085705.

Poveda, G., Jaramillo, L., Vallejo, L. F. (2014) Seasonal precipitation patterns along pathways of South American low-level jets and aerial rivers, Water Resour. Res., 50, 98-118, doi:10.1002/2013WR014087

Arango-Ruda, E., Poveda, G., (2018) Efectos de El Niño y La Niña sobre la hidrología de la Amazonia colombiana, Colombia Amazónica, No. 11, 2018, 33-58.

Hersbach, H., et al., The ERA5 global reanalysis, Q. J. R. Meteorol. Soc., 2020.

Von Storch, H. Bürger, G., Schnur, R., Von Storch, J-S (1995) Principal oscillation patterns: A review, Journal of climate, 8, 377-399.

Bedoya-Soto, J.M., Aristizabal , E., Carmona, A. M., Poveda, G. (2019) Seasonal Shift of the Diurnal Cycle of Rainfall Over Medellin's Valley, Central Andes of Colombia (1998-2005), Front. Earth Sci., 16 May 2019 — https://doi.org/10.3389/feart.2019.00092.

Stein, K., Timmermann, A., Schneider (2011) Phase synchronization of the El Niño-Sourthern Oscillation with the annual cycle, *Physical review letters*, PRL 107, 128501.

Stein, K., Timmermann, A., Schneider, N., Jin, F.F., Stuecker, M.F. (2014) ENSO seasonal synchronization theory, *Journal of Climate*, 27(14), 5285-5310.